ABSTRACT

GHARAGOZLOU, ALIREZA. Coupling of Deterministic and Probabilistic Models for Prediction of Storm-Driven Erosion on Barrier Islands. (Under the direction of Casey Dietrich.)

Coastal areas are subjected to storms and subsequent erosion and flooding. Waves and storm surge can cause damage to infrastructure and short- and long-term changes to coastal morphology. These morphodynamic changes can range from mild beach erosion to severe dune removal, overwash, and breaching. In this dissertation, a combination of models are used to explore the storm-driven hydro- and morphodynamic processes on different scales and their interactions over time. Additionally, their application is extended for prediction of beach response to sea-storms by coupling deterministic and probabilistic models.

In this dissertation, first a morphodynamic model is used to explore the effects of Isabel (2003) on the NC Outer Banks, with the focus on a large domain that covers 30 km of the barrier island from Rodanthe to Avon. It is hypothesized that the model can be coarsened and expanded to a large domain while preserving accuracy. Model predictions for dune erosion and overwash are in good agreement with post-storm observations. Sensitivity studies show that the model accuracy is less sensitive to the alongshore resolution of the mesh. Then, the topographic elevation changes are upscaled to a region-scale flooding model to allow overwash and inundation behind the dunes. The loose coupling of these process-based models improves the flooding predictions in region-scale model significantly.

Then, a more complex case of beaching and its impacts on larger-scale circulations are explored. Isabel (2003) breached the barrier island near the town of Hatteras and formed three channels connecting the ocean to the sound. Two-way coupling of high-resolution numerical models for coastal erosion and flooding is implemented to study the temporal and spatial evolution of the breach and its contribution to the hydrodynamics in the sound. It is hypothesized that the channels were formed due to the combined effects of ocean-side dune erosion and lagoon-side elevated water levels. The model shows that the flow from the sound to the ocean has an important role in deepening the breached channels. The morphodynamic model can predict the initiation and approximate location of the breach. However, it failed to accurately capture the channels' depths. Several flooding scenarios are considered to implement the ground surface changes in the flooding model. The evolving breach can affect the timing and extent of flow into the lagoon. The model results show that the breach has region-scale effects on flooding that extend about 10 km into the lagoon.

Finally, the erosion of nourished beaches subjected to multiple storms is investigated. Beach nourishment provides a buffer during extreme events in the short-term but has a finite lifespan as the beach responds to subsequent storms. Numerical models are widely used to predict the beach morphodynamics, however, they are computationally expensive. In this research, a surrogate model is developed by coupling deterministic and probabilistic models to improve the computational

efficiency and to include the randomness of possible future scenarios. A large data set of storm data and beach profiles is used to create a library of thousands of hypothetical scenarios to train the surrogate model. It is hypothesized that adding the beach profile variability in the analysis can improve the model in the sense that it can be applied to any beach state. The results show that predicted erosion volume by the surrogate model is very close to the numerical model prediction with an average error of $E_{volume} = 2.53\ \mathrm{m}^3/\mathrm{m}$ for the synthetic scenarios and $E_{volume} = 11.13\ \mathrm{m}^3/\mathrm{m}$ for the predictions of 2019 storms. The model produced the results in a few seconds which shows a significant improvement in computational time compared to numerical models.

This research has the potential to improve the prediction of storm-driven erosion, overwash, inundation and breaching. The loose coupling of hydro- and morphodynamic models allows for better predictions of storm-driven flooding into previously protected areas, such as coastal communities and back-barrier regions. The use of observed beach profiles in the development of a surrogate model can improve its predictions of nourishment response to single and successive storms. These better predictions can enable better planning and design for mitigation of future hazards.

Coupling of Deterministic and Probabilistic Models for Prediction of
Storm-Driven Erosion on Barrier Islands

by
Alireza Gharagozlou

A dissertation submitted to the Graduate Faculty of
North Carolina State University
in partial fulfillment of the
requirements for the Degree of
Doctor of Philosophy

Civil Engineering

Raleigh, North Carolina

2021

APPROVED BY:

Rafael Canizares External Member	Helena Mitasova
Alejandra Ortiz	Margery Overton

Casey Dietrich
Chair of Advisory Committee

DEDICATION

To my parents Farahnaz Nouri and Hamidreza Gharagozlou, and my brother Pouria
For their unconditional love and support.

BIOGRAPHY

Alireza Gharagozlou was born in Hamedan, Iran in 1989. He grew up there, where he attended Allameh-Helli High School. Alireza pursued an undergraduate degree in Civil Engineering at Bu-Ali Sina University. He then continued his education in Civil Engineering with a focus on Coastal Engineering at the University of Tehran, where he worked on modeling the coastal hydrodynamics and sediment transport near breakwaters and jetties. In 2015, he obtained his M.S. degree and then moved to the United States to pursue his doctoral studies under the direction of Dr. Casey Dietrich at NC State University. Beyond the academic world, Alireza enjoys listening to classical music, playing guitar, and computer games.

ACKNOWLEDGEMENTS

I would like to first thank my advisor, Dr. Casey Dietrich for his incredible patience, support, and mentorship. He was always available, supported me through every step of my PhD, and taught me to be a better person. I would never have been as successful without his help and guidance.

I am also thankful to my committee members, Dr. Overton, for her constructive advising and comments, Dr. Ortiz, for all her kind support during my PhD, Dr. Mitasova, for her suggestions and all she taught me about GIS, and Dr. Canizares, for his support and valuable suggestions regarding my research. I also would like to thank Dr. Sciaudone, for her support and helpful suggestions, and Dr. Anderson for his incredible insights and feedback on my research, and for teaching me a lot about machine learning.

Many thanks to Jessica and Tucker who worked hard and helped me with setting up the model, running simulations, and visualizing the outputs. I am grateful to be meeting and working with incredible people in the coastal team at NC State. Many thanks to Lily, Ayse, Rosemary, Ajimon, Russell, Nelson, Katie, Johnathan, Hanieh, and many others that supported me in the past six years.

Lastly, I would like to thank my amazing parents, and my brother, who always supported me from miles away. They selflessly encouraged me to explore this new path in my life and seek my destiny. This journey would not have been possible if not for them.

TABLE OF CONTENTS

LIST OF TABLES

LIST OF FIGURES

CHAPTER

1

INTRODUCTION

1.1 Overview

The research in this PhD dissertation will focus on the coupling of deterministic and probabilistic models to improve predictions of barrier-island erosion during single and successive storm events. Deterministic models can represent the erosion and flooding processes with high fidelity and have been applied successfully in numerous studies, but this research will address gaps related to the timing and extents of erosion and breaching on the barrier islands during storms and their interactions with hydrodynamics in small- and large scales. Probabilistic models can overcome the computational costs of deterministic models and have been applied successfully in recent studies to understand barrier island response over many years, but this research will address gaps related to assessment of volume of sand required for beach nourishment, the sustainability and frequency of the nourishment, and the response of nourished beaches to possible future scenarios. In this chapter, the background of these nearshore processes and predictive models will be discussed, the research gaps will serve as motivation for novel contributions in this PhD research, and the roadmap for the dissertation will be described.

1.2 Background

1.2.1 Nearshore Processes

About 10 percent of the world's open coasts are barrier coasts, formed as a result of sea level rise [Stutz & Pilkey, 2011]. These coasts occur all over the world but mostly in areas with a low gradient in the slope of the shore. A barrier coast consists of six elements: the coast, back-barrier lagoon, inlets, barrier islands, barrier platform, and shore face (shore zone of the sea floor) [Oertel, 1985]. Of these elements, barrier islands are natural storm defense systems and protect the back barrier region from flooding [Morton & Sallenger, 2003]. However, these features are highly vulnerable to erosion and flooding during storms [Doran et al., 2013]. Predictions of the morphodynamic response of the barrier islands and their impact on the regional circulation are crucial for flood risk assessment.

During storms, erosion and breaching of barrier islands is driven by nearshore hydrodynamics. Previous studies have explored these processes by using field and remotely sensed data to find the vulnerable locations for breaching and analayze the erosion of the dunes [Hardin, 2013; Donnelly et al., 2006]. Low dune elevations at the site of the breach prior to Irene's (2003) landfall had significant contribution to severity of the damages and formation of a breach [Clinch et al., 2012]. The locations that are most vulnerable to major damages usually are specified as hotspots [Overton & Smyre, 2013]. The morphodynamic response of the dune system during the storm can be categorized into four regimes of swash, collision, overwash, and inundation [Sallenger, 2000]. These regimes are linked to the total water level (TWL), which is the combined contributions of tides, surge, and run-up. In the swash regime, the TWL is below the dune toe elevation, and the erosion and deposition occur on the beach. In the collision regime, TWL exceeds the toe elevation and initiates the dune face erosion. In the overwash regime, TWL reaches the dune crest elevation, and overtopping occurs. In the inundation regime, TWL is higher than the dune crest, and the barrier is fully submerged. Thus, depending on the nearshore hydrodynamics, the morphodynamics of the beach and dune system can be very different.

These linked processes can be devastating to barrier islands. When the TWL on one side of a narrow barrier island exceeds a certain level in relation to dune elevation, strong waves and current erode the sediment on the dune and beach. Depending on the local topography and geology of the barrier island, as well as the intensity of the storm, the storm-driven erosion can develop a channel through the barrier. Water flow through the channel is driven by a difference between bay and ocean water levels, influenced by wave run-up and overwash. There are three causes of natural barrier island breaching: (1) run-up or inundation overwash, (2) liquefaction and piping due to elevated water level, and (3) narrowing of the barrier island due to a reduction in alongshore sediment supply [Kraus et al., 2002]. This breaching process can happen both from lagoon [Velasquez-Montoya et al., 2018; Safak et al., 2016] and ocean side [Karanci et al., 2014; Kurum & Overton, 2013; Ormondt et al., 2020]. After its formation, the initial channel will expand vertically and horizontally to reach its dynamic equilibrium dimensions [Kraus & Wamsley, 2003]. Barrier island erosion and breaching can be linked to several parameters such as island width [Morton, 2002], offshore wave conditions [Gracia et al., 2013a], and geology of the region [Riggs et al., 1995]. The response of barrier islands to major storms is critical in the assessment of coastal resiliency and vulnerability [Canizares & Irish, 2008; Sherwood et al., 2014], both during the event and in the future, as morphology changes can increase the vulnerability of communities and infrastructure to flooding [Ruggiero et al., 2001]. Therefore, it is important to understand and to predict these morphological behaviors.

To protect against these erosion hazards, coastal communities use a range of mitigation techniques. Beach nourishment is the leading form of coastal protection in the U.S. [Armstrong et al., 2016]. Beach nourishment design is a multi-disciplinary approach which requires a deep knowledge of the coastal zone and its processes to define equilibrium profile and depth of closure, suitable type of beach nourishment, characteristic of fill material, availability of submarine borrow sites, and environmental quality and suitability of resources [Giordano et al., 2006]. Beach nourishment is used on beaches with a variety of sedimentary characteristics from sand to gravel [Hanson et al., 2002]. Beach nourishment is an effective shoreline stabilization strategy [Luettich et al., 2014] which creates a buffer between the infrastructure and the storm impact. It also provides a source for natural growth of the beach and dunes [Kaczkowski et al., 2018]. A combination of wider beaches and larger dunes can mitigate storm impacts as observed in North Carolina coast during Floyd (1999) where the buildings near nourished beaches were protected and the ones in unnourished regions were damaged [Rogers, 2007]. Similarly during Sandy (2012) the homes behind unnourished beaches were flooded while the nourished beaches prevented overwash and breaching [Barone et al., 2014].

Beaches are dynamic systems that experience significant changes in short- and long-term. Placement of sand and constructed profiles are expected to change during the first several years after the nourishment, thus, requiring regular maintenance and monitoring of the subsequent morphodynamic changes to compensate the erosion from episodic events [Landry, 2011]. Typical nourishment frequencies in the U.S. are every 10 years, with variability dependent on the local background erosion rate [Cuttler et al., 2019]. However, the specific storm scenarios that a nourishment may experience in its lifetime are unknown. Therefore, there is a need to predict beach erosion and sustainability under futuristic storms as well as frequency and cost of the nourishment projects.

1.2.2 Predictive Models

These morphodynamic and hydrodynamic processes can be predicted using numerical models. For the morphodynamics, a widely used model is eXtreme Beach (XBeach) [Roelvink et al., 2009], which can simulate the sub-aerial response of a beach and dune system during an extreme event. The model solves the time-varying, short-wave action balance equation on wave-group scale and includes dissipation [Roelvink, 1993] and roller models [Svendsen, 1984]. This wave-group forcing drives infragravity waves and longshore and cross-shore currents. Infragravity waves can contribute to dune erosion, and XBeach includes their effects by resolving the short wave variation and the long waves associated with them.

Morphodynamic models are applied typically on small domains, due to their computational cost. These models require resolution of the dune-scale coastal features (e.g. dune shape, small inlets, etc.), as well as of the physical processes. Storm-driven erosion, breaching, and inlet formation affect nearshore hydrodynamics and morphodynamics in the region [Elsayed & Oumeraci, 2017; McCall et al., 2010; Harter & Figlus, 2017]. Kurum & Overton [2013] modeled a breach in Pea Island, North Carolina (NC), during Irene (2011) on a domain that included 1 km of coastline with a minimum resolution of 1 to 2 m. This resolution is similar to studies in other regions, e.g. Texas [Harter & Figlus, 2017], Louisiana [Lindemer et al., 2010], and Florida [Passeri et al., 2018], with larger domains that include up to 10 to 20 km of island coastline. While these models can predict the erosion at specific locations, their domain sizes can limit their predictions of how erosion may interact with waves and flooding throughout the larger region.

The large-scale storm effects on nearshore waves and circulation can be predicted with nearshore wave and coastal circulation models. A widely-used model is the tightly-coupled ADvanced CIRCulation (ADCIRC) [Luettich et al., 1992; Westerink et al., 2008] and Simulating WAves Nearshore (SWAN) [Booij et al., 1999], which have been applied for storm surge and coastal flooding [Bunya et al., 2010; Hope et al., 2013; Cyriac et al., 2018]. ADCIRC uses the continuous-Galerkin, finite-element method to solve modified forms of the shallow water equations on flexible, unstructured meshes. SWAN solves the wave action density equation for the evolution of wave energy, and it was extended to use unstructured meshes [Zijlema, 2010]. When coupled tightly, the ADCIRC+SWAN models can pass information through local memory without the need for interpolation between models [Dietrich et al., 2011b]. The coupled models can provide predictions of water levels, depth-averaged currents, and wave parameters (significant height, peak period, etc.)

Storm surge and flooding models are applied typically on large domains. The computational domains in these models can include the lagoon-barrier-ocean system or even extend to the entire Gulf and ocean scale [Sheng et al., 2010; Cyriac et al., 2018]. Recent studies for coastal NC have applied models on unstructured meshes, which allow for computational resolution to vary from kilometers in open water, to hundreds of meters near the coastline and through the floodplains, and to tens of meters in the small-scale natural and man-made channels that convey surge into inland regions [Blanton & Luettich, 2008]. For perturbations of storm forward speed and timing, the storm surge can interact nonlinearly with the tides, thus increasing and decreasing the total water levels in regions along the coastline of the South Atlantic Bight, including NC [Thomas et al., 2019]. While these studies considered the storm-induced waves and flooding near the barrier islands, they did not consider the erosion of beaches and dunes due to overwash and inundation.

Region-scale flooding models incorporate much coarser meshes compared to morphodynamic models, and thus they cannot consider the erosion of coastal features with spatial scales of a few meters. This is a problem in flooding and surge predictions, especially when the storm causes erosion of the dune, breaches a channel in the barrier island, and results in a low-lying area that is prone to inundation. Recent studies have shown that, with an *a priori* adjustment of the ground surface to represent erosion during the storm, then extensive dune and beach erosion and breaching can contribute to flooding extent predictions and storm surge level in back-barrier regions [Gharagozlou et al., 2020; Velasquez et al., 2015]. Therefore, we need to understand the gap between these deterministic models by investigating the resolution requirement and coupling the models to account for morpho- and hydrodynamic interactions in small- and large-scales.

Many modeling approaches have been developed to understand the interactions between storms and coastal dune and beach dynamics. However, deterministic process-based models are complex and are usually used to explore the impacts of a single or a few storms. They are also computationally expensive, which limits their applicability to be used as forecasting tools for multiple storm sequences. Additionally, the uncertainties in futuristic scenarios require a probabilistic analysis of the information and a probabilistic approach to predict the beach response. Therefore, a combination of statistical tools and numerical models is suitable for this purpose.

Recent studies have used probabilistic approaches in different fields such as storm surge predictions [Jia et al., 2016a], flooding in tidal channels [Moftakhari et al., 2019], shoreline change [Plant et al., 2014b], and coastal erosion [Santos et al., 2019]. They were able to improve computational time while preserving the accuracy of deterministic models. These probabilistic models define a relationship between the input and output parameters, thus removing the need for time-consuming numerical models. however, the variation in the beach profile and initial state of the morphology was not considered in any of these studies. Including the initial state of the beach, however, is an essential component of the coupled deterministic-probabilistic model and expands the application of the model to different scenarios of beach sustainability and nourished beach response to futuristic storm sequences.

1.3 Motivation

This PhD dissertation will initially address the gaps of connecting morphodynamics to larger-scale flooding. Our motivation is to improve the understanding of erosion, overwash, inundation, and breaching and their interaction with coastal circulations. This research will investigate the gaps between the small- and large-scales models to address the temporal and spatial requirements for coupling these models. Then, using the coupled models, we explore how the breach evolution affects the large-scale hydrodynamics and how the flow though the breached channels contributes to the flooding in the coastal communities.

Then, the models will be extended in a probabilistic framework for predictions over longer time periods and for consideration of futuristic scenarios. We address the gaps of combining deterministic and probabilistic models by describing the component of each model and their contribution to the predictions. Our motivation is to improve the understanding of nourished beaches response to successive storm events. We will investigate the requirements for parameterizing storm and beach profiles to develop a surrogate model. The developed surrogate model is an efficient tool that allows us to predict and study how the futuristic storm sequences affect the beach morphology, how the nourishment extends the beach sustainability, and how much sand is required to compensate for erosion after storms.

1.4 Roadmap of the Dissertation

The research in this PhD dissertation will focus on storm effects in North Carolina (NC). The NC coastline is characterized by barrier islands called the Outer Banks, which stretch 320 km, have a typical width of about 500 m, and contain natural and man-made dunes with typical crest elevations of 3 to 10.5 m [Sciaudone et al., 2016]. The Outer Banks are vulnerable to inlet breaching [Overton & Fisher, 2004; Mallinson et al., 2010] during storms, which happen frequently in NC. Isabel (2003) produced storm surge as high as 2 to 3 m above normal tide level [Beven & Cobb, 2003]. Dune overwash and inundation occurred at several locations along Hatteras Island [Sallenger et al., 2004; Morgan & Sallenger, 2009; Gencarelli et al., 2009], and 'Isabel Inlet' was formed between the communities of Hatteras and Frisco [Wamsley & Hathaway, 2004]. Irene (2011) moved over the sounds and barrier islands of NC as a weak Category 1 hurricane, pushing water levels above 2 m along the Outer Banks [Avila & Cangialosi, 2013] and causing erosion and several breaches of NC12 [Overton & Smyre, 2013]. Similar flooding occurred during Arthur (2014) [Berg, 2015], Matthew (2016) [Stewart, 2017], Florence (2018), and other storms moving over or near the Outer Banks. Different mitigation plans are used to reduce the impact of storms. Beach nourishment is the preferred plan in North Carolina and is conducted frequently at different beaches. North Carolina has spent more than $465 million on about 38 million cubic meters of sand for shore protection and emergency nourishments since 2010, not including nourishments resulting from navigation-related dredging [APTIM, 2021].

The Outer Banks response to extreme events will be explored via coupling of deterministic and probabilistic models for the erosion, overwash, and breaching during storms. Initially, the storm effects on a long stretch of the Outer Banks will be modeled with XBeach. The predictions are compared to the observations and model performance is quantified. Additionally, a new metric is developed to assess the available flow pathway over a topographic feature. This metric can be used for coupling the region-scale and small-scale models. Then, an approach to model a more-complex case of breaching and channel formation is presented. A methodology for a loosely-coupled ADCIRC-XBeach model is provided. Two-way coupling of high-fidelity, high-resolution numerical models for coastal erosion and flooding are used to better understand the formation of the breach, as well as scenarios of the breach's effects on the circulation in the region. Additionally, a surrogate model is developed based on the parameterized sea-storm, parameterized beach profiles, and parameterized erosion predicted by XBeach. The model is trained with 1,250 synthetic scenarios, and its performance and accuracy is quantified for prediction of erosion during four storms in 2019. The developed surrogate model can be used to study the erosion of nourished beaches and their sustainability to futuristic storm sequences. A brief overview of each chapter of this report is provided below.

In Chapter 2, the requirements for bridging the gap between dune-scale morphodynamic and region-scale flooding models are explored. A high-resolution XBeach model is developed to represent the morphodynamics during Isabel in the NC Outer Banks. The model domain is extended to more than 30 km of Hatteras Island and is thus larger than in previous studies. The erosion and overwash on the dune is modeled with XBeach. The predicted dune erosion is in good agreement with post-storm observed topography, and an "excellent" Skill Score of 0.59 is obtained on this large domain. Sensitivity studies show the morphodynamic model accuracy is decreased as the mesh spacing is coarsened in the cross-shore direction, but the results are less sensitive to the alongshore resolution. A new metric to assess model skill, Water Overpassing Area (WOA), is introduced to account for the available flow pathway over the dune crest. Together, these findings allow for upscaled parameterizations of erosion in larger-domain models. The updated topography is applied in a region-scale flooding model, thus allowing for enhanced flooding predictions in communities along the Outer Banks. It is found that, even using a fixed topography in region-scale model, the flooding predictions are improved significantly when post-storm topography from XBeach is implemented. These findings can be generalized to similar barrier island systems, which are common along the U.S. Gulf and Atlantic coasts.

In Chapter 3, the formation of a breach during Isabel is modeled on Hatteras Island. A range of possible breaching scenarios is considered. XBeach and ADCIRC+SWAN are coupled to predict the small-scale morphodynamics of breaching on Hatteras Island and its effects on lagoonal circulation in Pamlico Sound. The ground surface elevation in ADCIRC+SWAN is updated dynamically with a time-varying bathymetry module to represent the evolution of the breach. The dynamic mode is implemented both by using the surveyed DEMs and XBeach model predictions, and the results are compared to the static mode, in which the bathymetry is fixed. The flooding of the island during the storm is explored, and the flowrate for each case is calculated. It is shown that the breach has region-scale effects on flooding that extend 10 to 13 km into the lagoon, increasing the local water levels by as much as 1.5 m.

In Chapter 4, a probabilistic model is developed to represent beach erosion during storms over longer time periods. Ten years of beach profile surveys are analyzed and used to create DEMs that cover more than 20 km of the beach in the town of Nags Head, NC. These data are used to generate thousands of hypothetical beach profile scenarios for XBeach. Additionally, the storm parameters (waves height, period, angle, storm duration, tide, and storm surge) of the last 40 years are analyzed to generate thousands of hypothetical storm scenarios. The model compiles storm data into possible future scenarios. Synthetic storm data are used as boundary forcing to develop a library of XBeach simulations that each predict a unique beach profile response under varying storm conditions. In this model, the beach geometry and the nourishment will be parameterized by using Empirical Orthogonal Functions from Principal Component Analysis. Therefore, not only the storm parameters are included, but also the initial beach profile will be used to create the surrogate model. In this chapter, we assess if a library of synthetic storms and idealized nourishment profiles produces an emulator with the ability to simulate realistic nourishment response to storm sequences. And we predict the erosion of the nourished beach during 2019 storm season with the surrogate model.

Finally, a summary of findings, conclusions, the importance of this study, and suggestions for future work are presented in Chapter 5. Together, the research in this PhD dissertation is a major contribution to our understanding of small- and large-scale erosion and breaching and their interaction with hydrodynamics and surrogate model development and its application for predicting nourished beach response to storm sequences.

CHAPTER

2

STORM-DRIVEN EROSION AND INUNDATION OF BARRIER ISLANDS FROM DUNE- TO REGION-SCALES

2.1 Overview

Storm surge and flooding due to hurricanes can cause significant damage to property, loss of life, and long-term changes to coastal landscapes. In this chapter, models are developed for the prediction of erosion of the NC Outer Banks during Isabel (2003), including the development of an XBeach model for storm-driven erosion along 30 km of Hatteras Island (larger than other XBeach models in the literature) and the loose coupling of the eroded ground surface to ADCIRC. This chapter has been published as a research article in *Coastal Engineering* [Gharagozlou et al., 2020].

2.2 Abstract

Barrier islands are susceptible to erosion, overwash, and breaching during intense storms. However, these processes are not represented typically in large-domain models for storm surge and coastal inundation. In this study, we explore the requirements for bridging the gap between dune-scale morphodynamic and region-scale flooding models. A high-resolution XBeach model is developed to represent the morphodynamics during Hurricane Isabel (2003) in the North Carolina (NC) Outer Banks. The model domain is extended to more than 30 km of Hatteras Island and is thus larger than

in previous studies. The predicted dune erosion is in good agreement with post-storm observed topography, and an “excellent” Skill Score of 0.59 is obtained on this large domain. Sensitivity studies show the morphodynamic model accuracy is decreased as the mesh spacing is coarsened in the cross-shore direction, but the results are less sensitive to the alongshore resolution. A new metric to assess model skill, Water Overpassing Area (WOA), is introduced to account for the available flow pathway over the dune crest. Together, these findings allow for upscaled parameterizations of erosion in larger-domain models. The updated topography, obtained from XBeach prediction, is applied in a region-scale flooding model, thus allowing for enhanced flooding predictions in communities along the Outer Banks. It is found that, even using a fixed topography in region-scale model, the flooding predictions are improved significantly when post-storm topography from XBeach is implemented. These findings can be generalized to similar barrier island systems, which are common along the U.S. Gulf and Atlantic coasts.

2.3 Introduction

Barrier islands are common coastal features and storm defenses. They line 10% of the world’s open coasts, with 24% of the total within the U.S., including most of the Gulf and Atlantic coasts [Stutz & Pilkey, 2011]. The coastline of North Carolina (NC) is characterized by barrier islands called the Outer Banks, which stretch 320 km, and contain dunes with typical crest elevations of 3 to over 10.5 m [Sciaudone et al., 2016]. They are highly vulnerable to erosion and flooding during tropical cyclones and winter storms [Doran et al., 2013], which occur frequently in NC.

Storm-driven surge and flooding have been studied in coastal NC, often via computational modeling on region-scales to include the barrier islands, lagoonal estuaries, and inner floodplains [Weaver & Luettich, 2010; Sheng et al., 2010]. For idealized storms in this system, the magnitude and extent of coastal inundation are sensitive to the storm’s forward speed, size, and track angle relative to the coast [Peng et al., 2004; Peng et al., 2006]. For perturbations of forecast storm tracks and intensities, accuracy can deteriorate significantly if the storm’s track over the NC sounds and barrier islands is not predicted correctly [Cyriac et al., 2018]. For perturbations of storm forward speed and timing, the storm surge can interact nonlinearly with the tides, thus increasing and decreasing the total water levels in regions along the coastline [Thomas et al., 2019]. All of these storm effects can be represented in a high-resolution modeling system, which was automated to provide forecast guidance about coastal circulation and flooding [Mattocks & Forbes, 2008; Blanton et al., 2012] and has been expanded for storms along the entire U.S. Gulf and Atlantic coast (e.g. `https://cera.coastalrisk.live`). However, while these studies considered the storm-driven waves and flooding near the barrier islands, they did not consider the erosion of beaches and dunes due to overwash and inundation.

Erosion and breaching of barrier islands during storms have an important role on nearshore hydrodynamics, and recent studies have explored these processes by using field and remotely-sensed data and numerical models. The Outer Banks vulnerabilities to inlet breaching have been identified at several locations [Overton & Fisher, 2004; Mallinson et al., 2010]. The opening and eventual closure of the breach at Pea Island due to Hurricane Irene has been characterized extensively with aerial photography and other remote sensing data [Clinch et al., 2012; Hardin, 2013; Overton & Smyre, 2013; Velasquez-Montoya et al., 2018; Safak et al., 2016]. Beach and dune erosion were modeled at cross-shore transects in the northern Outer Banks [Fauver, 2005; Gencarelli et al., 2009], but the sediment transport was found to be dominant in the alongshore direction. These predictions were improved with newer models to include land cover effects on the dune erosion [Karanci et al., 2014].

We emphasize the difference in scales between models for coastal flooding and erosion. Storm-driven waves and surge are modeled typically on region-scale domains to represent their interactions with the complex coastal landscape. Recent studies for coastal NC have applied models on unstructured meshes, which allow for computational resolution to vary from kilometers in open water, to hundreds of meters near the coastline and through the floodplains, and to tens of meters in the small-scale natural and man-made channels that convey surge into inland regions [Blanton & Luettich, 2008; Cyriac et al., 2018]. Circulation and flooding are predicted at the Outer Banks with a minimum resolution of 50 to 200 m, thus limiting the representation of cross-shore beach profiles and alongshore dune crest variations. This resolution is typical of similar studies at global scale [Muis et al., 2016] or region scales (e.g. in U.S. [Kennedy et al., 2011; Dietrich et al., 2018; Bilskie et al., 2016], Australia [Haigh et al., 2014], and Europe [Fernandez-Montblanc et al., 2019]).

In contrast, erosion of beaches, dunes, and inlets is modeled typically on smaller-scale domains. When breaches at Pea Island were predicted with a morphodynamic model, less than 1 km of coastline was considered with a minimum resolution of 1 to 2 m [Kurum & Overton, 2013]. This resolution is typical of similar studies in other regions, e.g. Texas [Harter & Figlus, 2017], Louisiana [Lindemer et al., 2010], and Florida [McCall et al., 2010; Passeri et al., 2018], although the domains have grown to now include 10 to 20 km of island coastline. While these models can predict accurately the erosion at specific locations, their smaller-scale domains can limit their interactions with waves and flooding throughout the region.

These interactions may be significant. Erosion of beaches, dunes, and inlets will allow changes to circulation on the open coast and behind the island. It has been suggested that Isabel Inlet contributed much more to the local currents than the water levels [Kurum et al., 2010], but that numerical study did not include waves, dune overwash, or morphodynamics. For the Chandeleur Islands in Louisiana, their removal could increase surge by 0.5 m near New Orleans [Wamsley et al., 2009] and wave heights by nearly 500 percent [Grzegorzewski et al., 2009], while restored islands could delay the peak surge by 1 to 2 hr [Grzegorzewski et al., 2009]. This erosion may have affected significantly the flooding in the region. However, in these studies, the updated ground surface elevations were taken from remote-sensing data, and not from model predictions, and thus they could not consider the evolution of these interactions during the storms.

This study will explore these interactions via hindcast of Isabel's effects on Hatteras Island, specifically the dune erosion along a 30-km portion between the communities of Rodanthe and Avon. Our hypotheses are that: (a) in regions with relatively-uniform topography, a process-based morphodynamic model can be coarsened and expanded to a relatively-large domain, without sacrificing accuracy; and (b) the topographic elevation changes can be further upscaled and passed to region-scale models to allow overwash and inundation behind the dunes. This study will require a loose coupling of process-based modeling systems: the ADvanced CIRCulation (ADCIRC, [Luettich et al., 1992; Westerink et al., 2008]) and Simulating WAves Nearshore (SWAN, [Booij et al., 1999; Zijlema, 2010]) models, known as ADCIRC+SWAN, which have gained prominence for simulations of storm-driven waves and surge; and the eXtreme Beach (XBeach, [Roelvink et al., 2009]) model, which was developed explicitly for beach erosion during storms. Sensitivity tests will explore the relationship between accuracy and structured-mesh resolution in XBeach. Dune crest elevations will be passed to the unstructured mesh used by ADCIRC+SWAN, to allow for inundation of the communities on Hatteras Island and the results will be compared to XBeach prediction and the observations. This study is a necessary step toward the tight coupling of storm-driven erosion and flooding on region scales.

2.4 Hurricane Isabel (2003)

2.4.1 Synoptic History

Isabel was the most powerful storm during the 2003 Atlantic hurricane season, and its winds, waves, and storm surge impacted the NC Outer Banks. Isabel formed as a tropical wave off the West African coast on 1 September [Beven & Cobb, 2003], strengthened into a tropical storm by 6 September, into a hurricane by 15:00 UTC 7 September, and became a Category-5 hurricane on the Saffir-Simpson scale by 18:00 UTC 11 September with maximum sustained winds estimated at 74 m/s. During the next week, the storm moved northwestward and weakened, becoming a Category-2 hurricane on 16 September with maximum wind speeds of 45 m/s (Figure 2.1). On 17:00 UTC 18 September, Isabel made landfall near Drum Inlet in the NC Outer Banks as a Category-2 hurricane. The storm continued to weaken as it moved across eastern NC and became a tropical storm over southern Virginia. A day later, the storm weakened to extra-tropical and was eventually absorbed by a larger baroclinic system at 06:00 UTC 20 September [Beven & Cobb, 2003].

Isabel produced significant wave heights of about 8.1 m at the USACE Field Research Facility in Duck, NC. This observation exceeded the previous 27-year record by 1.8 m [U.S. Geological Survey, 2018]. Peak storm surge of 1.5 m occurred in phase with the time of high tide, which resulted in almost equal surge level along the northern Outer Banks and near the landfall location [Wamsley & Hathaway, 2004]. The National Oceanic and Atmospheric Administration (NOAA) water level gauge at the ocean-side of Cape Hatteras, recorded a water level of 2.05 m before failing during the storm [Hovis et al., 2004]. A maximum water level of 1.45 m was recorded at the NOAA station at Oregon Inlet, NC, at 04:00 UTC 19 September, and 1.72 m at Duck station at 18:00 UTC 18 September. These waves and surge caused damages to infrastructure and permanent changes to the landscape.

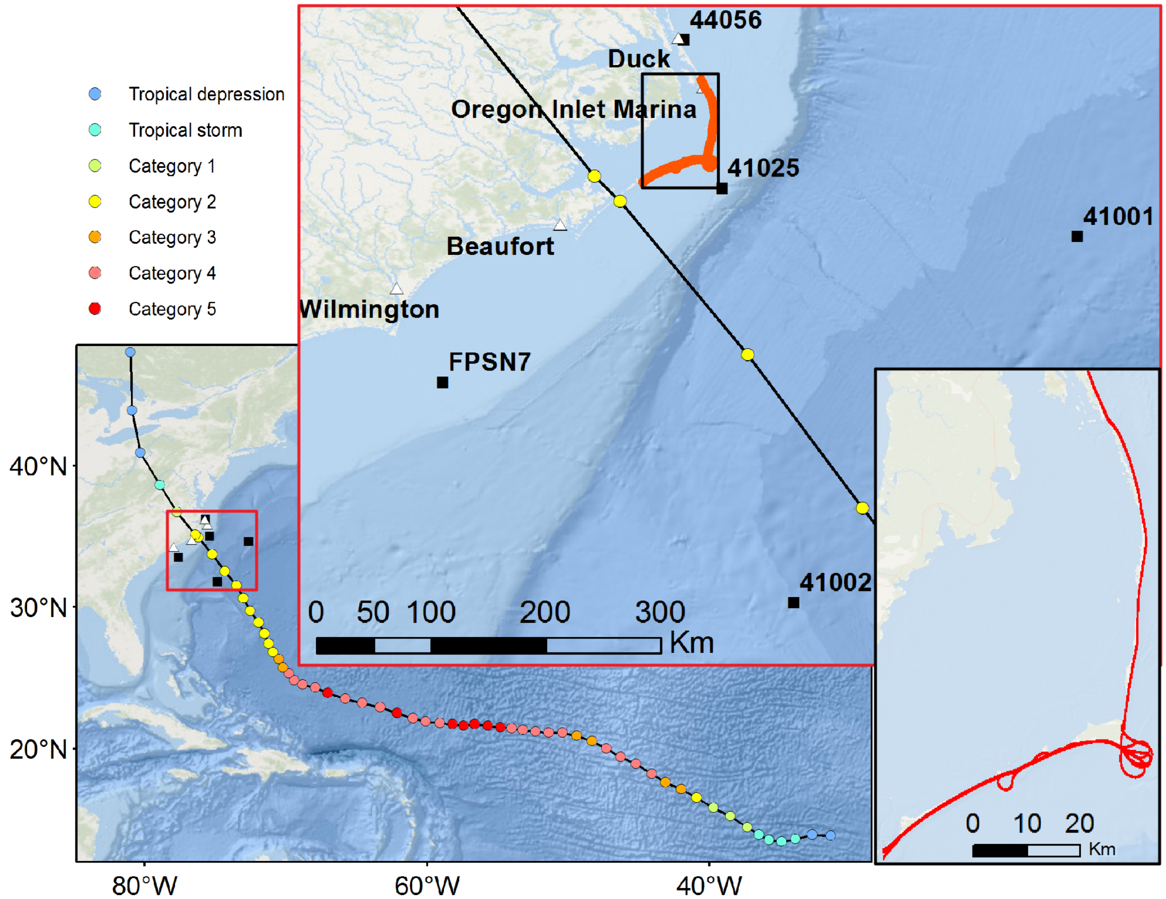

Figure 2.1 Hurricane Isabel (2003) track (colors show the storm intensity), with successive insets to show coastal NC and Hatteras Island. The extents of available pre- and post-storm LiDAR surveys (red line), and the locations of wave buoys (black squares) and water level stations (white triangles) are also shown.

2.4.2 Observed Erosion on Hatteras Island

Isabel caused erosion at several spots along the Outer Banks. The largest individual erosion event occurred near the western end of Hatteras Island, about 60 km east of Isabel's landfall location, where the island was breached due to extensive erosion, overwash, and flooding. The village of Hatteras was inaccessible due to the 520 m-wide inlet that connected the ocean and the sound. At this section, the island was narrowest with a width of about 150 m and the dune crest elevation was lower than other points along the island [Wamsley & Hathaway, 2004]. Elsewhere on the island, dunes were washed away at many locations, leaving sand deposits behind the dune, on the road, and against homes and other infrastructure. Dune erosion events occurred between the towns of Avon and Salvo. The town of Rodanthe was also impacted by a very large amount of erosion and overwash, causing damage to the buildings and road closure.

We select Isabel as a test case because of the extensive observations of morphodynamic changes to the topography of Hatteras Island. These changes are described in pre- and post-storm Light

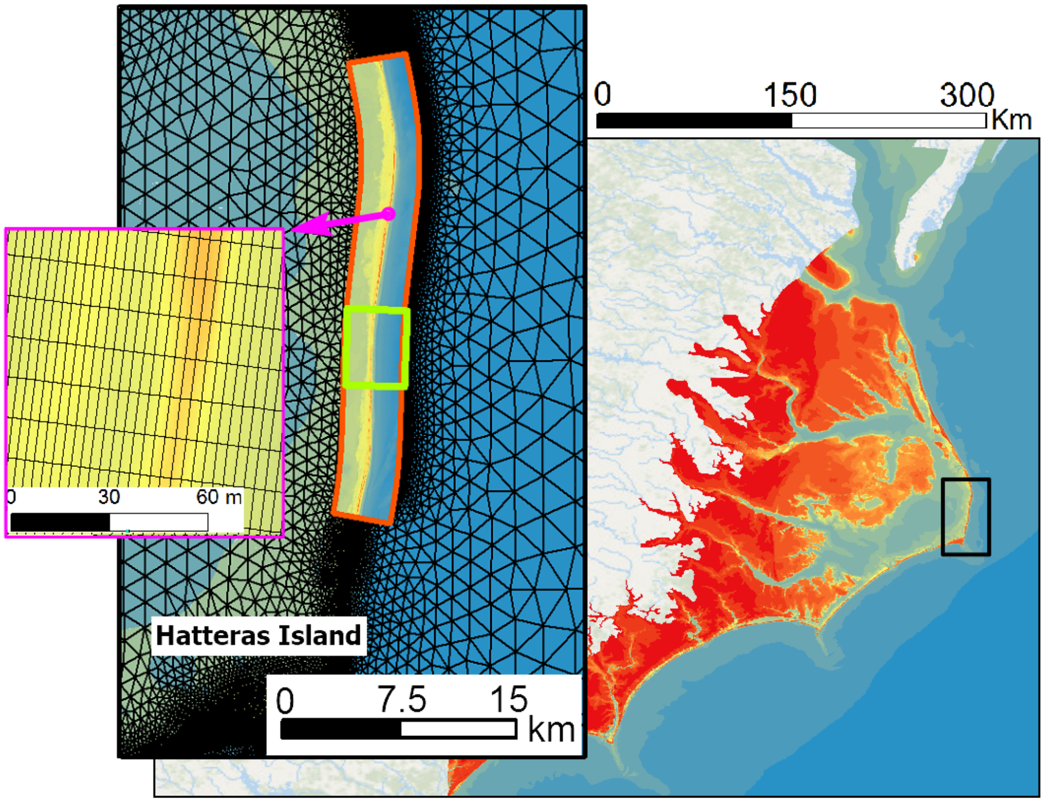

Figure 2.2 Comparison of meshes for ADCIRC+SWAN and XBeach. The region-scale ADCIRC+SWAN mesh is shown with contoured bathymetry/topography (right) and as black triangular elements in the first inset (center). The 30-km (red box) and 4-km (green box) extents of the XBeach mesh are shown in the first inset (center), with a maximum resolution shown in the second inset (left).

Detection and Ranging (LiDAR) surveys. Experimental Advanced Airborne Research LiDAR (EAARL) [Bonisteel et al., 2009] surveys were conducted on 16 September (two days before landfall) and 21 September (three days after landfall), and cover a width of 200 to 400 m of the beach topography for a 350-km stretch of the Outer Banks [Sallenger et al., 2004]. The vertical and horizontal accuracy of these data are within 0.3 m and 1 m, respectively [U.S. Geological Survey, 2019a]. These high-resolution LiDAR surveys are especially valuable for understanding of the morphodynamic changes on the barrier island during the storm.

This barrier island is characterized by two parallel dunes, which are not completely continuous, and which merge into one dune in a few locations. The study area includes 30 km of Hatteras Island between the towns of Rodanthe and Avon (Figure 2.2). The peak, pre-storm, dune crest elevation is about 10 m relative to the North American Vertical Datum of 1988 (NAVD88), and the average dune crest elevation change due to the storm was about 1 m (Figure 2.3). Aerial photos from the EAARL surveys show more than 20 erosion events with widths of 100 to 300 m in this region. The extent of overwash fans from the shoreline varies between 80 to 200 m, where the sand deposits cover the road. Rodanthe was impacted by overwash and the northern side was covered by sand

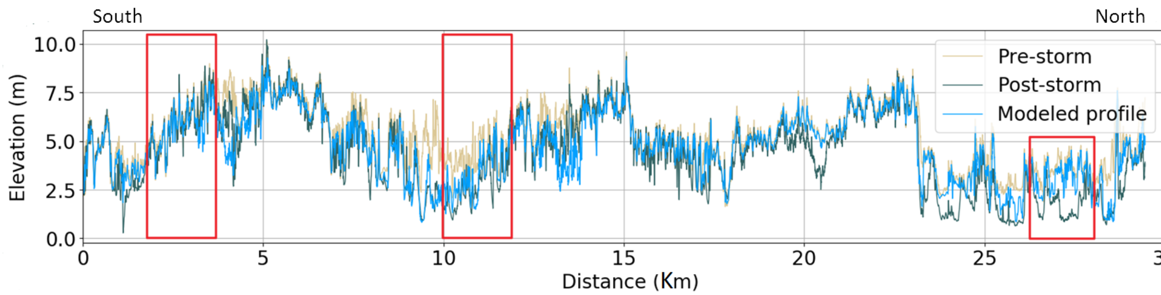

Figure 2.3 Observed and predicted dune crest profiles along the 30-km study area, for alongshore distances starting from north of Avon and ranging from south to north. The largest dune elevation change of about 4 m occurs near town of Salvo (at an alongshore distance of about 10 km), and the lowest dunes and extensive overwash were located near Rodanthe (at an alongshore distance of about 25 km). The red boxes correspond to the location of the three regions specified in Figure 2.7.

deposits with 5 km length and more than 200 m width.

2.5 Methods

2.5.1 Digital Elevation Model for Hatteras Island

The process-based, numerical models will require information about the pre-storm ground surface elevations as initial conditions, and about the post-storm ground elevations for validation. Thus, high-resolution digital elevation models (DEMs) were developed from existing sources. Bathymetric data were derived from a state-wide DEM with 10-m resolution that was developed for floodplain mapping studies [Blanton et al., 2008]. This DEM was then supplemented with high-resolution pre-storm and post-storm LiDAR data for Hatteras Island topography [Bonisteel et al., 2009]. To obtain high-resolution DEMs for the study area for both pre- and post-storm conditions, systematic errors were corrected in the raw LiDAR data [Mitasova et al., 2009]. Water turbidity, bubbles, and white foam in the surf zone can cause refraction of the laser beam that is emitted from survey equipment, so unreliable points in this region were removed from the dataset. The result point cloud covers 100 to 250 m width of the island. Each dataset was interpolated with the RST (Regularized Spline with Tension) method [Mitasova et al., 2005] into a 1-m raster. The bathymetry data and the LiDAR-based DEM may not align vertically on the edges of dataset, and thus a 30-m buffer zone was created to allow for a smooth linear transition between the LiDAR-based topography raster and the bathymetry DEM. The LiDAR point cloud is much denser on the dunes. Therefore, a uniform resolution of 1-m was selected to ensure efficiency and completeness of the raster. The resulting pre- and post-storm DEMs represent the ground surface elevations throughout the study area.

2.5.2 Large-Domain Models for Storm-Driven Waves and Circulation

2.5.2.1 Atmospheric Forcing

For storm simulations on large domains, atmospheric pressure and wind velocities are used as surface forcings for waves and circulation. This study uses a re-analysis product from OceanWeather Inc. based on land-, sea-, air-, and satellite-based observations [Bunya et al., 2010]. For Isabel, the wind fields consist of surface pressures and wind velocities on a nested set of regular grids. The larger grid spans over 60° to 85° W longitude and 15° to 48° N latitude with a regular 0.125° resolution, and the nested sub-grid extends over 74° to 78° W longitude and 36° to 40° N latitude with a regular 0.025° resolution. Surface pressures and wind velocities are interpolated in time and space from these regular grids onto the unstructured mesh used by the hydrodynamic models.

2.5.2.2 ADCIRC+SWAN

The large-scale effects of Isabel on nearshore waves and circulation are predicted by using the tightly-coupled ADCIRC [Luettich et al., 1992; Westerink et al., 2008] and SWAN [Booij et al., 1999] models, which are widely-used for storm surge and coastal flooding [Bunya et al., 2010; Hope et al., 2013; Cyriac et al., 2018]. ADCIRC uses the continuous-Galerkin, finite-element method to solve modified forms of the shallow water equations on flexible, unstructured meshes. SWAN solves the wave action density equation for the evolution of wave energy, and it was extended to use unstructured meshes [Zijlema, 2010]. When coupled tightly, the ADCIRC+SWAN models can pass information through local memory without the need for interpolation between models [Dietrich et al., 2011b]. The coupled models can provide predictions of water levels, depth-averaged currents, and wave parameters (significant height, peak period, etc.) throughout a large domain, but with focused resolution in the coastal region of interest. ADCIRC+SWAN has been validated for coastal flooding applications along the U.S. Gulf (e.g., [Dietrich et al., 2018]) and Atlantic (e.g., [Dresback et al., 2013]) coasts.

ADCIRC+SWAN predictions were saved at specific locations near Hatteras Island, and then used as boundary conditions for XBeach. Time series of ADCIRC water levels were saved at two locations offshore and two locations in the sound, and then used as boundary conditions at the four corners of the mesh used by the morphodynamic model (Figure 2.4). Time series of SWAN wave parameters (significant height, peak period, and mean direction) were saved at 15 locations at the offshore boundary in XBeach (Figure 2.4), which then uses the parameters to generate a JONSWAP spectrum with $\gamma = 3.3$ and directional spreading of 20, which is consistent with similar studies on the U.S. Atlantic [Schambach et al., 2018] and Gulf coasts [Passeri et al., 2018]. The morphodynamic model interpolates spatially and temporally the input boundary conditions to generate values along its boundaries.

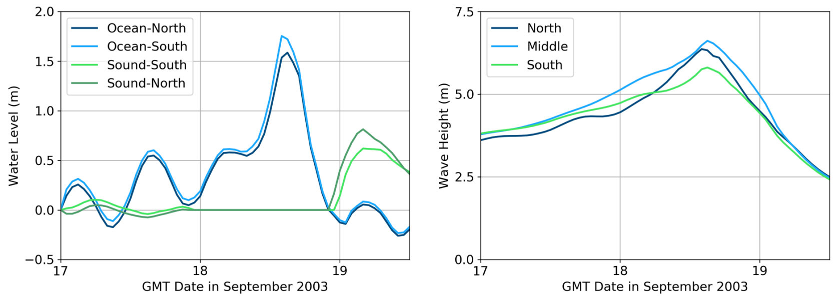

Figure 2.4 Boundary conditions extracted from ADCIRC+SWAN and used in XBeach. The water levels are interpolated from ADCIRC to the four corners of the XBeach mesh; the left sub-figure shows the time series used for the 30-km XBeach mesh. During the peak of the storm, water levels are set to zero at the sound-side boundary to maintain a positive water depth in XBeach. The wave parameters (significant height, peak period, mean direction) are interpolated from SWAN at 15 points along the offshore boundary; the right sub-figure shows the time series for significant wave heights at three locations in the 30-km XBeach mesh.

2.5.2.3 Unstructured Mesh

This study uses an edited version of the high-resolution NC9 mesh (v9.98) [Blanton & Luettich, 2008], which has more than 90 percent of its mesh resolution in the NC coastal region (Figure 2.2). The resolution varies from 100 km in the Atlantic Ocean to 50 m in the nearshore of NC. The mesh extends inland to the 15-m topographic contour to allow for storm surge and flooding prediction. Ground elevations at the mesh vertices were interpolated from several high-resolution DEMs to resolve bathymetric and topographic features such as inlets, dunes and rivers [Blanton & Luettich, 2008].

The typical mesh resolution on Hatteras Island was about 100 m, and thus the beach and dune system was represented with only 1–2 elements in the cross-shore direction. To improve the representation of this system, the maximum resolution was increased to about 20 m on the Outer Banks between Cape Hatteras and Oregon Inlet. This resolution was selected partly due to concerns about model stability (i.e. to maintain an efficient time step under the Courant-Friedrichs-Lewy condition), but it was also informed by the XBeach mesh sensitivity results, as described in Section 2.6.3.

2.5.3 Process-Based Model for Morphodynamics

2.5.3.1 XBeach

XBeach [Roelvink et al., 2009], is a robust morphodynamic modeling tool for nearshore processes during extreme events. The model solves the time-varying, short-wave action balance equation and two-dimensional, depth-averaged shallow water equations of momentum and continuity and includes infragravity wave effect, avalanching, wave breaking, dissipation, etc.

For this study, several XBeach settings were calibrated differently from their defaults, but consistently with other recent studies. Table 2.1 describes these parameters and their associated values in

Table 2.1 Settings for XBeach input parameters in this study.

Parameter	Description & Typical Value(s)	This Study
`morfac`	Morphological acceleration factor, $f_{\text{mor}} = 1$ to 10 [McCall et al., 2010; Lindemer et al., 2010]	10
`smax`	Maximum shields parameter, $\theta_{\text{max}} = 0.8$ to 1.2 [McCall et al., 2010; Harter & Figlus, 2017]	0.8
`facua`	Wave asymmetry and skewness, $\gamma_{ua} = 0.1$ to 0.3 [Nederhoff, 2014; Schambach et al., 2018]	0.3
`wetslp`	Critical avalanching slope under water, 0.1 to 1.0 [McCall et al., 2010; Roelvink et al., 2010]	0.2
`hmin`	Threshold water depth to include Stokes drift, $h_{\text{min}} = 0.001$ to 1.0 [McCall et al., 2010; Roelvink et al., 2010]	0.05

this study. The time scale of bed level change is often much longer than for hydrodynamic processes, so XBeach uses an acceleration scheme [Roelvink, 2006] to speed up the morphological evolution by a factor f_{mor} relative to the hydrodynamic time scale. Sensitivity tests have shown an improvement in computation time for f_{mor} up to 20 [Lindemer et al., 2010], while the difference in model results was less than 2 percent; this study used $f_{mor} = 10$. The model was calibrated using two parameters. One parameter, γ_{ua}, accounts for the effects of wave asymmetry and skewness, which can have a significant influence on the sediment transport rate during overwash in the surf zone [Nederhoff, 2014]. Sensitivity tests have shown an optimal value of $\gamma_{ua} = 0.3$ [Schambach et al., 2018], which was used in this study. The other parameter, S_{max}, is the Shields parameter and limits the returning flow speed during overwash. It has been shown that XBeach overestimates the erosion of the dunes during overwash, and this limiting parameter is needed to control the flow speed [McCall et al., 2010; Harter & Figlus, 2017]. Similar to previous studies, the best results were achieved by using $S_{\text{max}} = 0.8$. The `wetslp` parameter defines the threshold for the start of avalanching on wet nodes. The h_{min} parameter prevents very strong return flows in very shallow water conditions. The values for these parameters were calibrated within their default ranges.

2.5.3.2 Structured Meshes

XBeach is applied on a large domain with a total length of about 32 km. A high-resolution mesh was generated to represent the bathymetry and topography of the barrier island (Figure 2.2). The model incorporates this curvilinear mesh with 2100×420 cells with coverage of the island between the towns of Avon to Rodanthe. To allow for development of waves at the boundary, the mesh extends 2 km offshore and 1.8 km on the lagoon side. Mesh resolution varies locally in cross-shore direction with minimum of 3-m cell spacing on the beach and on the surf zone, and maximum of 30 m at the offshore boundary. Alongshore spacing of this mesh is about 15 m.

In addition to the large-domain mesh, smaller meshes with varying resolutions were generated to analyze the sensitivity of model accuracy. These smaller meshes cover a 4-km sub-region of the larger mesh, extend 2 km in offshore direction and 1.8km on the lagoon side (Figure 2.2). The sub-region coincides with the largest dune erosion of 3 m during Isabel. All XBeach parameters are consistent between region and sub-region, and boundary conditions were implemented from ADCIRC+SWAN simulation results. In the sub-region, a 'base' mesh was constructed to have a constant alongshore spacing of 15 m and minimum cross-shore spacing of 3 m (Table 2.4). Then in sensitivity studies, the mesh spacing in alongshore direction is increased up to 200 m and decreased down to 5 m, and the cross-shore mesh spacing is changed from 3 m to 30 m.

2.5.3.3 Representation of Dunes on Coarser Meshes

The dune system is an important topographic feature which acts as a hydraulic obstacle and prevents flooding into the lagoon. We used a method (see Appendix) to represent the dune crest in the models (XBeach and ADCIRC). This process informed a method to evaluate the dune crest elevation and is the basis for the Water Overpassing Area (WOA), a new metric developed for this study. The WOA is calculated along the dune crest line by integrating the vertical area above the dune crest and below a given elevation, e.g. the area between the dune crest and an elevation of 4 m. Thus it is an estimate of the available pathway for flow over the dunes and into the back-barrier area. This metric can be calculated for a variety of dune crests, as represented at different scales in the DEMs and models, and for a variety of potential water levels, as represented by different elevations, and thus it can be used to evaluate the upscaling process. If the WOA matches between the source and target, the potential for water to overpass the dune crest is maintained. In this study, the WOA was used to assess the accuracy of upscaled dune crest lines in model inputs, to assess the accuracy of predicted dune crest erosion for a single XBeach simulation, and also to compare results between XBeach and ADCIRC.

2.5.4 Model Accuracy

XBeach model predictions are compared to pre- and post-storm observations, and the model accuracy is calculated with several metrics. These calculations are performed only on the region that contains the LiDAR survey data. We use three metrics: the water overpassing area WOA, the bias B_{MN}, the skill score SS.

Bias (B_{MN}) is the mean error between predictions and observations, and it is calculated as a point-to-point difference. A negative B_{MN} will indicate an overestimation of erosion, while a positive B_{MN} will indicate an underestimation in erosion. The B_{MN} is computed as:

$$B_{MN} = \frac{1}{N}\sum_{i=1}^{N}(z_{p,i} - z_{o,i}) \tag{2.1}$$

where N is the number of points (described later), z_p is the predicted topographic elevation (from XBeach), and z_o is the observed topographic elevation (from DEM).

Skill Score (SS) is a comparison of the error in predicted bed level change to the variance of observed bed level change. A SS value of unity indicates a perfect match between predictions and observations, and lesser values indicate a progressively worse match. The SS is computed as:

$$SS = 1 - \frac{\sum_{i=1}^{N}(\Delta z_{o,i} - \Delta z_{p,i})^2}{\sum_{i=1}^{N}(\Delta z_{o,i})^2} \tag{2.2}$$

where Δz_o is the change in observed elevation (between pre- and post-storm conditions), and Δz_p is the change in predicted elevation (again, between pre- and post-storm conditions).

For both B_{MN} and SS, we emphasize a difference between our method and previous studies [McCall et al., 2010; Harter & Figlus, 2017], which calculated SS at the XBeach mesh resolution, i.e. by comparing erosion predictions only at the computational points. However, our analyses will show that SS is sensitive to the resolution over which the calculation is performed. Therefore, we will compute B_{MN} and SS with two methods. (1) Similar to the previous studies, pre and post-storm DEMs are interpolated onto the XBeach mesh, and then B_{MN_1} and SS_1 are calculated over the XBeach mesh vertices. Thus, the number of points (N) depends on the the resolution of the mesh. (2) Model outputs are linearly interpolated into a 1-m DEM, and then SS_2 is calculated using this DEM and pre- and post-storm DEMs. In this method, the number of raster cells is constant for all 4-km meshes regardless of their resolution.

It is noted that, for the second method, the interpolation of XBeach results onto the 1-m DEM can add error to the B_{MN_2} and SS_2 calculations. To quantify the contribution of this interpolation error, we calculated an SS_2 value by examining only the observed topographic changes, without any XBeach simulation. The post-storm DEM was interpolated onto the base 4-km XBeach mesh and back onto the 1-m DEM, and then this double-interpolated DEM was used as the 'predicted' post-storm condition in an SS_2 calculation. If the interpolation did not introduce any errors, then this SS_2 value should be unity; instead, we found $SS_2 = 0.94$ for this case. It is noted that this interpolation error does contribute to the overall error, but it is relatively small compared to the SS_2 values computed from the XBeach predictions (Table 2.4), described in the following section.

2.6 Results and Discussion

The ADCIRC+SWAN predictions are validated for waves and water levels during Isabel. XBeach model performance is analyzed via comparisons with post-storm DEM and aerial imagery. Then, the sensitivity of XBeach to its mesh resolution is quantified by varying systematically the alongshore and cross-shore mesh spacings. Finally, the predicted topographic changes are upscaled for use in a repeated ADCIRC+SWAN prediction, but now representing the lower beach and dune elevations, and thus allowing more flooding into coastal communities.

2.6.1 Predictions of Storm Waves and Surge in Coastal NC

The SWAN predictions are a good match to observations at buoys ranging from deep water to the nearshore (Table 2.2, Figure 2.5). At NDBC buoys 41001 and 41002, which are located in deep water to the east and south of Cape Hatteras, respectively, the significant wave heights increase to peaks of about 10 m, although the records are missing data as the storm passed nearby. The SWAN

Table 2.2 Locations near NC where observations were collected during the study period. Significant wave heights were observed at four buoys operated by the NOAA National Data Buoy Center (NDBC) and at a directional waverider operated by the USACE Field Research Facility (FRF) in about 17 m depth offshore of Duck. Water levels were observed at four stations operated by the NOAA National Ocean Service (NOS).

Agency	ID	Name	Longitude	Latitude	Waves	Water Levels
NDBC	41001	East of Cape Hatteras	72.617 W	34.625 N	X	
NDBC	41002	South of Cape Hatteras	74.840 W	31.760 N	X	
NDBC	41025	Diamond Shoals	75.403 W	35.005 N	X	
NDBC	FPSN7	Frying Pan Shoals	77.590 W	33.485 N	X	
FRF	44056	Offshore of Duck	75.700 W	36.168 N	X	
NOS	8658120	Wilmington	77.953 W	34.227 N		X
NOS	8656483	Beaufort, Duke Marine Lab	76.670 W	34.720 N		X
NOS	8652587	Oregon Inlet Marina	75.548 W	35.795 N		X
NOS	8651370	Duck	75.747 W	36.183 N		X

predictions match the development of the largest significant wave heights at these locations. At NDBC buoy 41025 on the shelf at Diamond Shoals, close to the storm's landfall, the observations show a significant wave height of almost 14 m before the buoy failed. The SWAN predictions match the magnitude of this peak, but are delayed by 6 to 8 hr after the buoy failure. At buoys on the shelf but farther from the storm's landfall, such as the NDBC buoy 44056 at the USACE Field Research Facility near Duck and NDBC buoy 41013 at Frying Pan Shoals near Wilmington, the observed significant wave heights are smaller, with peaks of about 8 m and 6 m, respectively. The SWAN predictions show similar peaks, and they fill the gaps in the observed record during the storm.

Water levels were observed at NOAA tide gauges along the NC coast, and they show variations in the peak water levels (Figure 2.6). At gauges to the south of the storm's landfall, the observed peak water levels are not much larger than the tide range. At NOAA station 8658120 at Wilmington, there is no observed storm peak, while at NOAA station 8656483 at Beaufort, the observed peak water levels are about 1 m, and are matched within 0.1 m by the ADCIRC predictions. At gauges in the northern part of the coast near Oregon Inlet and Duck, which are closest to our study area on Hatteras Island, the peak water levels were observed as large as 1.5 to 2 m. The ADCIRC predictions show the timing of these peaks, and they match their magnitudes within 0.1 to 0.25 m. Although the Oregon Inlet station is located on the sound side of the Outer Banks, the ADCIRC predictions match the observed water levels. On the ocean side, the predictions agree with the observations at the buoy and gauges, thus giving confidence in the ADCIRC+SWAN predictions. The accuracy of predicted significant wave heights and water levels at the stations near the study area is acceptable for the purposes of this study, and the extracted boundary conditions from ADCIRC+SWAN will be used for the XBeach simulations.

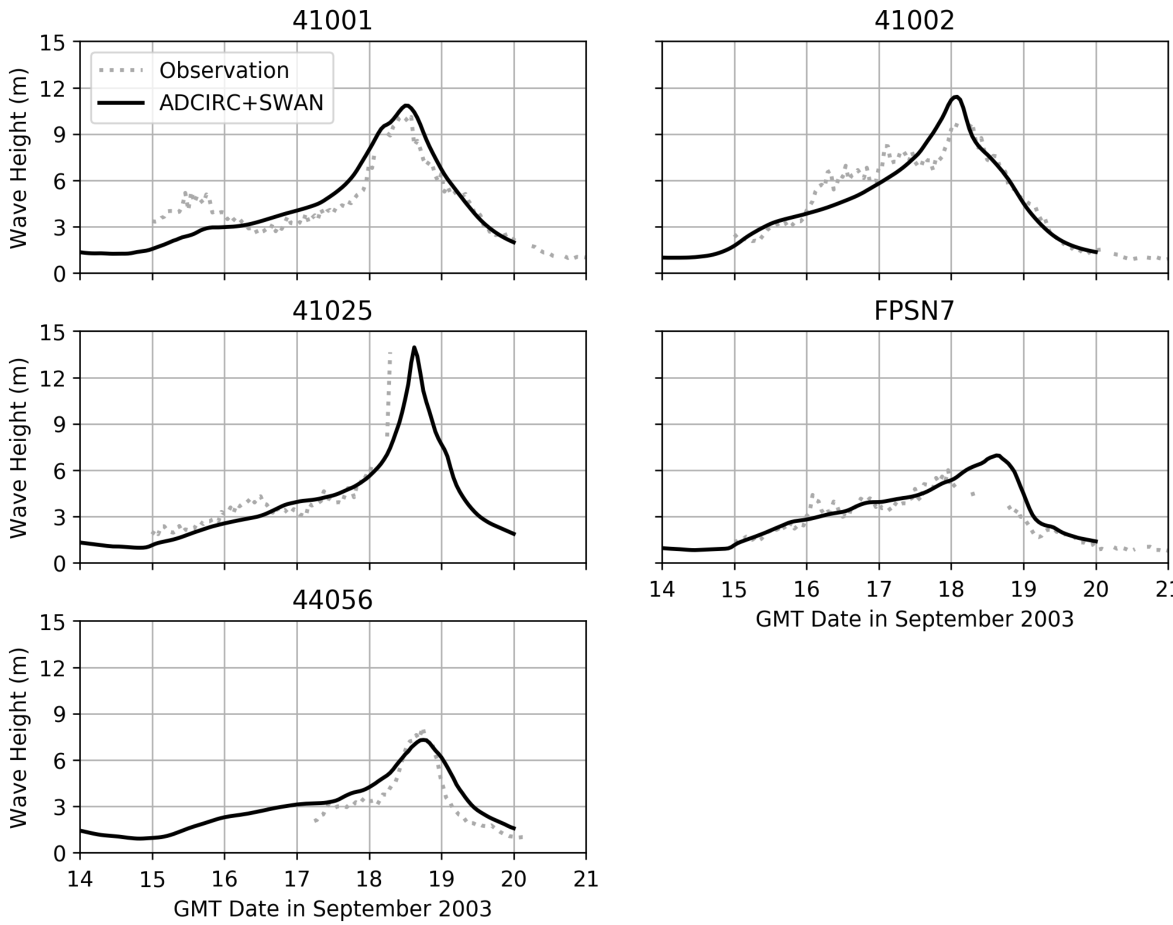

Figure 2.5 Time series of observed and predicted significant wave heights (m) from simulations at 5 stations with locations described in Table 2.2 and Figure 2.1.

2.6.2 Erosion of Beach-Dune System on Hatteras Island

Model simulations can predict the timing and evolution of the erosion events, relative both to each other and to the incoming waves and surge during the storm. Furthermore, the extent and volume of erosion and deposition of sediments, and the growth pattern of the overwash fans relative to time-varying water levels, are investigated via analyses of the model predictions. Along the 30-km portion of the island, the beach and dune systems are in the swash regime at the start of the storm. Increasing wave height and water level initiate collision regime and the dune face gets eroded gradually. Inundation occurs in several locations where the dunes are lowered. To better understand and describe these morphodynamic changes, three locations that contain erosion events are selected (Figures 2.7a and 2.8a).

In the northernmost part of the domain near Rodanthe (Figures 2.7b-c), the water level starts to increase at 11:00 UTC 18 September, or 6 hr before landfall. About 6 hr later, the water levels reach their maxima, and the beach undergoes its maximum inundation. Relatively-low dune elevations, as well as dune and beach erosion (Figures 2.8b-c), lead to inundation at this region. XBeach

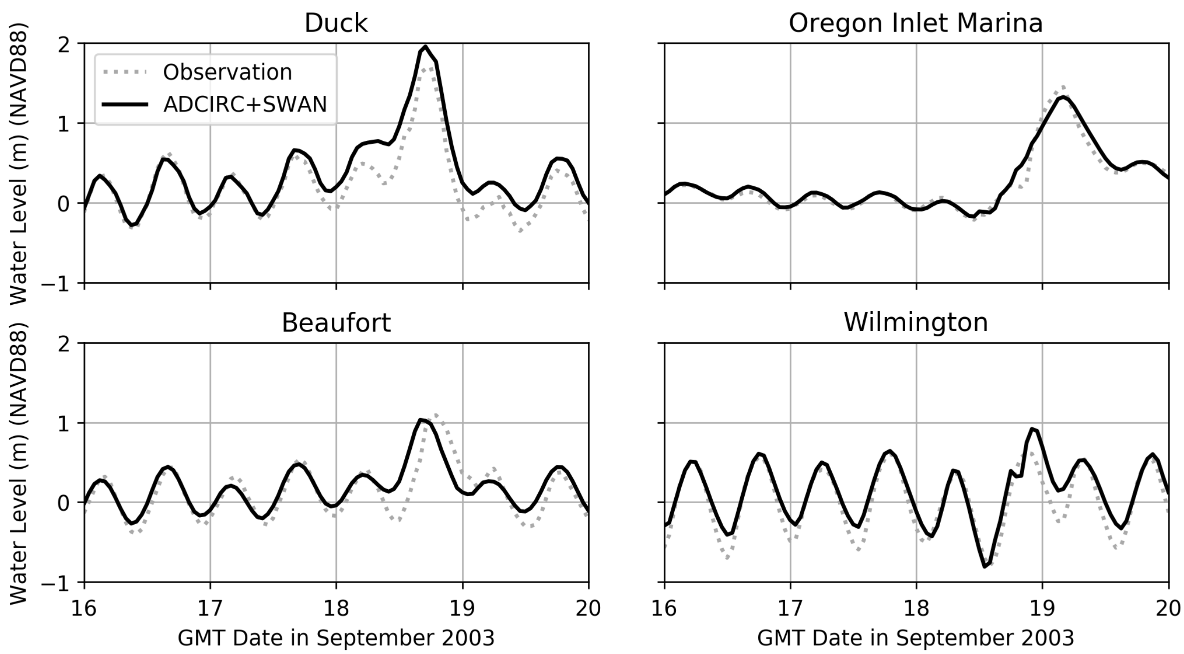

Figure 2.6 Time series of observed and predicted water levels (m) (NAVD88) from simulations at 4 stations with locations described in Table 2.2 and Figure 2.1.

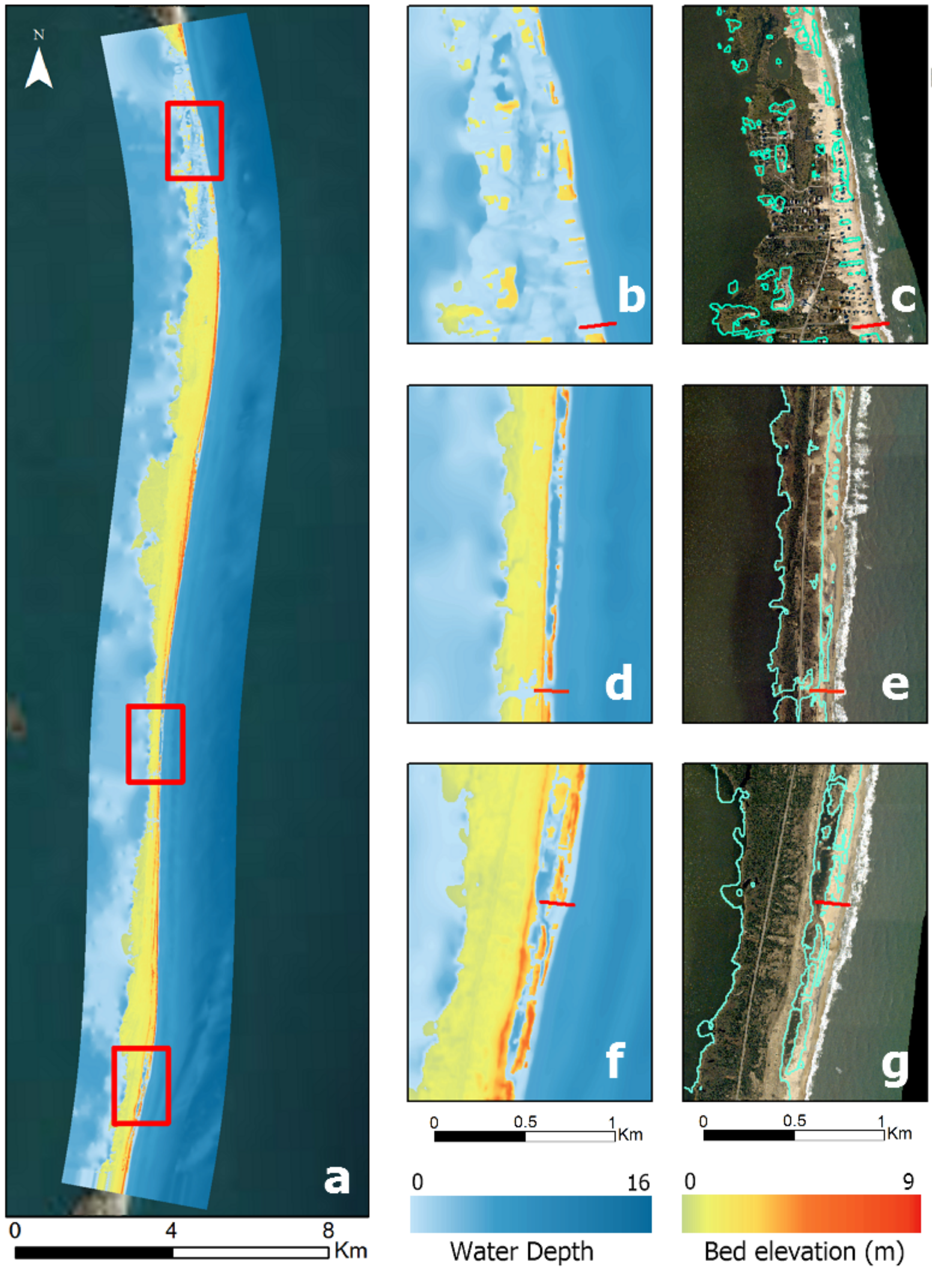

Figure 2.7 XBeach-predicted peak water levels on the (left column) full, 30-km domain and (middle) at selected locations, with comparisons to (right) aerial photos. In the aerial photos, the XBeach-predicted flooding extents are shown in a cyan line, and match well with the observed overwash fans. The red lines in panels b, d and f show the location of beach profiles in Figures 2.9 and 2.16.

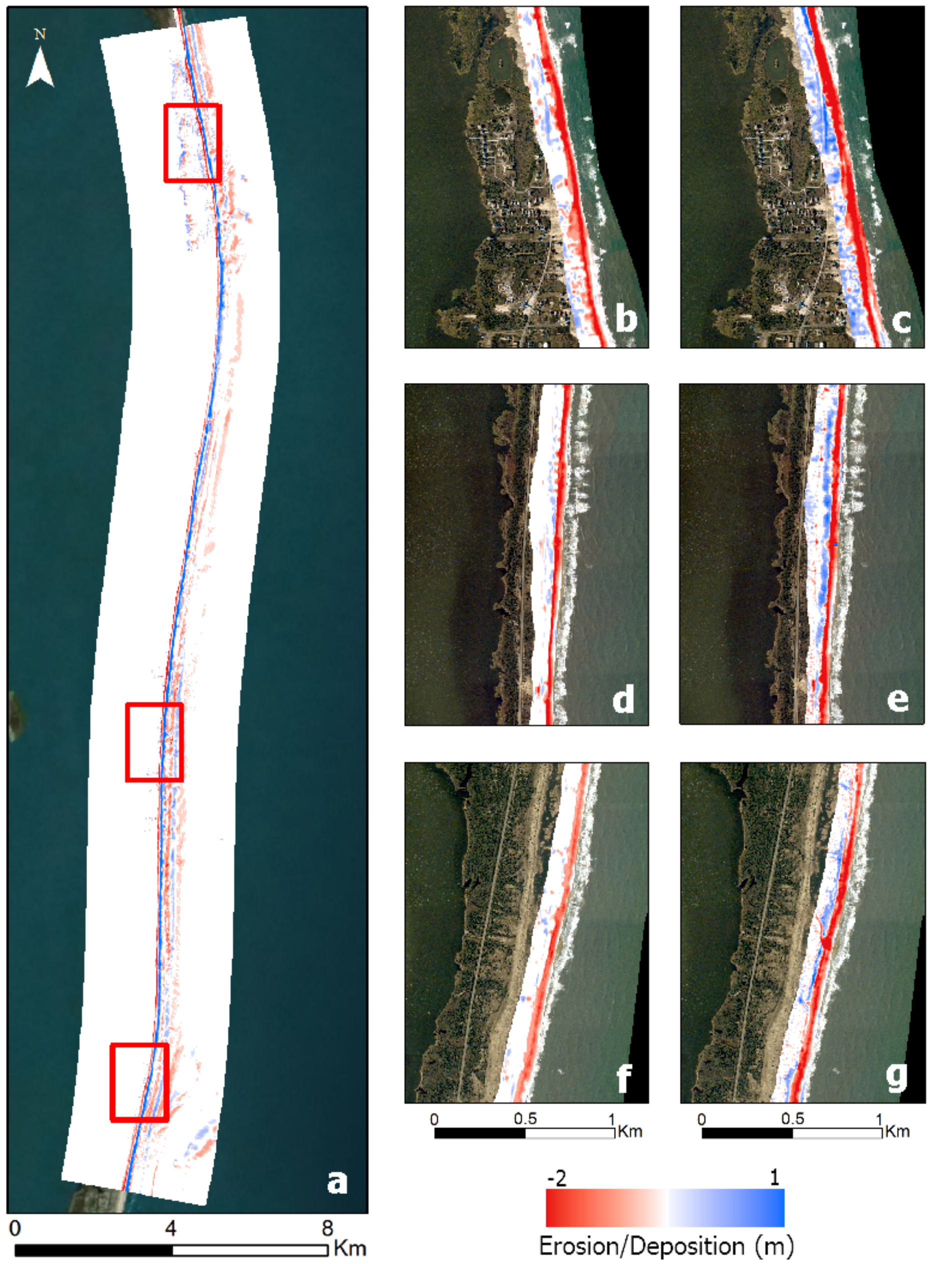

Figure 2.8 Erosion and deposition predicted by XBeach on the entire computational domain (left). XBeach prediction at the selected locations and only to the extent of available LiDAR data (middle) with comparison to observed erosion and deposition (right) extracted from LiDAR. Red and blue colors indicate erosion and deposition, respectively.

predicts peak water levels that inundate much of the island. This is an overestimation; the aerial photos show evidence of overwash fans and inundation, but only in specific locations. However, extensive deposition of sand in this region implies relatively larger flooding, and it is noted that the predicted peak water depths are only about 10 cm over much of this region. Additionally, our XBeach implementation does not include effects of land cover and vegetated areas, which would likely limit the flooding area behind the dune system.

Dune removal and inundation, followed by dune face erosion, are visible in the beach profiles as they evolve in the XBeach predictions (Figure 2.9a). By 17:00 UTC 18 September, the dune has been removed completely, and the peak ground elevation is within 0.5 m of the observed peak in the DEM. The volume of sub-aerial erosion between 11:00 and 21:00 UTC 18 September is $0.58 \cdot 10^5$ m^3, and, during this time, the maximum erosion rate of $5.9 \cdot 10^3$ m^3/hr has occurred at this section of the beach. Observations show more than 3 m of erosion on the beach, and sand was moved onto the road behind the dunes. Predicted erosion on the beach and dune is close to the observations. Although XBeach predicted the overwash fans behind the dunes, the extent and amount of sand deposition is underestimated. The total predicted deposition volume is 72 percent of the observed deposition.

Erosion and overwash were similar on the primary dune in the middle part of the domain, but the inundation was slowed by a secondary dune. The overwash started at 13:00 UTC 18 September or 4 hr before landfall, as the water crossed the primary dune. However, the secondary dune prevented flooding in the road and back-dune. The extent of overwash fans and flooding in this region were much smaller than in the northern region near Rodanthe, likely because the relatively higher dune crest acted to hinder the flooding (Figure 2.3). Maximum flooding coincided with the highest surge level at 17:00 UTC 18 September. In this portion of the island, the predicted overwash extent and the flooded wet areas in the aerial photos are represented well by the model. The erosion events and the extent of eroded dunes are also predicted accurately in XBeach (Figures 2.7d-e and 2.8d-e). In this region, the maximum erosion rate was $3.54 \cdot 10^3$ m^3/hr between 11:00 and 21:00 UTC 18 September, with a total dune and beach erosion of $1.11 \cdot 10^5$ m^3 ,which is close to observation ($1.21 \cdot 10^5$ m^3). But the amount of deposition on the road is not predicted accurately. The dunes in this region have generally higher elevation and are not removed completely, however, local erosion is predicted well. Figures 2.8d-e show the amount of erosion and deposition on the beach and behind the dune system. The maximum of 4 m dune crest elevation change occurred at this section where the dune is removed.

At the southern part of the domain, the overwash starts at 16:00 UTC 18 September or 1 hr before landfall. Similar to the middle section, high dunes (Figure 2.3) prevent flooding until the maximum surge reaches the coast. In this region, two parallel dunes protect the rest of the island from erosion and overwash. In Figures 2.7f-g, the primary dune has eroded, but the secondary dune has blocked and trapped the flood waters between the dunes. The accuracy of XBeach in predicting the locations of the erosion events and overwash fans in this region is encouraging. Figure 2.7 shows the extents of maximum flooding during the simulation at different locations on the beach. A

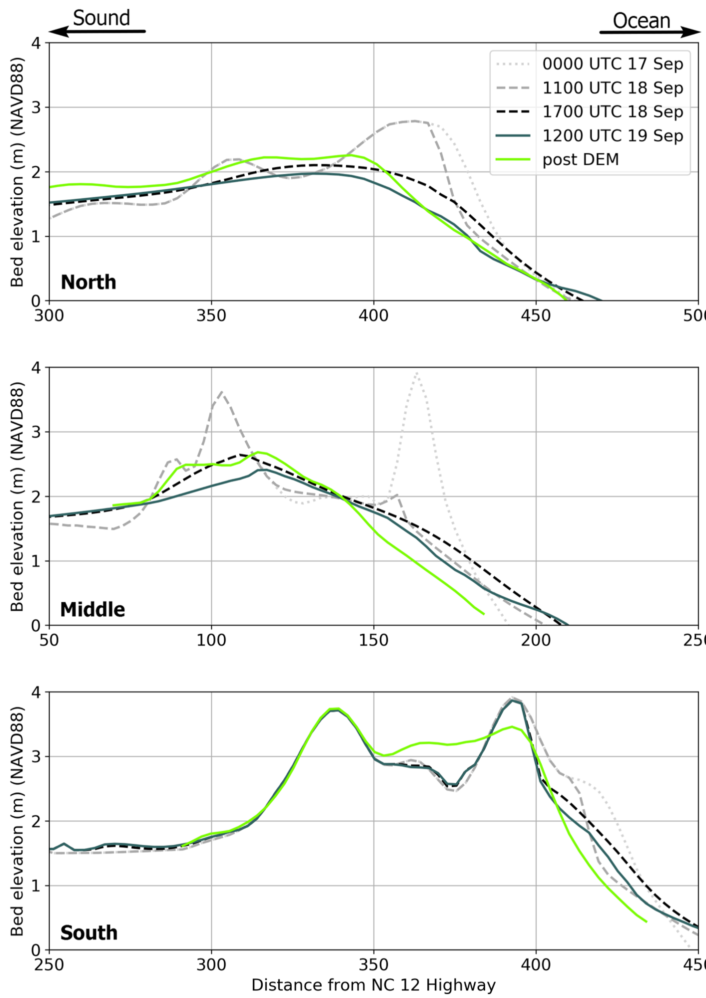

Figure 2.9 Beach profile at different time steps compared to the LiDAR post-storm profile at the locations specified in Figure 2.7.

qualitative comparison of these results and post-storm aerial photos confirms that XBeach captured these events. The extents of erosion and deposition at the southern region is provided in Figure 2.8f, and comparison to Figure 2.8g confirms that the predictions are very close to observations. The total amount of deposited sediment behind the dunes is underestimated in XBeach by 15% (Figure 2.8 and Table 2.3). The volume of erosion computed from observed DEMs ($0.94 \cdot 10^5$ m^3) is close to the prediction ($0.88 \cdot 10^5$ m^3).

The predicted erosion and deposition are compared to observations of topographic elevation changes (Figure 2.8), and the corresponding volume of sediment transported is calculated over the extents of available LiDAR observations (Table 2.3) and also the rate of erosion and deposition for each region is computed over time (Figure 2.10). As the waves and water levels increase, the erosion rate also increases. The maximum rate of sediment transport occurs between 11:00 and 21:00 UTC 18 September during the overwash and inundation regimes. Figure 2.9 shows the beach

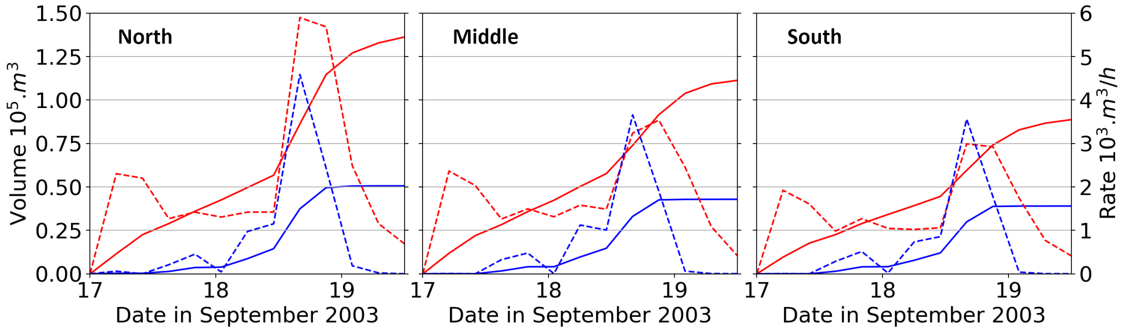

Figure 2.10 Volume (solid) and rate (dashed) of erosion (red) and deposition (blue) on 30-km domain.

profile evolution at several time steps. The evolution of the profile is in agreement with the regimes that occur on the beach. The erosion on the dune face happens during the collision regime, and, after 11:00 UTC 18 September as the water levels and wave heights increase, the overwash and inundation regimes start and sediment transport reaches its maximum rate. After 02:00 UTC 19 September, with water levels receding and the wave heights decreasing, the erosion slows down and deposition rate goes to zero. The final profile matches the post-storm DEM, and the shape of the dune is predicted well in cases that the dune is eroded partially or removed entirely.

The accuracy of morphodynamics predictions can be quantified via the SS_1 and B_{MN} metrics, which were computed for topographic elevation changes in more than 92,000 model cells. For the overall study domain, the $B_{MN} = 0.03$ m and $SS_1 = 0.59$, which can be categorized as 'Excellent' [Sutherland et al., 2004; Bosboom et al., 2014]. When the observed and predicted elevation changes are compared (Figure 2.11), areas of high observed erosion are slightly under predicted by the model, however, most changes are near the 1-to-1 line. The good agreement between predicted and DEM-observed elevation changes can also be seen in the final XBeach profiles and the post-storm conditions. In most regions, XBeach represents well the dune erosion and removal. These predictions are promising for implementation of XBeach for morphodynamics on larger domains. In this large-domain modeling approach, the general behavior of the beach and dune erosion is more important than small-scale changes, and we will use the response of the beach to improve the flood prediction in larger-domain models.

Dunes are the primary hydraulic barriers to prevent flooding from extending over the island.

Table 2.3 Total Volume (10^5 m^3) of erosion and deposition for each section on 30-km domain compared to observation. The area of computation is limited to each section and the extent of available LiDAR data

	Prediction		Observation		Area (10^3 m^2)
Section	Erosion	Deposition	Erosion	Deposition	
North	1.36	0.51	1.45	0.70	320.6
Middle	1.11	0.43	1.21	0.53	309.5
South	0.89	0.39	0.95	0.46	301.7

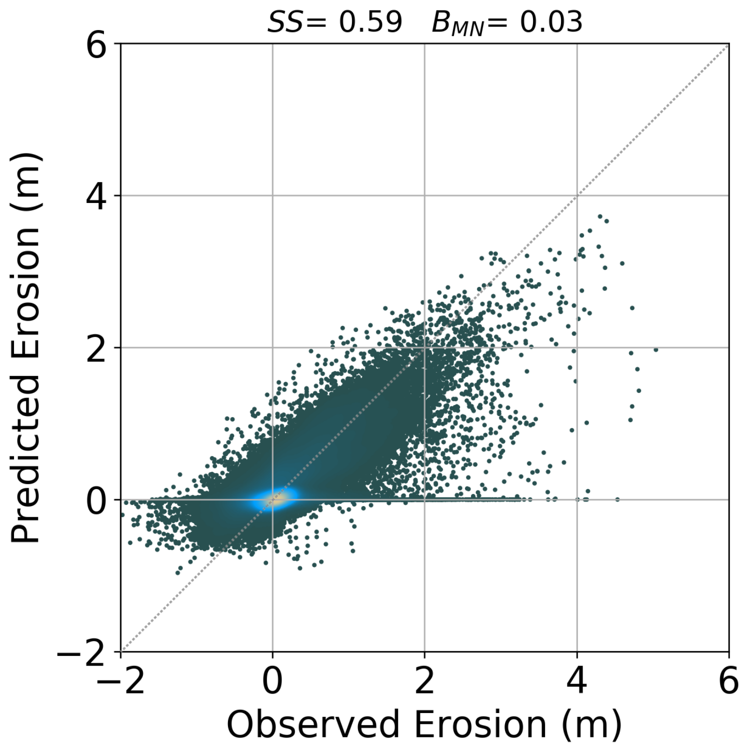

Figure 2.11 Scatter plot comparing observed and predicted elevation changes for the XBeach simulation on the 30-km domain.

Thus, predictions of the dune crest elevation change will be critical for coupling to larger-domain flooding models. To quantify the accuracy of XBeach predictions of dune crest elevation change, the WOA parameter is used to estimate the pathway for water to overpass the dune. As mentioned in 2.5.3.3, WOA uses the dune crest shape and the water level to calculate the available area for the overpassing flow. In large-scale models like ADCIRC, the mesh resolution is coarser than what is needed to capture the shape of the dunes. WOA provides the required information for mapping the hydraulic barrier elevation from XBeach to ADCIRC. Additionally, it is a useful error metric for comparing the accuracy of predicted and observed dune crest elevation. The result analysis indicates that prediction of post-storm WOA is close to observed condition (Figure 2.12a). For water levels of up to 1.5 m, predicted WOA is zero. This means that the dune crest elevation is high enough to block the water below this level. The predicted WOA, however, starts to increase gradually as the water level exceeds 1.5 m and reaches $28 \cdot 10^3$ m^2 for water level of 6 m. The predicted WOA is very close to post-storm plot (Figure 2.12a) and the error is less than 10 percent for water levels above 4 m. To identify the source of this error, WOA was computed for every 5-km sub-sections in the domain. The analysis shows that the prediction of dune crest elevation is very good for the southern-half of the domain and there are some inaccuracies in the northern part where the town of Rodanthe is located.

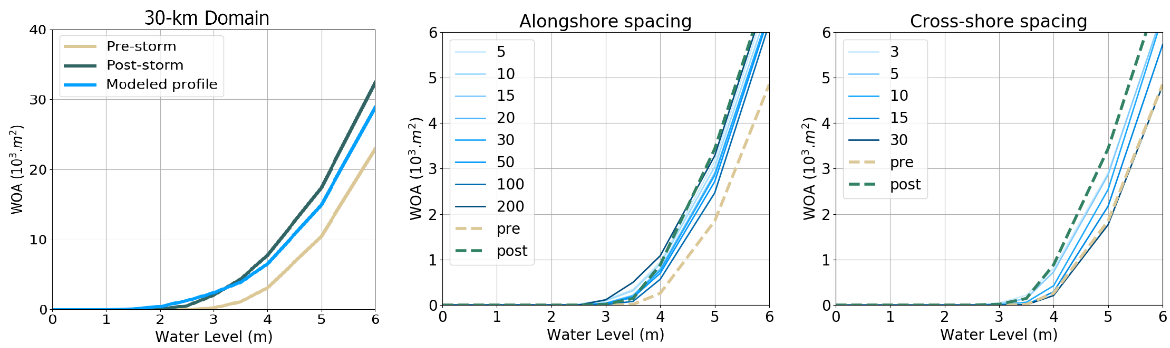

Figure 2.12 Water Overpassing Area (WOA) for the 30-km domain (left) and for meshes with varying spacing in alongshore (middle) and cross-shore (right) directions.

2.6.3 Sensitivity of Erosion Predictions to Mesh Resolution

The XBeach simulations in the previous section are critical steps toward predictions of storm-driven morphodynamics on large domains. However, for these predictions to be useful during real-time forecasting, they will need to be expanded to even larger domains (such as the entire 80-km of Hatteras Island) and then be coupled to models for storm surge and overland flooding (such as ADCIRC+SWAN). For both of these goals, it may be necessary to coarsen the XBeach mesh resolution to improve its computational efficiency. In this section, we explore the sensitivity of the XBeach prediction accuracy to changes in mesh resolution, by varying systematically the along-shore and cross-shore mesh spacings in a section of Hatteras Island.

Instead of using the full XBeach domain from the previous section, the resolution sensitivity tests were run on a smaller domain (described in Section 2.5.3.2). This mesh covers a sub-region that includes processes such as local dune removal and flooding, and the variation in dune shape and height can be representative of the larger domain. The 4-km base mesh was initialized with the same resolution as the larger 30-km domain mesh; the resolution has a minimum of 3 m in the cross-shore and a constant 15 m in the alongshore directions. The base mesh has coverage of a major erosion event where the washover sedimentation blocked the NC 12 Highway. On this smaller domain, the XBeach predictions were validated with the $B_{MN} = -0.06$ m and $SS_1 = 0.68$, which can be categorized as 'Excellent' [Bosboom et al., 2014; Sutherland et al., 2004]. In addition, the predicted dune crest shape and WOA are a good match to the post-storm profile (Figure 2.12).

This small-domain model was then used to investigate the effects of mesh resolution variation on accuracy. The alongshore and cross-shore mesh spacings were varied separately, by developing suites of meshes (Table 2.4). For each new mesh, the WOA metric and the additional pre-processing step (Section 2.5.3.3) were used to ensure that the pre-storm topographic condition as the initial setup in XBeach was similar for all meshes. Therefore, the differences in the XBeach predictions for each mesh are only influenced by mesh resolution.

For a range of alongshore mesh resolutions (Table 2.4), if SS is calculated at the mesh resolution, then it is not sensitive to alongshore spacing. The SS_1 values are relatively constant between $SS_1 =$

Table 2.4 Details of mesh resolution and model performance for the sensitivity tests on the 4-km mesh.

	Spacing (m)		Performance					
			On Mesh			On Raster		
Mesh	Alongshore	Cross-shore	SS_1	B_{MN_1}	N_1	SS_2	B_{MN_2}	N_2
Base	15	3	0.68	-0.06	15423	0.68	-0.06	641893
C5	15	5	0.6	-0.05	9260	0.58	-0.06	641893
C10	15	10	0.51	-0.03	4620	0.34	-0.04	641893
C15	15	15	0.27	-0.03	3086	0.21	-0.03	641893
C30	15	30	0.07	0.334	1521	-0.03	0.2	641893
L5	5	3	0.68	-0.06	46299	0.72	-0.07	641893
L10	10	3	0.69	-0.07	23134	0.7	-0.07	641893
Base	15	3	0.68	-0.06	15423	0.68	-0.06	641893
L20	20	3	0.69	-0.06	11556	0.68	-0.06	641893
L30	30	3	0.69	-0.06	7706	0.65	-0.05	641893
L50	50	3	0.67	-0.05	4603	0.6	-0.05	641893
L100	100	3	0.69	-0.03	2279	0.53	-0.02	641893
L200	200	3	0.69	-0.03	1159	0.44	-0.02	641893

0.67 and $SS_1 = 0.69$ even for alongshore spacings up to 200 m, thus indicating that XBeach is predicting well the erosion at its mesh nodes. However, when the erosion predictions are evaluated on the higher-resolution 1-m raster, and thus closer to the resolution of the observed topography, the SS_2 values are decreased as the mesh spacing is coarsened. From an 'Excellent' value of $SS_2 = 0.72$ for an alongshore spacing of 5 m, the predictions are decreased to a 'Good' value of $SS_2 = 0.44$ for an alongshore spacing of 200 m. The largest dropoff in accuracy occurs at alongshore spacings of about 50 m. These findings quantify the relationship between XBeach mesh resolution and predictive accuracy, and they provide an upper limit on alongshore mesh resolution for use in future models.

The WOA metric (Figure 2.12) also can vary as the resolution changes. For an alongshore mesh spacing of 5 m, the WOA is very close to the post-storm condition, and as the spacing increases to 100 m, the graph slightly deviates from post-storm and shows less WOA. This trend indicates that the dune crest is eroded less with the larger alongshore spacing, and thus there is less WOA to allow overwash and inundation. However, the $L200$ mesh does not follow the same pattern, and its higher WOA is a good match to the post-storm conditions. When the WOA for the $L200$ mesh is considered alongside the $SS_2 = 0.44$ in Table 2.4, it is clear that this mesh resolution is insufficient to represent the erosion elsewhere in the beach and dune system. The WOA analysis of dune crest shape reveals the difference between each mesh resolution, where the dune crest in finer meshes is very close to post-storm. Even for an alongshore mesh spacing of 100 m, the predicted crest line is a good representation of the larger-scale high and low points on the crest.

These results suggest that very coarse meshes with alongshore spacing of more than 50 m are not ideal for capturing the morphology and dune crest erosion. Although individual values of SS and WOA may seem to be acceptable, their combined usage can reveal inaccuracies in the results. It is critical to examine the accuracy of the erosion predictions for both the dune crest and the entire

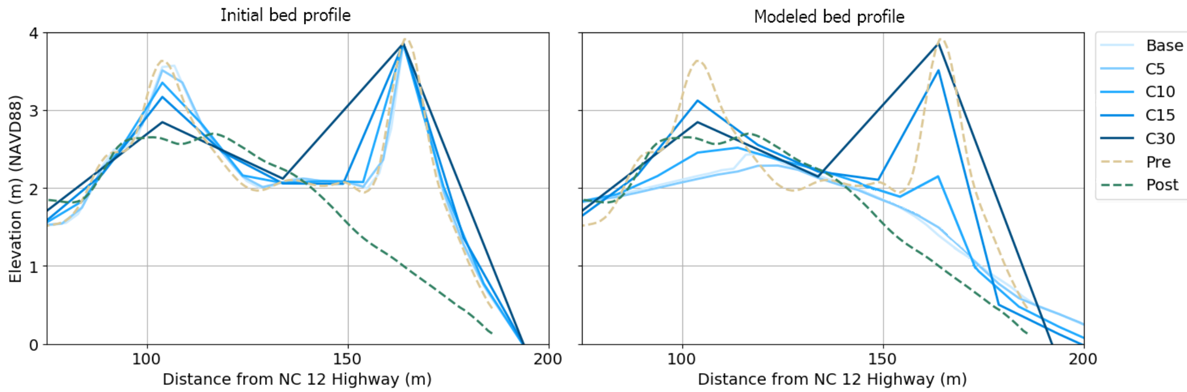

Figure 2.13 Effect of mesh resolution on predicted topographic elevations at the Middle profile with location shown in Figure 2.7e.

beach and dune system, at the same resolution as the observations.

The XBeach model accuracy is more sensitive to mesh resolution in the cross-shore direction (Table 2.4). The SS_1 and SS_2 values both decrease as mesh spacings are coarsened, and they drop to almost 0 for the $C30$ mesh. The prediction of WOA also diverges from post-storm observations (Figure 2.12) as the mesh is coarsened. For the $Base$ and $C5$ meshes, the WOA shows that XBeach predicts the dune crests to be eroded close to the post-storm observations, whereas for the $C30$ mesh, the WOA shows no difference between the post-storm predictions and pre-storm observations. To better illustrate the effect of cross-shore mesh spacing on the predicted dune crest, modeled cross-shore beach profiles for each mesh are depicted in Figure 2.13. It can be seen that the dune erosion is not modeled correctly in coarser meshes, which fail to predict the removal of the primary dune. However, in the finer meshes, the first dune removal is predicted, and erosion is also seen at the second, higher secondary dune.

Interpolation and coarse representation of topographic features, in both the alongshore and cross-shore directions, can contribute to decay in predictive accuracy. The beach and dune erosion must be represented with sufficient resolution for XBeach. Otherwise, the model physics are impacted and consequently alter the results. For example in the $C30$ mesh, the beach and dune are represented with only 3 vertices, and thus the model cannot predict the erosion. For the alongshore variability, the decrease in WOA for the $L5$ to $L200$ meshes is less than what we observe in cross-shore resolution sensitivity. The dune crest elevation does not vary rapidly along the island, and thus the WOA has smaller changes as the alongshore mesh resolution is coarsened.

Coarsening the mesh will change the slope of the beach and dunes that are represented in the mesh and consequently hinder the avalanching and erosion. In order to investigate the effects of slope and to find the optimal performance for each mesh, the `wetslp` parameter is changed for each mesh separately. It should be noted that the impact of this parameter is more significant when the mesh spacing is changed in cross-shore direction. Calibrating the `wetslp` parameter for each mesh (Table 2.5) improved SS_1, and even for a very coarse $C30$ mesh we obtained $SS_1 = 0.92$. However, SS_2

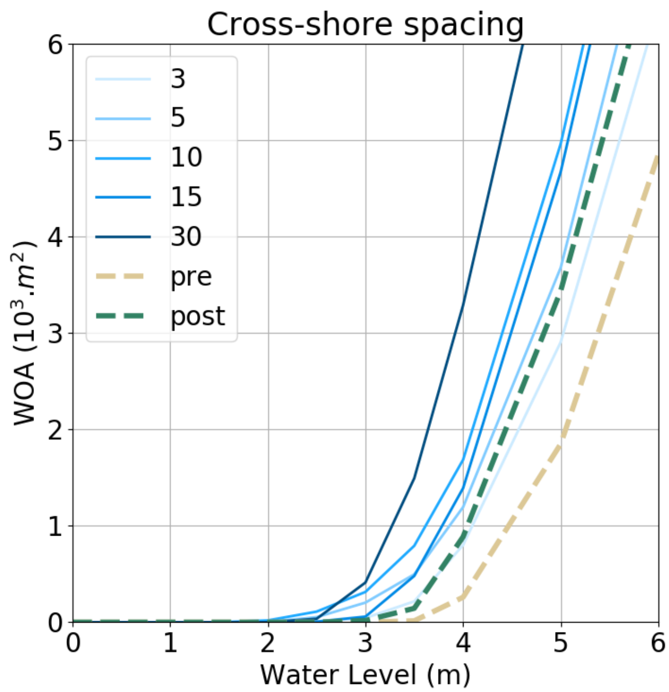

Figure 2.14 Water Overpassing Area (WOA) for meshes with varying spacing in cross-shore directions and with different $wetslp$ – refer to Table 2.5.

decreases for higher cross-shore spacing (similar to the pattern observed when we used a constant `wetslp` for all meshes), and the WOA plots (Figure 2.14) for these tests show that the modeled dune crest is significantly lower for coarser meshes than the observed dune crest. Thus, calibrating with `wetslp` can improve accuracy in SS_1, but the other metrics show the model performance is still sensitive to the mesh resolution. We expect these findings to be similar for other storms in other coastal regions.

Thus, the XBeach predictions are sensitive to its alongshore and cross-shore mesh spacings, with significant changes in accuracy as represented by SS and WOA. The trends in SS depend on the resolution at which this metric is calculated. While SS_1 is in 'Excellent' range for alongshore-coarsened meshes, SS_2 drops to 0.44 for the $L200$ mesh. However, the SS is more sensitive to cross-shore spacing, and both SS_1 and SS_2 decrease to zero for the $C30$ mesh. The erosion predictions deviate from post-storm conditions with coarsened resolution. These findings can provide guidance for the development of meshes to optimize accuracy and efficiency. Additionally, understanding the impacts of mesh resolution is the preliminary step toward upscaling the XBeach results to large-domain flooding models like ADCIRC.

Table 2.5 Optimum "`wetslp`" value and model accuracy for each mesh.

				On Mesh		On Raster	
Mesh	Alongshore	Cross-shore	$wetslp$	SS_1	B_{MN_1}	SS_2	B_{MN_2}
Base	15	3	0.2	0.68	-0.06	0.68	-0.05
C5	15	5	0.15	0.71	-0.04	0.68	-0.05
C10	15	10	0.1	0.79	0.02	0.64	-0.03
C15	15	15	0.1	0.73	-0.02	0.48	0.04
C30	15	30	0.05	0.92	0.01	0.25	-0.05

2.6.4 Upscaling Eroded Topography to Larger-Domain Wave and Surge Models

Lastly, XBeach outputs are used to update the topographic features in ADCIRC+SWAN and to investigate the improvement of flooding predictions in region-scale models. We examine ADCIRC+SWAN simulations in which the island topography has been represented in three cases: (1) from a pre-storm DEM, (2) from a post-storm DEM, and (3) from the post-storm XBeach predictions.

Using the findings on mesh resolution in Section 2.6.3, the operational ADCIRC+SWAN mesh was refined in our study area on the Outer Banks. This refined mesh has a minimum resolution of 20 m on the study area, which is finer than its original resolution of $50-100$ m but is still coarser than the minimum cell size of 15×3 m in the XBeach mesh. In Cases 1 and 2, pre- and post-storm DEMs are interpolated onto the ADCIRC mesh. And in Case 3, the XBeach-predicted post-storm topography is used to update the island in the ADCIRC mesh. Then the large-scale model is run on each mesh to hindcast Hurricane Isabel, and the results are compared. To better focus the discussion, we analyze three regions, that include differences in the results of each Case (Figure 2.15); a section near Rodanthe, a section near the middle, and a section at the south part of the study area with discrete erosion events.

Near Rodanthe, ADCIRC+SWAN simulations for Cases 1 and 2 illustrate how the updated topography can impact the flooding prediction. The largest difference in flooding occurred at the northern part of the study area. Figures 2.15b-d show the maximum water elevation near Rodanthe, where extensive erosion allowed for dune removal and overwash from ocean to lagoon. In Case 1 with the pre-storm observed topography, the surge is pushed onto some parts on the beach, but the static dunes protect the back-barrier region and no flooding is observed on the island. However, in Case 2 with the post-storm observed topography, the dunes are fully eroded and flooding has occurred in this region. In the town of Rodanthe, the ocean and the lagoon are connected due to flooding (Figure 2.15c). This prediction was also observed earlier in XBeach (Figure 2.7b) as well as in post-storm aerial photos (Figure 2.7c). The results indicate that flood prediction can be improved considerably by integrating the topographic changes due to erosion in the model. In Case 3, the flooded area has even larger extents compared to Case 2 and it has a better match to flooding extent predicted in XBeach (Figure 2.15c). When the dune erosion and low-lying topography are updated from the XBeach results into the ADCIRC predictions, then there is a good match between the flooding predictions.

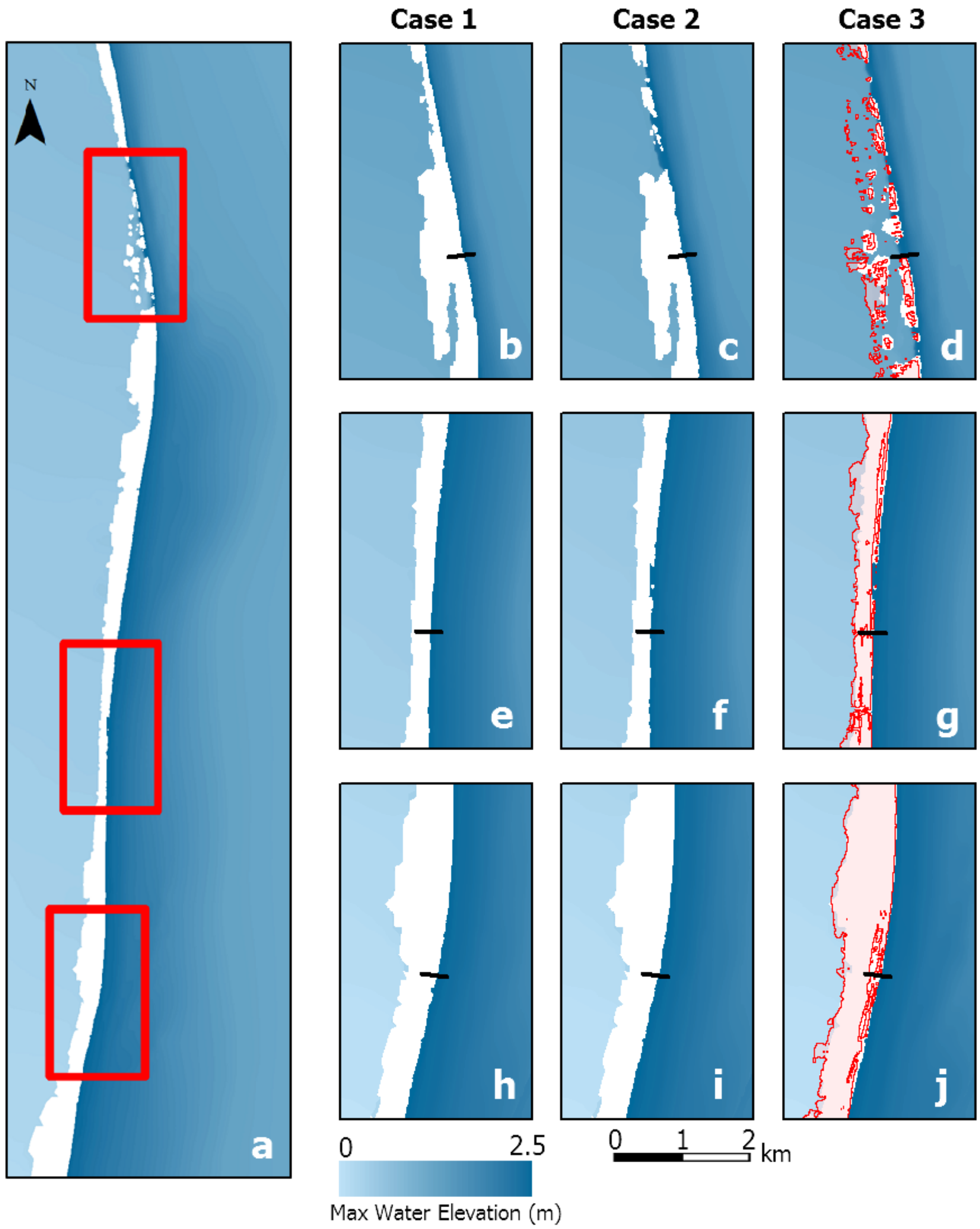

Figure 2.15 Maximum water levels from ADCIRC+SWAN for Cases: (1) pre-storm topography (b, e, h), (2) post-storm topography (c, f, i), and (3) XBeach predicted topography (d, g, j). The top, middle and bottom row correspond to the red boxes. In the last column, the red lines show the extents of the XBeach-predicted maximum flooding, and the black lines show the locations of profile transects in Figure 2.16.

The models also provide information about how the flooding evolved during the storm. We consider transects at each of the three regions (with locations in Figure 2.15 and results in Figure 2.16a-b). At 11:00 UTC Sep 18, the ADCIRC water level exceeds 1 m on the ocean side of the island and initiates the flooding. At 17:00 UTC Sep 18, the water level reaches its maxima of 2.1 m and subsequently the flooding extent grows. At the same time on the lagoon side, the wind pushes the water away from the island. The water level gradient between the ocean and the sound lets the water flow into the lagoon. The water level predicted by ADCIRC is discontinued near the shoreline because its mesh resolution does not allow the water line to extend to the true beach profile. Comparing the profiles at the northern section shows than the sand dune in Case 1 blocks the water flow ,however, in Case 3, the elevation of the dune is low enough to let the maximum surge at 17:00 UTC Sep 18 overtop the crest and flood the island. This result is very promising, and ADCIRC has shown a significant improvement in flood prediction with updated topography.

In the southern and middle sections with discrete erosion events, ADCIRC does not allow the overland flooding, even with the updated topography on the beach and dune system. In the middle section, ADCIRC predictions for Cases 1, 2 and 3 are very similar (Figure 2.15e-g), while the observation and XBeach prediction shows local flooding at this locations. Even in Case 3, ADCIRC could not capture the flooding in this region and the dunes prevented the flooding. The cross-section profiles (Figure 2.16c-d) show that the maximum water level exceeds 2.1 m at the coast, but the flooding is limited to the beach, and the water does not flow past the lowered dunes. ADCIRC does not represent the extra wave runup on the beach, and therefore the water level on the beach is slightly lower and water cannot cross the island. In the southern section, the dune is not fully eroded and is able to prevent flooding (Figure 2.16e-f) . These findings are encouraging, but more work is needed to upscale accurately the overwash and erosion processes to the region-scale models.

2.7 Conclusions

In this study, we explored the coupling of storm-driven erosion on beach and dune scales, with storm waves and flooding on region scales. ADCIRC+SWAN and XBeach models were developed for the impacts of Hurricane Isabel (2003) on Hatteras Island. Time series of offshore waves and water levels were predicted by ADCIRC+SWAN, and then used as boundary conditions for simulations of morphodynamics by XBeach. Overwash and inundation predictions were validated on a portion of the island including the towns of Rodanthe, Salvo, and Avon, and then the sensitivity of the erosion predictions was explored relative to the XBeach mesh resolution. Lastly, island topography in the ADCIRC mesh was updated by using the XBeach predictions. The major findings of this study are:

1. *XBeach was extended for predictions on a* 30*-km-wide domain, larger than any previous study.* Using default model settings and high-resolution pre-storm topography, we developed and validated an extensive model for storm-driven overwash and inundation. The accuracy with $SS = 0.59$ is in the 'Excellent' range [Sutherland et al., 2004]. There is a good match between the predicted inundation extents and erosion events to the post-storm observation, and the

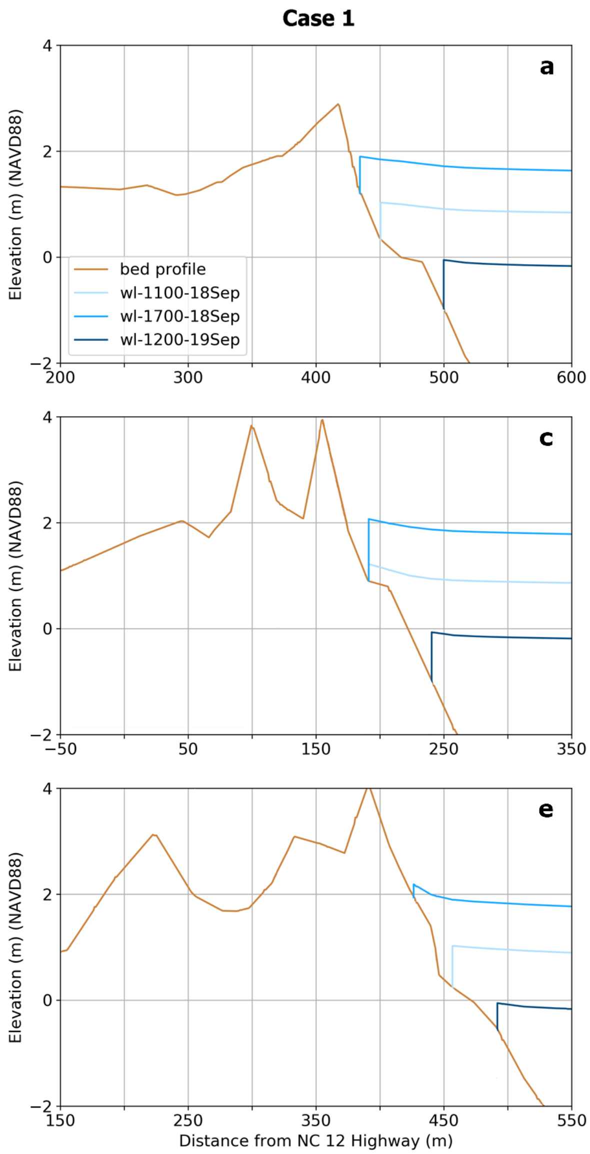

Figure 2.16 Bed profile and predicted water levels in Case 1 (left column) and Case 3 (right column) at sections shown in Figure 2.15. Sub-figures at top, middle and bottom correspond to the north, middle and south sections.

general behavior of dunes during various stages of the storm was modeled correctly.

2. *The Skill Score SS metric is sensitive to the mesh resolution.* This metric is used widely to assess the performance of morphodynamic models including XBeach, but it has considered differences between observations and predictions only at the computational points. In our sensitivity study, we showed that SS should be computed at the same resolution as the observations.

3. *The XBeach accuracy is highly sensitive to its mesh resolution.* In the alongshore direction, the relatively-uniform dune crest along Hatteras Island allows for larger mesh spacings, and we did not see a decrease in model accuracy until the mesh was coarsened to an alongshore spacing of 50 m or larger. However, in the cross-shore direction, the accuracy was decreased significantly for mesh spacings larger than 5 to 10 m. These findings will have implications both for future studies with XBeach, as well as for coupling of XBeach predictions with other models.

4. *Even using a fixed topography in ADCIRC+SWAN, the flooding predictions are improved significantly when using post-storm topography from XBeach.* The differences in model prediction for each case are proof that accounting for morphodynamics in large-scale flooding models is critical. In island sections with extensive overwash, the updated topography can allow predictions of flooding across the island and through the coastal communities. However, more work is needed to represent the flooding allowed by discrete erosion events in the region-scale models.

These results are encouraging, especially given the relative simplicity of this XBeach model setup without vegetation or variability in sediments and other physical properties (i.e. bed friction, sand size, etc.). This level of simplification allows for transition of our findings to other regions. These finding may be specific to this region, however, the methodology can be applied in similar studies in other regions. Using a coarser mesh can improve the computational time, however, the SS_2 shows a significant reduction. Additionally, the prediction of the dune crest and WOA is very sensitive to the cross-shore resolution. Therefore, the optimal resolution depends on the purpose of the modeling and the accuracy and efficiency metrics that are of more interest and future testings will be necessary in other regions.

In this large-scale modeling approach, focus is on the general behavior of the beach and dune erosion, rather than small-scale changes. These findings will be used to provide a method for updating the topographic data in large-scale models based on the morphodynamic model results. This is a preliminary step toward two-way coupling of region-scale coastal flooding models such as ADCIRC and morphodynamic model such as XBeach. We explored the resolution requirements in each model, and the next goal is to find an optimal way of updating the topography, which may include correction or calibration of topographic data in order to accurately model the flooding. The findings of this study, including the morphodynamics of the beach and resolution requirements, can be used for bridging the gap between region-scale and dune-scale models and, therefore, improving the flooding predictions during storms.

Acknowledgements

The authors thank Dr. Helena Mitasova for her continuous help and support. This work was made possible by grants from the National Oceanic and Atmospheric Administration through the North Carolina Sea Grant, and from the U.S. Army Corps of Engineers through the U.S. Coastal Research Program. This material is also based upon work supported by the National Science Foundation under Grant Award Number ICER-1664037, and by the U.S. Department of Homeland Security under Grant Award Number 2015-ST-061-ND0001-01. The views and conclusions contained in this document are those of the authors and should not be interpreted as necessarily representing the official policies, either expressed or implied, of the U.S. Department of Homeland Security.

Appendix: Mapping the Dune Crest on the Mesh

To represent the dune crest line in our models (XBeach and ADCIRC), the dune crest elevations were assigned in an extra step after interpolation of topographic data on to the mesh. For all of the meshes in our study, the ground surface elevations at all computational points were interpolated (upscaled) from fine-scale sources to a coarse-scale target. The source could be either a pre-storm DEM, post-storm DEM, or XBeach model result, while the target could be either XBeach or ADCIRC meshes. Interpolating the data with IDW or cell-area averaging method can cause smoothing of the dune crest elevations, which are then too low in the initial model topography. To preserve the dune crest in the model, we implement an additional post-interpolation process to correct the dune crest on the mesh. First, for each row in the DEM (perpendicular to the shoreline), we find the cells with the highest elevation (shown as white squares in Figure 2.17b). Then, for each row in the XBeach mesh (again, perpendicular to the shoreline), we find the vertices with the highest elevations assigned from the interpolation (shown as dark-red dots in Figure 2.17c). Finally, the elevations from the nearest DEM cells are averaged onto each of the dune-crest vertices (Figure 2.17d). This method has the benefit of maintaining the dune crest as a hydraulic obstacle to flow over the dune and island, while still being fully automated.

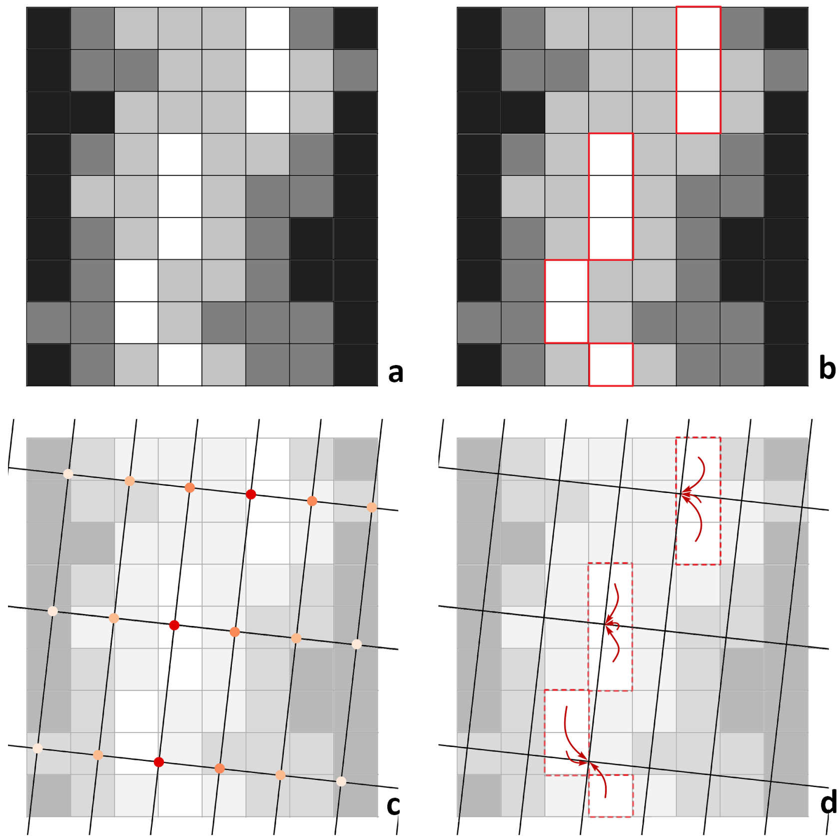

Figure 2.17 Schematic representation of the post-processing steps toward correcting the dune crest elevation: (a) the DEM, (b) finding the highest points (dune crest) on the DEM, (c) finding the highest cells in the XBeach mesh, and (d) assigning the average of the nearest highest points from the DEM onto the XBeach mesh.

CHAPTER

3

FORMATION OF A BARRIER ISLAND BREACH AND ITS CONTRIBUTIONS TO LAGOONAL CIRCULATION

3.1 Overview

Morphology changes in coastal areas during storms can have a wide range of effects on the hydrodynamics of the region. However, many large-scale modeling tools neglect these changes due to computational constraints. In this chapter, the erosion and breaching of the NC Outer Banks near town of Hatteras during Isabel are modeled with XBeach. Then, XBeach and ADCIRC are coupled to explore the interactions of breaching and flooding on the barrier island and in the sound. This chapter has been submitted for publication in *Estuarine, Coastal, and Shelf Science*.

3.2 Abstract

Barrier islands are a primary coastal defense and often experience erosion during storms. When they fail due to storm-induced breaching, there can be significant changes to the small- and large-scale hydrodynamics and morphodynamics of the region. In this study, we explore the formation of a breach on Hatteras Island, North Carolina, during Isabel (2003) and the subsequent flooding into Pamlico Sound. Two-way coupling of high-fidelity, high-resolution numerical models for coastal erosion and flooding enables a better understanding of the formation of the breach, as well as

scenarios of the breach's effects on the circulation in the region. The breach connecting the ocean to the sound formed during the day of landfall. It is shown that, during the storm, overwash and inundation from the ocean led to deterioration of the beach and dunes, and then after the storm, the creation of channels through the island was sensitive to elevated water levels in the lagoon. Then flooding scenarios are considered in which the ground surface of the hydrodynamic model was (a) static, updated with the (b) pre- and post-storm observations, and updated dynamically with (c) erosion model predictions and (d) erosion model predictions with elevated lagoon-side water levels. The model results show that the breach has region-scale effects on flooding that extend 10 to 13 km into the lagoon, increasing the local water levels by as much as 1.5 m. These results have implications for similar island-lagoon systems threatened by storms.

3.3 Introduction

Coastal storms can cause significant morphological changes to barrier islands, as demonstrated by the numerous breaches in the past 10 years due to Irene (2011) in North Carolina [Clinch et al., 2012], Sandy (2012) in the mid-Atlantic coast [Sopkin et al., 2014], Isaac (2012) in Louisiana [Sherwood et al., 2014], Matthew (2016) in the southeast-Atlantic coast [Birchler et al., 2019], and Michael (2018) in northwest Florida [FEMA, 2020]. When these breaches are initiated, they can allow flooding into lagoons that were otherwise protected, e.g. into the bays on Long Island [Canizares & Irish, 2008], often with negative effects on the lagoonal ecosystem, e.g. the rapid changes in water quality in Barnegat Bay due to island breaching during Sandy [Miselis et al., 2016; Smallegan & Irish, 2018]. These events are likely to occur more often due to rising sea levels [Passeri et al., 2015] and as storms become stronger due to climate change [Kossin et al., 2020; Emanuel, 2020], increasing the likelihood of beach erosion, breaching, and coastal flooding. Predictions of the morphodynamic response of the beach and its impact on the regional circulation are crucial for flood risk assessment.

Researchers understand the causes for discrete erosion events. The morphodynamic response can be categorized from the swash regime, where the waves and water levels impact only the beach, to the inundation regime, where overland flow can cause dune erosion and breaching [Sallenger, 2000]. Barrier islands can be inundated and eroded from both the ocean- [Ormondt et al., 2020] and lagoon-sides [Safak et al., 2016], and flow can concentrate within low areas to scour a channel [Pierce, 1970]. Although barrier islands can be large, breaches often occur in specific locations [Fritz et al., 2007; Sallenger et al., 2007; Fearnley et al., 2009]. Barrier island erosion and breaching can be linked to island width [Morton, 2002], persistent rip channels [Thornton et al., 2007], offshore wave conditions [Gracia et al., 2013b], and geologic formations like relict river channels [Riggs et al., 1995].

Predictive morphodynamic models are applied typically for studies on small domains, due both to their computational cost and the need to resolve the dune-scale coastal features (e.g. dune shape, small inlets) and physical processes [Elsayed & Oumeraci, 2017]. The eXtreme Beach (XBeach) model [Roelvink et al., 2009] has evolved significantly during the last decade to better predict storm effects on coastal regions. Early studies used bulk parameters within the models to control erosion, such as limiting the Shields parameter of erosion and overwash in Santa Rosa Island during Ivan (2004) [McCall et al., 2010]. However, later studies have represented the effects of land covers (e.g. sand, vegetation, pavement) as multiple sediment layers [Kurum & Overton, 2013] or spatially varying bottom friction, like for the erosion and overwash in Dauphin Island [Passeri et al., 2018]. Physics-based improvements were implemented in XBeach to account for dilatancy and bed slope [de Vet, 2014] and for temporally-varying bed roughness [Lugt et al., 2019], thus allowing for predictions of the general behavior of the barrier breaching. In a study of erosion along the mid-Atlantic coast due to Sandy (2012) and Matthew (2016), the model was able to predict some of the breach locations, but not all of them, and the predicted channel depths were shallower than observed after the storm [Lugt et al., 2019]. These results are encouraging for risk assessment; even a limited prediction of barrier breaching can be useful to locate vulnerabilities in the overall system. However, more research is needed to improve understanding of how breaches form and evolve during storms.

Storm surge in a shallow lagoonal system can contribute to the flooding of nearby communities. These effects can be predicted with region-wide models for wind waves, tides, and circulation [Dietrich et al., 2013], but these models often include a static ground surface. For Ike (2008) in Texas, it has been shown that the early easterly winds pushed water into the communities on the west side of Galveston Bay, which was later flooded by storm surge through the Bolivar Roads inlet and over Galveston Island and the Bolivar Peninsula [Sebastian et al., 2014]. In North Carolina (NC), wave-induced set-up contributes to inundation along the ocean-side of the Outer Banks [Sheng et al., 2010] and throughout the Pamlico and Albemarle Sounds [Mulligan et al., 2015]. For the few studies in which barrier erosion was included, the simulations used a static ground surface with the post-storm topography and bathymetry [Canizares & Irish, 2008]. These studies have shown the removal of the Chandeleur Islands in Louisiana could increase surge by 0.5 m near New Orleans [Wamsley et al., 2009] and wave heights by nearly 500 percent, while restored islands could delay the peak surge by 1 to 2 hours [Grzegorzewski et al., 2009], although the effect is spatially variable [Grzegorzewski et al., 2011]. Similarly, erosion on Bolivar Peninsula could increase the surge volume in Galveston Bay by 50 to 60 percent [Rego & Li, 2010]. While these studies have shown the importance of the barrier island system, they did not include the timing of erosion and breaches and their effects on flooding and surge on the back-barrier.

Recent studies with a tight coupling of hydro- and morphodynamics have shown that adjustment of the ground surface to represent beach and dune erosion can improve accuracy of flooding predictions [Velasquez et al., 2015], including for storm surge along the Outer Banks of North Carolina [Gharagozlou et al., 2020]. Herein, we extend these studies to also consider storm-induced breaching and its contribution to lagoonal circulation. *We hypothesize that: (1) the breaches were formed due to the combined effects of ocean-side erosion of the beach and dunes during the storm and lagoon-side elevated water levels and scour after the storm, and (2) the evolving breach can affect the timing and extent of flow into the lagoon.* We test these hypotheses via simulations of a breach on Hatteras Island, NC, during Isabel (2003), which is well-described with pre- and post-storm observations of the island topography and a post-storm survey of the breach bathymetry. First, a high-resolution, morphodynamic simulation of the so-called 'Isabel Inlet' is validated and then used to understand the evolution of the breaches. The model predicts the initiation of the breach during the day of the storm's landfall and its approximate location, even with minimal information about variations in subsurface and sediment properties. However, there are differences between the channels' exact locations and depths as predicted by the erosion model and observed in the post-storm surveys. Then a larger-domain circulation model is applied for simulations in which the ground surface is (a) static, updated linearly between the (b) pre- and post-storm observations, and updated dynamically with the (c) full breach evolution from the morphodynamic model and (d) full breach evolution with elevated sound-side water levels. The results show that the breach can affect circulation more than 10 km into the lagoon.

3.4 Methods

3.4.1 Storm and Study Area

Isabel was the most powerful storm during the 2003 Atlantic hurricane season [Beven & Cobb, 2003]. It organized as a tropical depression and then a tropical storm on 6 September, and it increased in intensity over the next five days. Isabel became a Category-5 hurricane by 18:00 UTC 11 September with maximum sustained winds estimated at 74 m/s. It continued to move northwestward over the next several days, weakening to a Category-2 hurricane on 16 September. Isabel maintained this intensity through its landfall near Drum Inlet in the Outer Banks at 17:00 UTC 18 September [Beven & Cobb, 2003] (Figure 3.1). Its winds, waves, and storm surge affected most of coastal North Carolina. Isabel generated waves with maximum significant heights of about 8.1 m at the US Army Corps of Engineers (USACE) Field Research Facility in Duck, NC. At the ocean-side of Cape Hatteras, the National Oceanic and Atmospheric Administration (NOAA) gauge recorded a total water level of 2.05 m before failing during the storm [Hovis et al., 2004]. The waves and surge caused damages to infrastructure [Rogers & Tezak, 2004] and made significant changes to the landscape [Sallenger et al., 2004].

The largest individual erosion event occurred near the western end of Hatteras Island, about 60 km east of Isabel's landfall location. The island topography was surveyed with Light Detection and Ranging (LiDAR) [Bonisteel et al., 2009] on 16 Sep, about two days before landfall, and again on 21 Sep, about three days after landfall. The LiDAR vertical and horizontal accuracies were within 0.3 m and 1 m, respectively [U.S. Geological Survey, 2019b]. Before the storm, the island was narrowest with a width of about 150 m at this section (Figure 3.2, top), and the dune crest elevation was lower than other points along the island [Wamsley & Hathaway, 2004]. During the storm, the island was breached, and the village of Hatteras became inaccessible due to the 520-m inlet that formed to connect the ocean and the sound. The newly formed inlet geometry was surveyed on 13-16 Oct, about four weeks after landfall (Figure 3.2, middle), when two 'breach islands' separated the opening into three channels. The western channel was filled with debris and had a width of about 105 m with

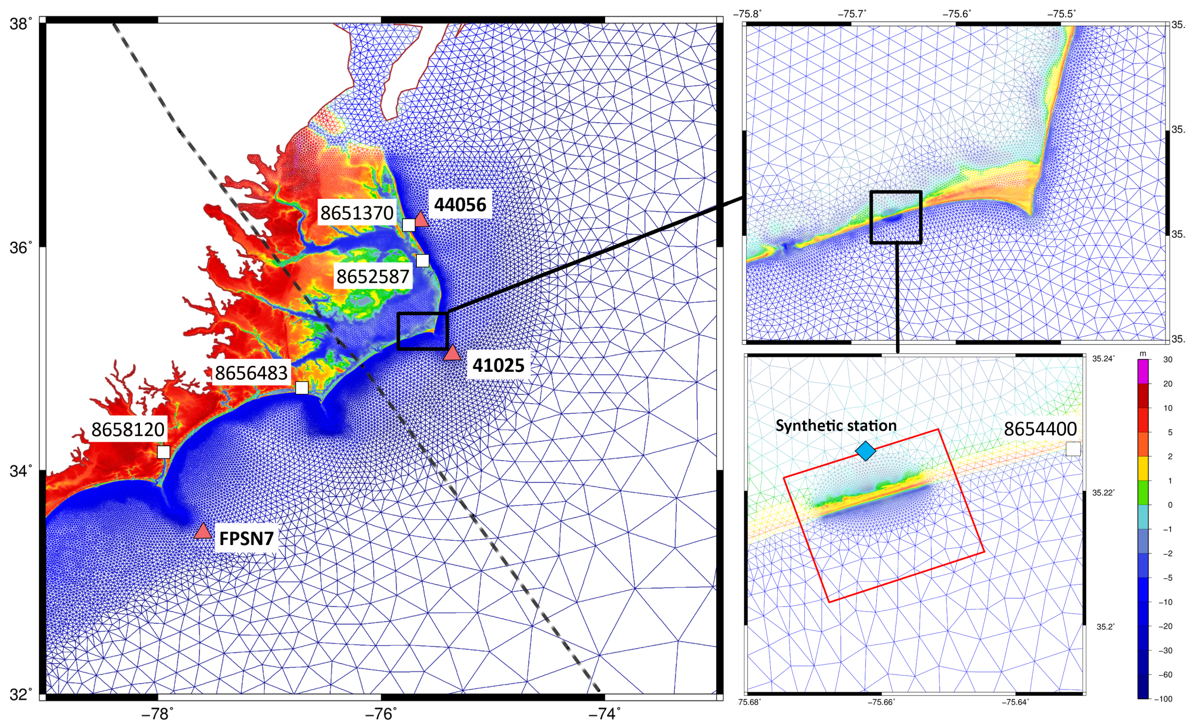

Figure 3.1 ADCIRC mesh coverage on North Carolina coast. Isabel's track is shown with a dashed line. The study area in Hatteras Island and the boundary of the XBeach domain (red box) are shown. The red triangles and white squares show the locations of NDBC buoys and NOAA gauges, respectively. Description of these stations and model validation of wave heights and water levels are provided in Gharagozlou et al. [2020]. In the bottom right figure, the location of the NOAA gauge that failed before Isabel's landfall is shown. Additionally, a synthetic station (blue diamond) is considered to show the wind velocity, direction, and water level time series on the sound side (Figure 3.3), which will be used as the back-shore boundary conditions in XBeach.

a maximum depth of 2 to 3 m, whereas the middle breach channel was 70 m wide and relatively shallower than the other channels with a maximum depth of 1.5 m. The middle channel only flooded at higher tide elevations because a peat terrace restricted the flow on the ocean side of this channel. The main channel on the east side was approximately 100 m wide on the sound side and 105 m wide on the ocean side. The unrestricted flow through this channel created scour depths down to 6 m [Wamsley & Hathaway, 2004] and consequently allowed more flow during ebb tide. The so-called 'Isabel Inlet' was closed by the U.S. Army Corps of Engineers (USACE) on 1 Nov [Wurtkowski, 2004]. These surveys provide valuable information about the island topography immediately before the storm and the channel geometries a few weeks after the storm.

For this study, the survey data were interpolated into high-resolution DEMs using the regularized spline tension method [Mitasova et al., 2005] (Figure 3.2). The DEMs have 1-m resolution and represent detailed topographic features. For the pre-storm DEM, we use the LiDAR survey from 16 Sep (about two days before landfall) to represent the sub-aerial ground surface on Hatteras Island. For the post-storm DEM, we use the LiDAR survey from 21 Sep (about three days after landfall) to represent the sub-aerial ground surface, and we use the USACE survey from 13-16 Oct (about four weeks after landfall) to represent the bathymetry in the breaches. These surveys are merged into a single post-storm DEM. This is imperfect, because it is possible that the breach channels evolved and deepened in the weeks following the storm. However, we assume that the majority of the erosion occurred during the storm's day of landfall, when the waves and surge were largest.

3.4.2 Models

3.4.2.1 ADCIRC+SWAN

The ADvanced CIRCulation (ADCIRC) [Luettich et al., 1992; Westerink et al., 2008] and Simulating WAves Nearshore (SWAN) [Booij et al., 1999] models are used to predict the region-wide effects of Isabel on nearshore waves and circulation. The models are widely-used for storm surge and coastal flooding [Hope et al., 2013; Cyriac et al., 2018; Suh et al., 2015] and have been validated for applications along the U.S. Gulf [Dietrich et al., 2018] and Atlantic [Thomas et al., 2019] coasts. ADCIRC uses the continuous-Galerkin finite element method to solve modified forms of the shallow water equations on unstructured meshes. SWAN solves the wave action density equation for the evolution of wave energy, and was extended to use unstructured meshes [Zijlema, 2010]. ADCIRC+SWAN are dynamically coupled to use the same mesh and allow information to pass through local memory without the need for interpolation between models [Dietrich et al., 2011b]. The coupled models can provide predictions of water levels, depth-averaged currents, and wave parameters (significant height, peak period, etc.) throughout a large domain, but with focused resolution in the coastal region of interest.

We used an edited version of the high-resolution NC9 mesh (v9.98) [Blanton & Luettich, 2008], with increased resolution in the NC coastal region (Figure 3.1). The resolution of the mesh varies from 100 km in the Atlantic Ocean to 50 m in the nearshore of NC. The mesh extends inland to the

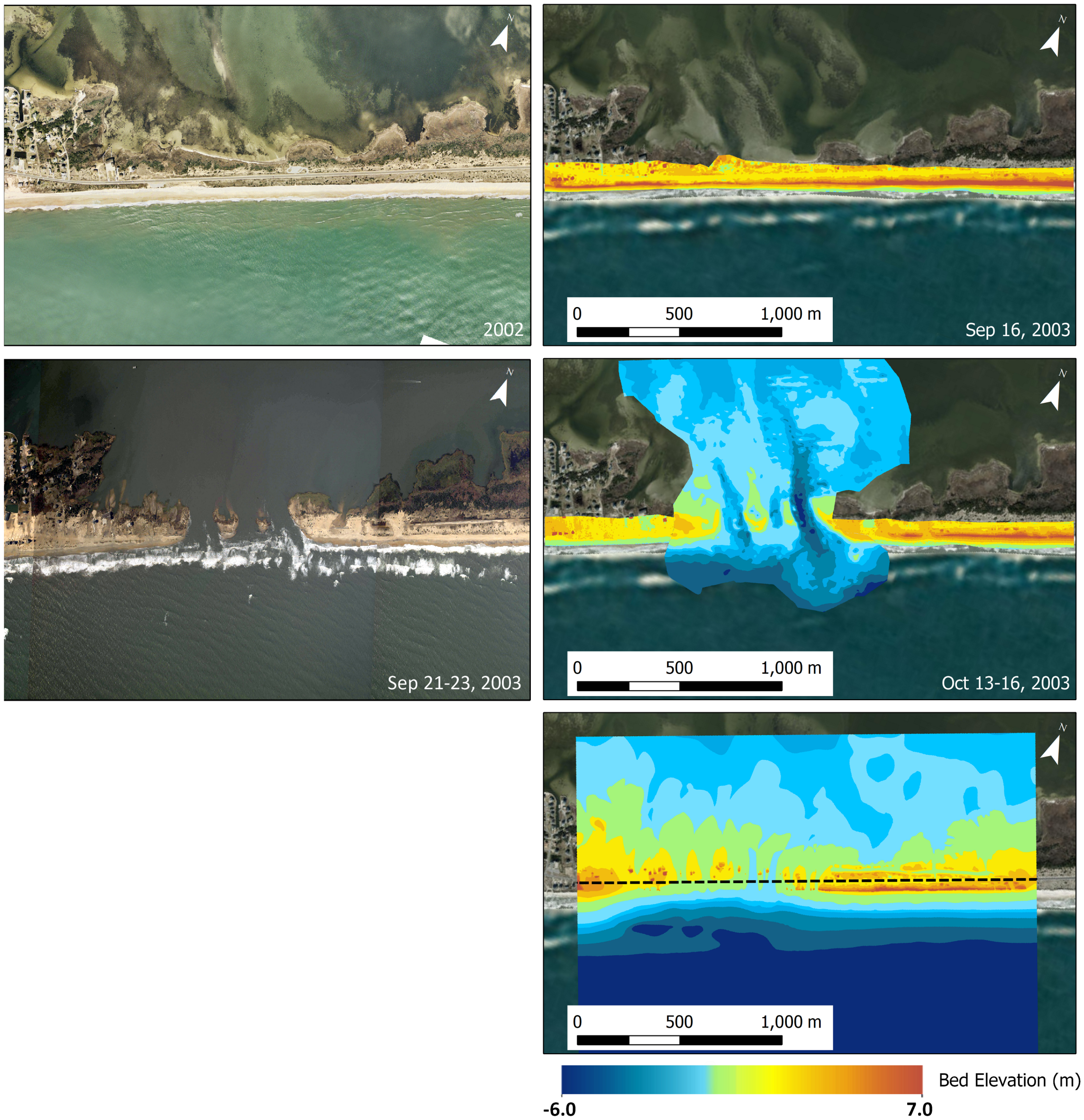

Figure 3.2 Isabel Inlet as described by pre- and post-storm (left) satellite images and (right) surveys and model predictions. The surveys were used to derive DEMs to represent (top-right) pre-storm and (middle-right) post-storm conditions. Three eroded channels were observed in the post-storm survey, with the deepest channel on the east side. The three breaches had a combined width of 500 m. These DEMs were used to initialize and validate the (bottom) XBeach-predicted final bathymetry and topography, with the 2 distinct channels in the middle and extensive dune erosion on the west side. The dashed line shows the transect of the alongshore profile, where the flow rate through the island was calculated in Figure 3.5.

15-m topographic contour to allow for storm surge and flooding prediction. Ground elevations at the mesh vertices were interpolated from several high-resolution DEMs to resolve bathymetric and topographic features such as inlets, dunes and rivers [Blanton & Luettich, 2008; Blanton et al., 2008]. The typical mesh resolution on Hatteras Island was about 50 m, and thus the beach and dune system was represented with only 1–2 elements in the cross-shore direction. In this study, to improve the representation near the breach, the maximum resolution was increased to about 20 m on the Outer Banks near the Hatteras Inlet. This resolution was selected to represent the shape of the breach in the model and also based on mesh sensitivity studies [Gharagozlou et al., 2020]. Then the ground surface was re-interpolated from the pre-storm DEM.

The SWAN+ADCIRC simulations are for 23 days, with a 15-day tides-only simulation from 00:00 UTC Aug 28 to 00:00 UTC Sep 12, and then an 8-day storm simulation until 00:00 UTC Sep 20. ADCIRC uses a time step of 1 sec (due to the constraints of its wet/dry algorithm and the Courant-Friedrichs-Lewy condition), while SWAN uses a time step (and coupling interval) of 1200 sec (due to its implicit solver). Tides are specified with 8 harmonic constituents (M_2, S_2, N_2, K_2, K_1, O_1, P_1, and Q_1). From land-use/land-cover data, spatially varying inputs are included for bottom stress, which is computed from Manning's n values, and surface stress, which is reduced both partially due to overland roughness and fully due to blocking from forest canopies [Westerink et al., 2008]. Average horizontal eddy viscosities are specified in two classes of 2 m^2/s and 10 m^2/s, while the primitive weighting in the modified continuity equation is specified in three classes of 0.005, 0.02, and 0.03. Advective terms are enabled. SWAN settings are similar to previous studies [Thomas et al., 2019; Dietrich et al., 2018]. For the transfer of momentum to the wave and circulation models, the wind drag coefficient has an upper limit of 0.002; this is balanced in ADCIRC with no lower limit on the bottom friction coefficient.

Atmospheric pressure and wind velocities from OceanWeather Inc. [Cox et al., 1995] are used as surface forcings for waves and circulation. The wind fields consist of surface pressures and wind velocities between 00:00 UTC Sep 12 and 00:00 UTC Sep 20 at 15-minute intervals and on a nested set of regular grids with the coverage over 60° to 85° W longitude and 15° to 48° N latitude. Surface pressures and wind velocities fields are interpolated in time and space onto the unstructured mesh used by ADCIRC+SWAN. Fields developed with this technique have been used in ADCIRC hindcasts of Katrina [Dietrich et al., 2010], Gustav [Dietrich et al., 2011a], Ike [Hope et al., 2013], and other storms.

3.4.2.2 XBeach

The eXtreme Beach (XBeach) model is used to predict the evolution of the breach on Hatteras Island during the storm. In 'surfbeat' mode, XBeach accounts for the waves motion by solving the time-varying, short-wave action balance equation on wave-group scale to generate the radiation stresses. The model solves the depth-averaged nonlinear shallow water equations for mean flow and includes dissipation [Roelvink, 1993] and roller models [Svendsen, 1984]. XBeach also includes the effects infragravity waves by resolving the short wave variation and the long waves associated with them. Sediment transport is modeled with a depth-averaged advection-diffusion equation, and bed elevations are updated according to the Exner equation. The model is capable of simulating the morphodynamic behavior of coastal dune systems under different storm impact regimes with excellent skill, as shown in other studies [Passeri et al., 2018; Lugt et al., 2019].

The model is calibrated using several parameters for bed friction, sediment transport, hydrodynamics, and wetting/drying and avalanching processes. These parameters differ from the default XBeach settings, but the selected values are consistent with other recent studies. To keep the dunes and the shape of the channels stable, the critical avalanching slope for the wet nodes is increased to `wetslp` = 0.6. We use $f_{\mathrm{mor}} = 10$ [McCall et al., 2010] to speed up the morphological evolution relative to the hydrodynamic time scale. Instead of the Shields parameter S_{max}, a uniform bed friction coefficient of $C = 30$ [Nederhoff, 2014] is used in the model. Additionally, the effect of wave asymmetry and skewness is included by increasing $\gamma_{\mathrm{ua}} = 0.18$. XBeach default settings tend to overestimate the erosion, so a non-physics-based approach was introduced [McCall et al., 2010] to hinder the erosion by limiting the Shields parameter. This method improves the results when the beach is in the overwash or collision regime. However, a physics-based approach to implement the land cover effects is suggested in recent studies [Passeri et al., 2018; Schambach et al., 2018], which used spatially-varying bed friction coefficient derived from land cover DEMs, where each type of coverage is assigned an equivalent Manning's n coefficient. A formulation was implemented in XBeach to account for vegetation impact by temporally changing the bed friction relative to the thickness of erosion and sedimentation [Lugt et al., 2019]. In this study, a uniform bed friction value was used to simplify the model and keep it applicable to other regions. Thus, the main morphodynamic behavior of the barrier system is determined by the topography and bathymetry of the region and the hydrodynamic forcing.

XBeach is applied on a domain with a total alongshore length of about 2.2 km (Figure 3.1). Using the DEM created from the pre-storm survey, a high-resolution mesh was generated to represent the bathymetry and topography of the barrier island with the focus on the breached inlet. The model resolves this ground surface by using a structured mesh with 600 cells along-shore and 490 cells across-shore. To allow for development of waves at the boundary, the mesh extends 1.5 km offshore and 0.8 km on the lagoon side. Mesh resolution varies locally in the cross-shore direction with minimum cell spacing of 2 m on the island and maximum of 20 m at the offshore boundary. The alongshore spacing also varies between 2 m and 10 m, with the minimum spacing located on the breach location. The model runs for three days of the storm starting at 00:00 UTC Sep 17. This XBeach start is five days later than the ADCIRC+SWAN start, and thus the waves and circulation will adjust to the atmospheric forcing before they are applied as boundary conditions to the morphodynamics.

3.4.2.3 Two-Way Coupling of XBeach and ADCIRC+SWAN

A one-way coupling is common, with predictions of the larger-domain waves and flooding to be used as boundary conditions for the smaller-scale erosion [Passeri et al., 2018; Schambach et al., 2018]. However, a two-way coupling is considered herein.

To XBeach, boundary conditions for water levels and waves were taken from ADCIRC+SWAN predictions (described above). Time series of water levels were applied at both the offshore and the lagoon boundaries, whereas time series of SWAN wave parameters (significant height, peak period, and mean direction) were only applied at the offshore boundary. This information is used by XBeach to generate a JONSWAP spectrum with $\gamma = 3.3$ and directional spreading of 20, which is consistent with similar studies on the U.S. Atlantic [Schambach et al., 2018] and Gulf coasts [Passeri et al., 2018]. The XBeach model interpolates the input boundary conditions spatially and temporally to generate values along its boundaries.

To ADCIRC, a dynamic approach for updating the topography was developed and implemented in version 53 of the ADCIRC source code; this approach allows the model to modulate the elevation of the nodes during simulation and incorporate the variation of the bed level due to erosion and deposition. Repeatedly during the simulation, the model reads data about the time-varying bathymetry, updates the ground surface elevations at the mesh vertices, and then continues with its computations. This method is not strictly mass-conserving (and this is a direction for future research) and relies on other sources to predict the ground surface variations spatially and temporally. However, it does allow ADCIRC to represent the effects of the morphodynamics while maintaining model stability. Additional information about the parameters and setup of this dynamic approach is provided in the Appendix. In this study, we use the dynamic bathymetry update to include the erosion and breaching of the barrier island in ADCIRC.

3.5 Results

3.5.1 Storm Effects near Hatteras Island

The storm's effects on waves and water levels are described at several locations (Figure 3.1). Observations are available at the NDBC buoys ranging from deep water to nearshore and at NOAA gauges along the NC coast. The maximum significant wave heights were 8.1 m at a gauge near Duck, NC, and the peak water level was 2.05 m at a gauge on the ocean-side at Cape Hatteras. A validation of ADCIRC+SWAN predictions of waves and water levels is included in Gharagozlou et al. [2020]. Here, it is noted that the gauge at Cape Hatteras failed before the peak of the storm, and there were no other gauges near the breach location to observe how waves and water levels varied on the ocean- and sound-sides. A synthetic station is selected on the sound side of the breach, where the boundary of the XBeach domain is located (Figure 3.1, bottom right) and the predicted wind speeds, wind directions, and water levels at this location are shown in figure 3.3. The wind speed was less than 15 m/s until 00:00 Sep 18. As the storm approached the region, the wind speeds increased to a maximum of about 39 m/s on 15:00 UTC Sep 18. The wind directions changed as the eye of the storm passed the barrier island. The wind direction changed abruptly from 250° at 8:00 Sep 18 to 90° at 18:00 Sep 18, with directions measured counter-clockwise from east.

The ADCIRC predictions are critical at this location, because they will be used as boundary conditions to the XBeach simulations of the island breach, which we will show was sensitive to waves

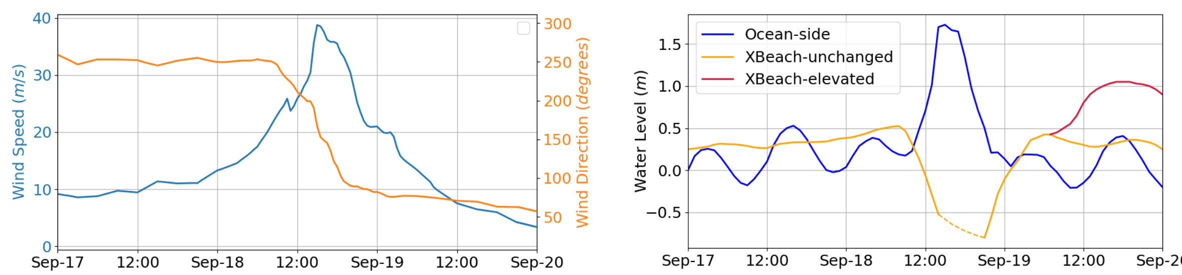

Figure 3.3 Storm effects at a synthetic station on the lagoon side of the breach (with location in Figure 3.1): (left) OWI wind speeds (m/s) and directions (degrees counter-clockwise from east); and (right) ADCIRC-predicted water levels (m) at the ocean (blue) and at the sound side when unchanged (orange) and elevated (red).

and surge from both the ocean- and sound-sides. Sound-side seiching and surge have been observed during recent storms, e.g. the rapid increase of water levels near Oregon Inlet during Arthur (2014) [Cyriac et al., 2018], or the multiple breaches of the Core Banks during Dorian (2019) [Sherwood et al., 2020]. In those storms, both the observations and model predictions showed elevated water levels, up to 1 m above mean sea level, in the sound for 12 to 24 hr after the storm landfall. However, in our ADCIRC simulation for Isabel, although the water levels are predicted to drawdown before landfall and then return to normal conditions, they are not predicted to rise and sustain at an elevated level after landfall. There was no sound-side gauge with observations to validate these water levels, but they may be an underprediction, similar to the ADCIRC underprediction by more than 0.5 m of the peak surge at Oregon Inlet during Arthur (2014) [Cyriac et al., 2018]. This underprediction may be caused by the relatively coarse temporal resolution of the atmospheric forcing, which slows the change in wind direction that is the primary cause of seiching and surge, and/or the bottom friction parameterization in Pamlico Sound, which may not account for muddy bottoms and lower friction that would allow seiching and surge to propagate to the Outer Banks. Thus, to test our first hypothesis in the following analyses, we apply boundary forcing to XBeach simulations with two scenarios: with ADCIRC water levels as predicted on the sound side, and with ADCIRC water levels but elevated artificially to 1 m above mean sea level for the last 12 hr of the XBeach simulation. These two scenarios of sound-side water levels are shown in Figure 3.3. It is noted that the elevated water levels are applied only as boundary conditions to XBeach; the water levels are not elevated artificially in any ADCIRC simulations to follow.

3.5.2 Erosion and Breaching at Isabel Inlet

We next explore the breaching of the Isabel Inlet by using XBeach to predict its timing and evolution at high resolution. We consider both qualitative (shape, location, and timing of the breach) and quantitative (volumetric sediment change and flowrate) characteristics of the breach. The focus is to understand how the storm waves and surge impacted the beach and dune system, how the breach was formed, and what were the channel depths immediately after the storm (before they could be deepened further by tidal currents).

3.5.2.1 Timeline of Island Response

The XBeach simulation covers 3 days of Isabel, starting at 00:00 UTC Sep 17 until 00:00 UTC Sep 20. At Hatteras Island, the peak of the storm occurred during the second day of the simulation, which is also when the channels developed through the island. At the start of the simulation (Figure 3.4a), the storm was 41 hours and 860 km from landfall. The ocean-side water level was less than 0.5 m (relative to NAVD88), and thus only the foreshore and the beach were eroded. However, the waves and water levels increased as the storm approached the coast. Later at 07:00 UTC Sep 18 (Figure 3.4b), the storm was 10 hr and 310 km from landfall. On the ocean side, the total water level due to waves, surge, and tide was larger than 1.0 m (NAVD88), and thus it extended to and started to erode the dune toe. By 14:00 UTC Sep 18 (Figure 3.4c), ocean water flowed through the dunes at a low point in the dune crest for beach access, and then spread alongshore to flood the road and other parts of the back-dune.

During the next 2 hr, severe dune erosion occurred, specifically in the middle and west parts of the domain. This prediction is in agreement with post-storm data that show the dunes on the west side were removed completely. The eroded sand was deposited in front of the dunes on the beach area. This collision process weakened the dune system by lowering the crest and reducing the dune thickness until 16:00 UTC Sep 18, when it switched to the overwash and inundation regimes (Figure 3.4d). When the storm was about to make landfall, the dunes had already been flattened. Strong flow and inundation through the island moved a considerable volume of sand to the back bay area. The topography of the island conveyed the flow through a specific section, which later led to the formation of channels. The water level then began to recede on the ocean side as the surge on the sound side increased. At 06:00 UTC Sep 19, about 13 hr after landfall, the water level on the sound exceeded the ocean side which forced a gradual back flow to the ocean (Figure 3.4e).

During the last 18 hours, the water flowed from the sound through the small channels, causing them to deepen. However, the channel depths were highly sensitive to the size of this water-level gradient across the island. For the scenario with the unchanged ADCIRC water levels as sound-side boundary conditions (Figure 3.4f-i), the flow conditions were not sufficient to scour the channels to have depths below sea level through the island. Instead, although the beach and dune have been eroded away, there is still a land connection. However, for the scenario with the elevated water levels as sound-side boundary conditions during the last 12 hr of the simulation (Figure 3.4f-ii), the channels were scoured to depths below sea level, and sediment was moved to the ocean side.

These findings provide a better understanding of the island response to the storm, especially the temporal evolution of the dune erosion and channel formation. The dunes protected the barrier island from flooding during the early part of the storm; however, sustained surge and waves weakened the system and eventually removed the dunes. The island topography conveyed the water flow through low-lying areas or possibly through smaller channels that had been scarped behind the dunes historically. In the narrow section of the island, the back flow from the lagoon side to the

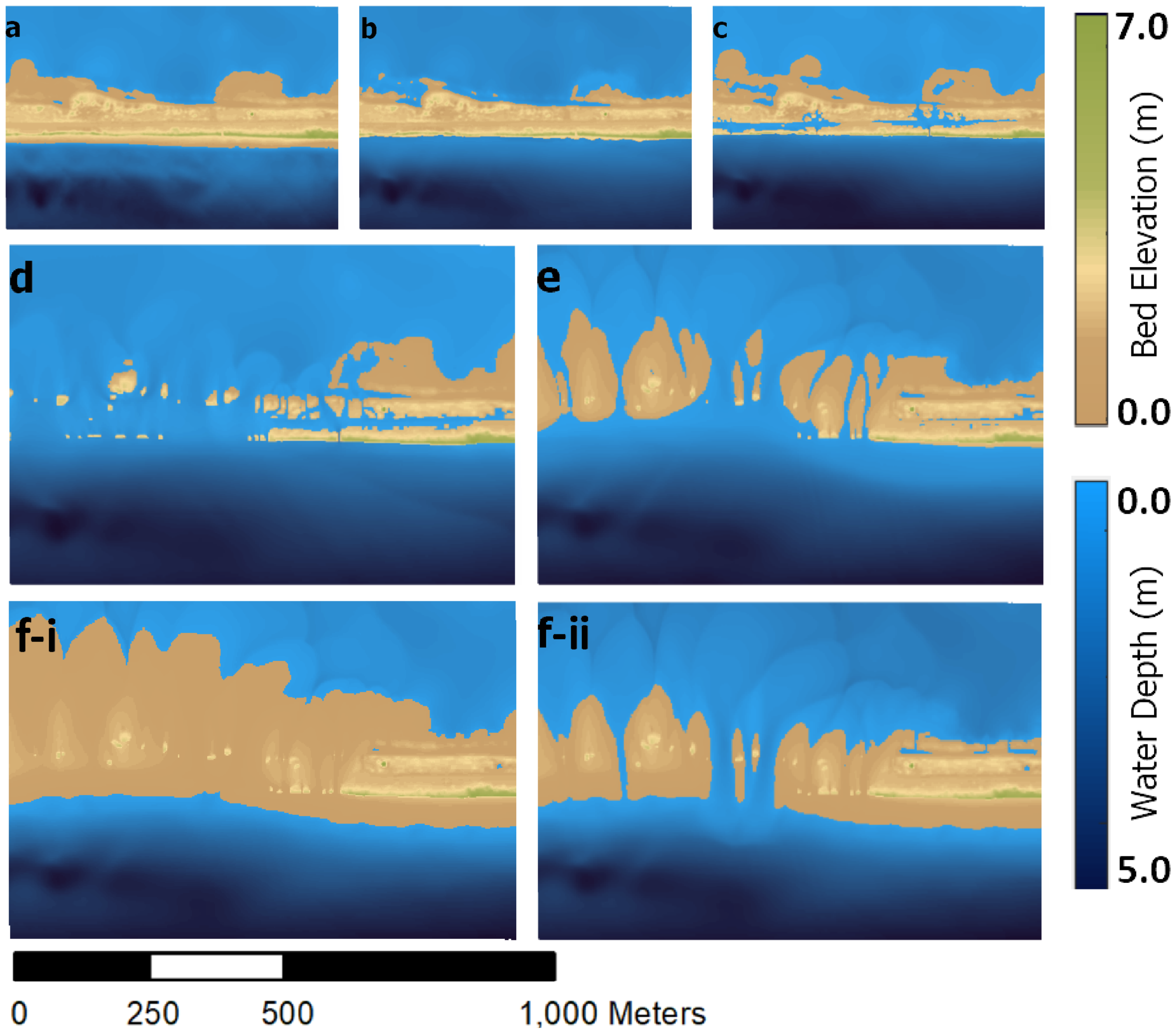

Figure 3.4 XBeach-predicted evolution of the Isabel Inlet: (a) the initial state at 00:00 UTC Sep 17; (b) the collision regime at 7:00 UTC Sep 18; (C) at 14:00 UTC Sep 18 when the overwash and flooding through beach access occurred; (d) at 16:00 UTC Sep 18, when the overwash and inundation on the west side of the domain occurred; (e) at 06:00 UTC Sep 19, the water level on the sound side exceeded the ocean side; (f-i) the final condition at 00:00 UTC Sep 20 using ADCIRC-predicted sound-side water levels with shallow channels; and (f-ii) the final condition at 00:00 UTC Sep 20 using elevated sound-side water levels with two deeper channels in the middle of the domain.

ocean formed and deepened the channels, but the amount of scour was sensitive to the water-level gradient across the island.

3.5.2.2 Rates and Quantities of Erosion and Discharge

To better understand the erosion and breaching process, we calculated the erosion rate and total volumetric change of sand on the sub-aerial part of the island. This information agrees with the storm phases and additionally can inform the coupling with the flooding model. A total volume of about 160 000 m^3 was removed during the XBeach simulation (Figure 3.5 top). Initially, the erosion rate was very small and most of the sediment transport occurred on the beach. At 06:00 UTC Sep 18, the total water level reached the dunes. The erosion and deposition increased, and dunes eroded rapidly. However, because the sand was deposited in front of the dunes, the erosion rate during this time was about 2500 m^3/hr. The cumulative erosion volume until 14:00 UTC Sep 18 was 40000 m^3. At the peak of the storm, the most significant erosion of the dunes occurred, which resulted in 90000 m^3 volume of sand loss at a rate of 13000 m^3/hr. This large erosion occurred mostly on the middle and west side of the domain and comprised about 55 percent of the total sand loss over 7 to 8 hr. At 00:00 UTC Sep 19, the erosion slowed down, and the water level decreased on the ocean side. For the scenario with elevated water levels on the sound side, a returning flow from the sound to the ocean eroded and deepened the channels. This scour caused an additional 10000 m^3 of erosion, compared to the scenario with unchanged water levels.

We also computed the discharge along 2 km of the island where the breaching occurred (red lines in Figure 3.5 bottom). For about half of the simulation time, the dunes protected the barrier island from inundation. However, erosion of the dunes during this time lowered the crest and, at 14:00 UTC Sep 18, the overwash and flow through beach access increased the discharge. At 16:00 UTC Sep 18 with the dunes removed entirely, maximum discharge of 1300 m^3/s was reached, corresponding to extensive inundation on the west and middle of the domain. Then the discharge decreased as the water level increased on the sound side. The direction of the current flowed between the ocean and the sound until 12:00 UTC Sep 19. After this time, there is almost no flow through the island for the XBeach (unchanged) scenario. However, for the XBeach (elevated) scenario, the water level gradient caused scour across the island and deepened the channels. Note the difference in discharge due to the higher sound-side water levels during the last 12 hours in the XBeach (elevated) results; the maximum discharge was about 190 m^3/s, compared to no discharge for the unchanged sound-side water levels as predicted by ADCIRC.

3.5.3 Breaching Effects on Larger-Scale Circulation

We next consider the storm's effects on the larger-scale circulation and flooding, via the coupling with ADCIRC+SWAN. Although similar models can predict the morphodynamics of large sand sheets or waves and nearshore evolution, morphodynamics of island breaches are dependent on local gradients in sediment transport, the scale of which is not feasible in larger-domain models like ADCIRC. Therefore the ground surface elevations at its mesh vertices are typically fixed during the

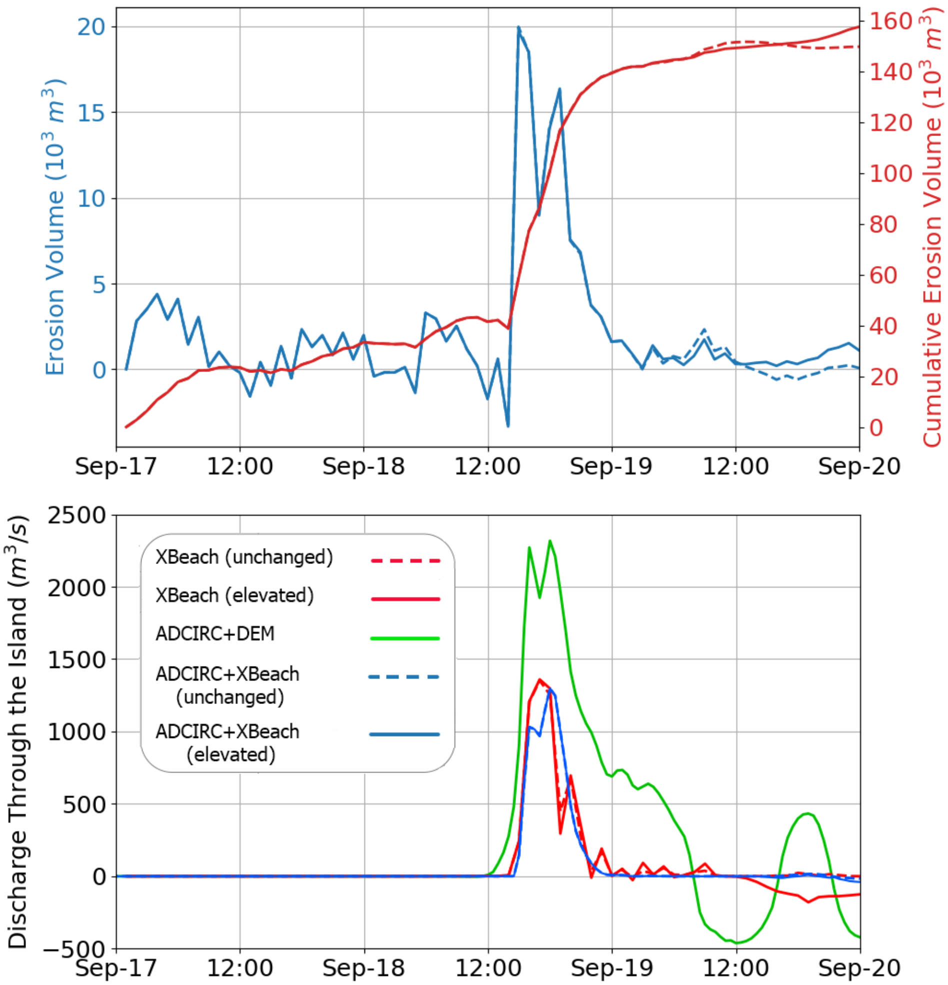

Figure 3.5 Erosion and discharge through the breach (with location in Figure 3.2: (top) erosion volume (m^3) and cumulative total sand loss (m^3) on the sub-aerial part of the barrier island during the storm, and (bottom) flow discharge (m^3/s) through the island during storm calculated from XBeach (red) as well as ADCIRC with surveys (green) and XBeach (blue).

simulation. In our first simulation with two-way coupling, we use (a) a static bathymetry, in which the pre-storm DEM is interpolated onto the mesh. Then in following simulations with two-way coupling, we allow the bathymetry to evolve. The time-varying bathymetry information is extracted from (b) a hypothetical linear transition from pre-storm to post-storm DEMs of the bathymetry and topography, (c) an XBeach simulation of island erosion with the unchanged ADCIRC boundary conditions, and (d) an XBeach simulation of breaching with the elevated sound-side water levels. It is noted that, in these ADCIRC simulations, the water levels are not increased artificially; instead, they will respond to the varying scenarios of ground surface evolution.

3.5.3.1 Static Scenario

In the static scenario, the ground surface elevation was fixed during the simulation, and thus the erosion during the storm was not included. Figures 3.6a show time snaps of the static mode before the storm peak, during the maximum surge, after the landfall, and the final condition. At 17:00 UTC Sep 18 when the maximum surge reached the coast, the water level on the ocean side was about 2.0 m (Figure 3.6a-iii). On the sound side, however, the wind pushed the water back and created a dry region behind the barrier island. At 00:00 UTC Sep 19, this region was flooded again as the water returned (Figure 3.6a-iv). The final results show that a fully-intact dune system would protect the barrier island from extensive flooding (Figure 3.6a-v).

3.5.3.2 Dynamic Scenario with Pre- and Post-Storm DEMs

The ground surface was updated dynamically in the ADCIRC simulation by using the pre- and post-storm DEMs. The initial elevation was obtained from the pre-storm DEM, corresponding to the island topography about two days before landfall. Then the elevation of each vertex was changed to reach the post-storm DEM, which has a combination of the topographic and bathymetric surveys collected after the storm. Because the exact timing of the breach cannot be known, we assume the major morphodynamic changes occurred during the storm's day of landfall. Thus, in the ADCIRC simulation, these ground-surface changes are applied linearly, starting at 00:00 UTC Sep 18 and continuing over 24 hr. This can be considered a 'worst-case' scenario with all of the erosion occurring during the storm.

In this scenario, the ground surface elevation was reduced during the simulation, and the channels developed as the storm approached the coast. This process allowed water to flood the barrier and cross the island onto the sound. At 06:00 UTC Sep 18, the elevation of the deeper channel was low enough to allow water to intrude the island from the sound side (Figure 3.6b-i). At 14:00 UTC Sep 18, three hours before landfall, the dunes were lowered and inundation occurred on the island (Figure 3.6b-ii). At 17:00 UTC Sep 18, the maximum surge flooded the island and the channels were deep enough to facilitate flow through the island (Figure 3.6b-iii). Contrary to the static scenario where the sound side became dry temporarily, in this scenario, the flow from the ocean to the sound kept the region flooded with a maximum water level of 1.2 m. After landfall, the wind pushed the water back toward the ocean. In the static scenario, the water piled on the sound side behind the

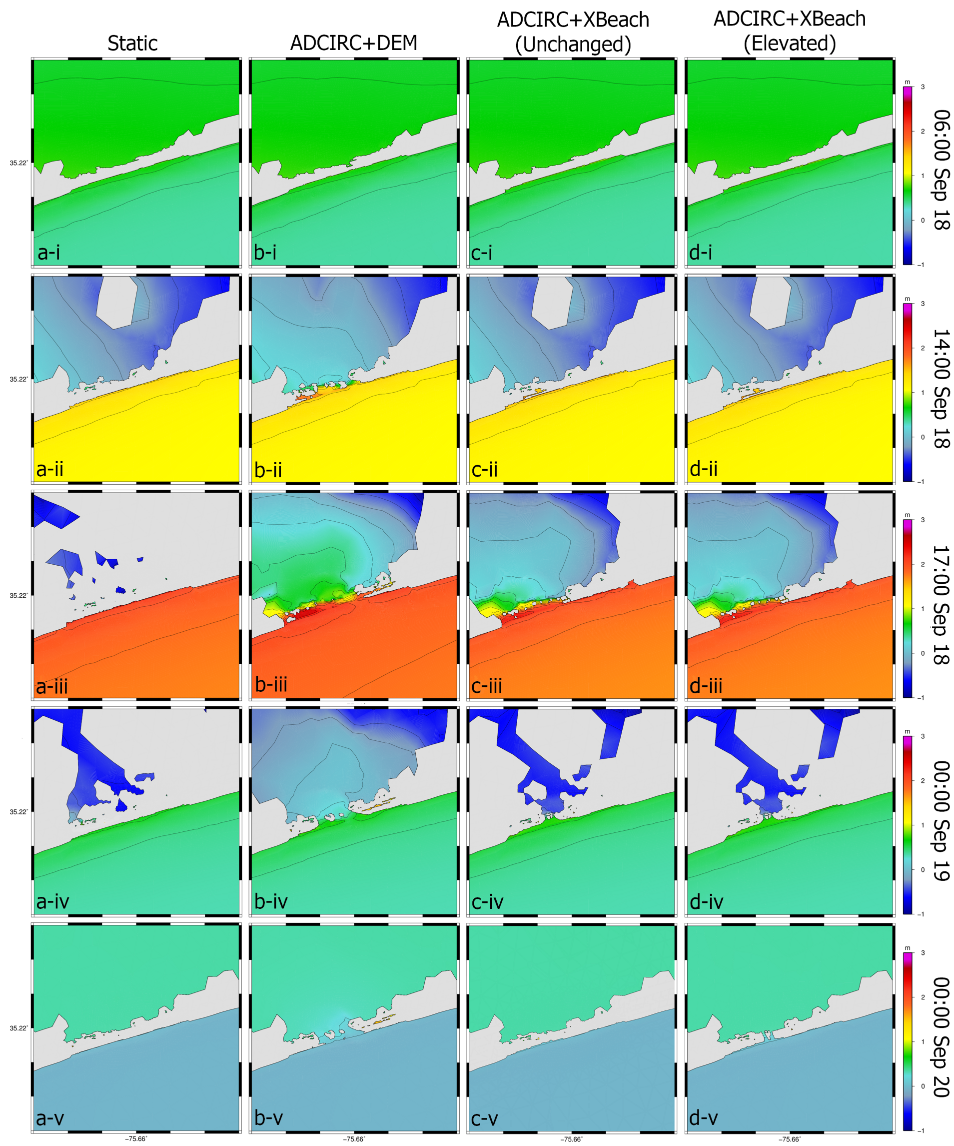

Figure 3.6 Water elevation during the storm in (a) static mode, (b) ADCIRC+DEMs, (c) ADCIRC+XBeach (unchanged), and (d) ADCIRC+XBeach (elevated). The water levels are shown at different time snaps during the storm.

barrier island, however, in this scenario, the channels conveyed the water back to the ocean and equalized the water level on both sides (Figure 3.6b-v).

For this scenario, the flow discharge through the barrier island was computed based on the current velocity and the depth of the water. Initially, the dunes prevented flooding into the island, however, when the elevation of the dunes reduced to below the total water level, flooding started at 12:00 UTC Sep 18. If the ground surface had eroded in this manner during the peak of the storm, then the flowrate would have increased rapidly reaching 2300 m^3/s (Figure 3.5 bottom). The flowrate reduced to 750 m^3/s over the next 6 hours with current restricted to the shallowly formed channels.

At 07:00 UTC Sep 19, the storm pushed water from the sound back to the ocean, and the flowrate reached 500 m^3/s at 12:00 UTC Sep 19. During the last 12 hours of the simulation, the channels were formed fully and allowed for water pass. The oscillations in the discharge graph correspond to the tide and ebb flows through these channels. The total volume of water exchanged between ocean and sound during the storm was about 58 million cubic meters.

Additionally, the maximum of differences in water level and current velocities between this mode and the static mode was calculated. Maximum difference is about 1.8 m in this scenario compared to the static scenario (Figure 3.7a-i). The differences in water level are limited to the sound near the breach extending to the northeast side. However, the differences near the northern part of Hatteras Island are caused by small delays in the phase of wetting and drying, and thus the main impact of the breach is observed roughly within 10 km of the opening and on the sound side. The velocity differences show a similar pattern with maximum differences near the breach of about 3 m/s (3.7a-ii).

To examine the current through the inlet and the larger-scale effects of the breach, we represented the flow with 20 Lagrangian particles. Their movement is based on the depth-averaged velocities as reported by ADCIRC [Dietrich et al., 2012]. The particles were released on the sound side at 06:00 UTC Sep 18, a few hours before the breaching started. Figure 3.7a-iii shows the tracks of these particles over time. Initially the particles are pushed into the sound in the northwest direction. Then, at 18:00 UTC Sep 18, they turn east and eventually follow a path northward. During the 40 hours after the breach is opened, these particles move northward 35 km (and far beyond the extents of the XBeach domain), thus demonstrating the breach's contribution to the circulation in the larger Pamlico Sound.

3.5.3.3 Dynamic Scenarios with XBeach

The XBeach simulations, which ideally include more realistic details of flood water timings and magnitudes, were also used to dynamically update the ground surface in ADCIRC. In these case, the ground surface elevation data are extracted hourly during the 3-day XBeach simulations, and then inverse-distance weighting (IDW) interpolation is used to upscale the XBeach-predicted bed levels onto the ADCIRC mesh.

Similar to the previous scenario, the results show that the barrier island was inundated and water passed through the breached channels. Initially, the dune system on the barrier island prevented the flooding until 14:00 UTC Sep 18 when the total water elevation on the ocean side exceeded the eroded dune crest, and overwash occurred (Figure 3.6c-ii and d-ii). This was similar to the XBeach prediction at 14:00 UTC Sep 18 (Figure 3.4c). The flooding through the island reached its maximum at 17:00 UTC Sep 18 when the storm made landfall (Figure 3.6c-iii and d-iii). The flooding extent was smaller compared to the ADCIRC+DEM results, and the water level elevation on the sound side was lower. This is because the channels predicted by XBeach were not as wide and deep as in the post-storm DEM. The dune system on the island was eroded but the channels were not fully formed, thus the volume of water crossing the barrier was limited. At 00:00 UTC Sep 19, the water on the

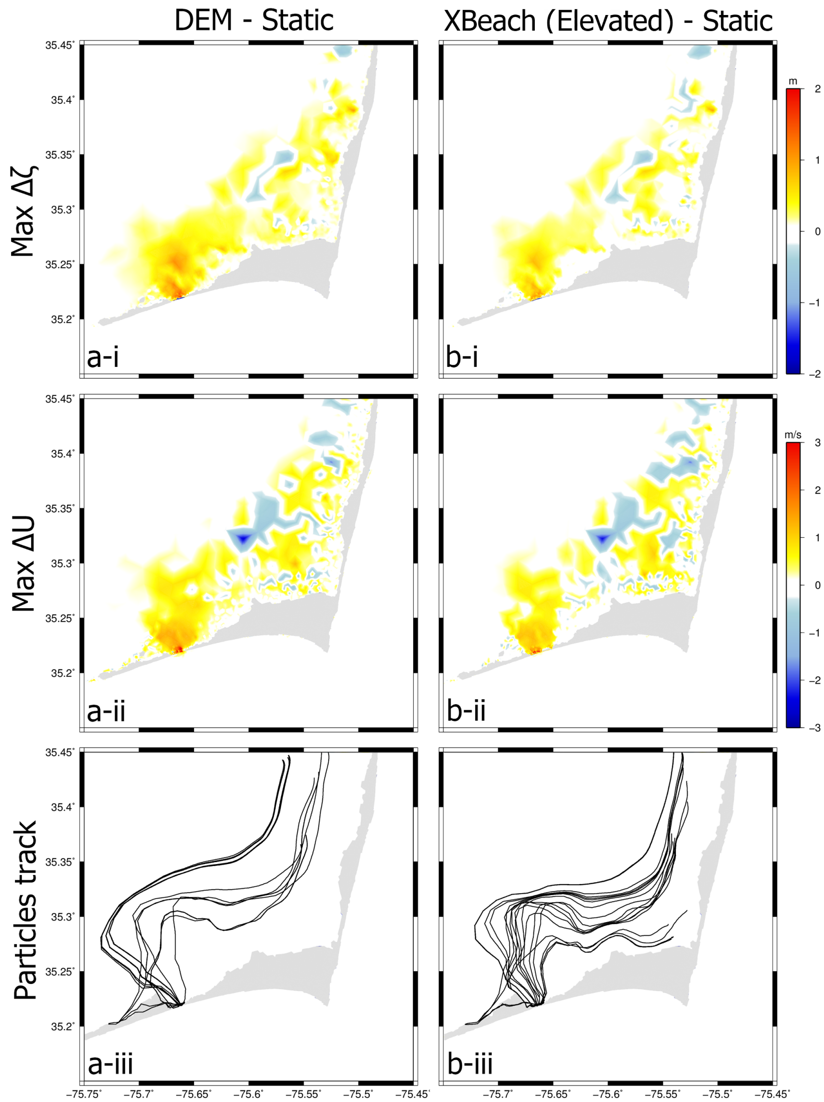

Figure 3.7 Maximum difference of water level (top) and velocity (middle) between (a) ADCIRC+DEMs and static mode, and (b) ADCIRC+XBeach (elevated) and static mode. The particle tracks (bottom) are shown for ADCIRC+DEMs and ADCIRC+XBeach (elevated) simulations. Note the differences and particle tracks for the ADCIRC+XBeach (unchanged) results were nearly identical to the ADCIRC+XBeach (elevated) results, and thus they are not shown.

sound was pushed back, but the flow through the small channels filled the region. However, some areas were still dry (Figure 3.6c-iv and d-iv). At 06:00 UTC Sep 19, the water level on the sound side increased and exceeded the ocean side water level, which forced a flow from the sound back to the ocean. In the case of XBeach (unchanged), the barrier island elevation is higher than water levels on both sides (Figure 3.6c-v). However, in the case of XBeach (elevated), the deeper channels connect the ocean and the sound until the end of the simulation at 00:00 UTC Sep 20 (Figure 3.6d-v).

The discharge computed for this scenario shows that the flooding started at 14:00 UTC Sep 18, or about 2 hr later than the previous scenario. The discharge through the island was 1250 m^3/s during the peak of the storm (Figure 3.5 bottom). Compared to the ADCIRC+DEM scenario, this flowrate was much smaller (about 50% less). The total volume of water exchanged between the ocean and sound in this case was about 19 million cubic meters, which was 33% of the volume calculated for the previous scenario, however, it was similar to the XBeach prediction for discharge through the barrier island.

The maximum of differences in water level and velocities between the ADCIRC+XBeach (elevated) scenario and the static scenario are shown in Figure 3.7b. The maximum water level difference was 1.5 m near the breach. Similar to the ADCIRC+DEM scenario, the differences are observable near the beach and further on the north-east along the sound-side of the barrier island (Figure 3.7b-i). The plume of water extends about 10 km in the sound, but it is slightly smaller than in the previous scenario. The maximum depth-averaged velocity difference is about 2.5 m/s compared to the static scenario (Figure 3.7b-ii).

The track of particles released on the sound is qualitatively similar to the previous scenario (Figure 3.7b-iii). However, the particles start to move into the sound half an hour later, due to a later opening of the breach in the XBeach predictions. Also, the particles do not extend as far to the west in the sound, and instead they track closer to the sound-side of Hatteras Island as they move northward. Thus, with a lower flow volume through the breach, the effects did not extend as far into Pamlico Sound.

3.6 Discussion

These results have several implications for our understanding of the formation of the Isabel Inlet and its effects on the larger circulation in Pamlico Sound, as well as our ability to predict breaches due to other storms.

XBeach predicted the Isabel Inlet breach with reasonable accuracy, similar to other studies [Nederhoff, 2014; Elsayed & Oumeraci, 2016]. The model represents the collision, overwash, and inundation regimes at appropriate times as the storm approached and made landfall, and the erosion of the dunes on the west side is comparable to the observations (Figure 3.2). Most importantly, the predicted breach is at the correct approximate location of the Isabel Inlet. These predictions were achieved with minimal model tuning – the sediment properties are uniform through the model domain, there is no use of a non-erodible layer, and the other model settings were derived from recent studies (as referenced in Section 3.4.2.2). These results are encouraging for the use of XBeach in regions where the subsurface properties are uncertain, and for coupling with larger-domain flood models for real-time predictions.

However, the predicted number, shape, and depth of the channels are not fully accurate, at least in comparison with the post-storm survey. In the XBeach prediction, two channels are breached, and they are located at 840 m and 930 m from the west boundary (Figure 3.8), which match the location of the western and middle channels in the post-storm survey. A third channel should have been breached and all channels should be deeper and wider. In the XBeach prediction, the two channels

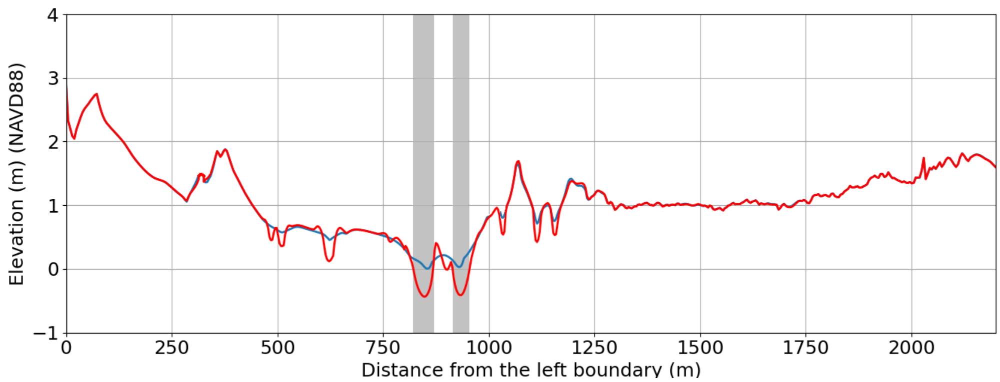

Figure 3.8 Alongshore profile of the XBeach-predicted final ground surface, for (blue) XBeach (unchanged) and (red) XBeach (elevated) (red). With the elevated water levels on the sound side, the formed channels are deeper by about 0.5 m. The location of this profile is shown with the dashed line in Figure 3.2. The locations of the breached channels are highlighted. These channels are located at $x = 850$ m and $x = 920$ m from the left (west) boundary of the XBeach domain.

have similar depths and widths of about 0.45 m and 40 to 50 m, respectively. In the post-storm survey four weeks after the storm, the three channels have widths of 105 m, 70 m, and 105 m, with the maximum depth of 6 m on the eastern channel.

These inaccuracies are likely caused by a combination of factors. First, the prediction of island breaching, especially the sub-aqueous transport to create channels, may be beyond the capabilities of XBeach. Several recent studies have focused on island breaching [de Vet, 2014; Nederhoff, 2014; Elsayed et al., 2018; Lugt et al., 2019] with similar results – the locations of the breaches are generally correct, but XBeach fails to erode channels to their full depths. Second, the subsurface geology can affect and control the erosion. Reports of this breach have mentioned the appearance of a peat layer [Wamsley & Hathaway, 2004; Wurtkowski, 2004], which would focus the erosion in the channels. The configuration of the peak layer is unknown, and thus it is not represented in our model. Third, the channel depths may be exaggerated in the post-storm survey, which was conducted a few weeks after landfall. A newly formed inlet can have a highly dynamic morphology, and the tidal current through the channels and ocean waves can change the shape and depth of the channel. It may not be reasonable to compare the XBeach-predicted channels immediately after the storm with the real channels as surveyed a few weeks later. Taken together, these factors are an indication that, although our simulation is a good qualitative depiction, it should be considered as one possible scenario of the island's response to the storm.

It is appropriate to consider several scenarios of how the breach may have affected the larger-scale circulation. The dynamic ADCIRC simulations show that including the morphodynamics can change the hydrodynamics and the flooding pattern significantly because the newly formed channels were deep enough to allow a considerable flow discharge through the island. In the scenario with the ground surface from the DEMs, we assumed a linear change in ground surface elevation can represent the morphodynamics, but this may not be an accurate match to the response of the barrier island. For example, in this scenario at 06:00 UTC Sep 18, flooding was initiated on the sound side (Figure 3.6b-i), when the immediate impacts of surge and waves were on the ocean side. Because of the linear transition of the ground surface in time, it was reduced to below mean sea level too early and before the storm affected the sound side. In contrast, in the scenario with the ground surface from XBeach (elevated), the flooding was initiated from the ocean side at the appropriate time (Figure 3.6c,d-ii). These scenarios show the channels conveyed water to maintain the elevated water levels on the sound side during the peak of the storm, and then also conveyed water to equalize the water levels between the ocean and sound after the storm.

The true flowrate through the breach was likely somewhere between these two scenarios. In the scenario with the ground surface from the post-storm survey, the channels were probably too deep, and thus the discharge of 2300 m^3/s was too high. In the scenario with XBeach, the channels were underpredicted in width and depth, and thus the discharge of 1250 m^3/s was probably too low. These scenarios are useful in that they provide a reasonable range for the true flowrate, and they are motivation for improved observation of subsurface properties to constrain the morphodynamic model predictions.

The maximum differences in water level show that erosion of the dunes on the barrier island as predicted by XBeach can impact the hydrodynamics on the sound at larger scales. However, compared to the case with a linear variation of the ground surface between the pre- and post-storm DEMs, the maximum differences are smaller in the XBeach cases both for water level and current velocity. Although the channel depths and widths in the DEM-based case were much larger than in the XBeach-based cases, the extent of water level, velocity differences, and particle tracks are similar in all cases. The particles tracks inside the lagoon are impacted by the wind force and the tidal current inside the lagoon, however, the breaching allows the water to push the particles from the sound-side shore further into the lagoon.

These results show that region-scale circulation can be affected by a breach. Consequently, higher water levels on the sound can result in local flooding in nearby communities, such as the town of Hatteras. These larger scale impacts can only be studied with a coupled model that resolves the temporal and spatial evolution of the breach and the subsequent flow through the barrier island. The plume jet through the breach extends to several kilometers into the lagoon and creates strong currents that push the particles into the lagoon. The extent of the region affected by the breach, both in terms of water level and current velocity, is several orders larger than the width of the breach, which again demonstrates the importance of small-scale morphodynamic changes on larger-scale hydrodynamics.

3.7 Conclusions

In this study for Isabel (2003), XBeach and ADCIRC+SWAN were coupled to predict the small-scale morphodynamics of breaching on Hatteras Island and its effects on lagoonal circulation in Pamlico Sound. We used a time-varying bathymetry module to dynamically update the ground surface elevation in ADCIRC+SWAN and represent the evolution of the breach. The dynamic mode was implemented both by using the DEMs and XBeach model predictions, and the results were compared to the static mode, in which the bathymetry is fixed. The flooding of the island during the storm was explored, and the flowrate for each case was calculated. The major findings of this study are:

1. *With a simple model setup and minimum tuning of the parameters, XBeach could predict the initiation and location of the breach.* This simplicity will allow the model to be applicable to other locations. Further improvement of the the results may require additional parameterization (e.g. spatially varying friction, multiple sediment layers, vegetation impact, etc.). Although the predicted depth and number of the breached channels did not match the conditions from several weeks after the storm, the information about the temporal evolution of the breach was useful for predicting the interaction of the breach with large-scale hydrodynamics near the barrier island.

2. *Flow from the sound to the ocean has an important role in deepening the breached channels.* Although there are no observations of water levels in the sound near the breach, the model predictions show that water level gradient from the sound to the ocean scarped the channels and increased the depth of the breach. These results support the behavior seen in Dorian (2019) [Sherwood et al., 2020], in which returning flow from the sound to the ocean may have caused breaching in the same barrier system.

3. *Breaching of the barrier island has significant large-scale impacts on the hydrodynamics.* When XBeach predictions of the temporal evolution of the erosion are included in an ADCIRC+SWAN simulation with a dynamic ground surface, a more realistic representation of the breach is captured by the model. The water level increased by 1 m near the breach, and the ocean waters extended to 13 km into the sound. These scenarios provide a reasonable range for the flow pattern through the breach, and they improve predictions of hazards from the sound side at nearby residential communities.

These results emphasize the need to consider coastal erosion in the prediction of storm surge and coastal flooding during storms, especially for real-time forecasting. Future studies will extend to other storms and coastal regions, further explore the applicability of a simple XBeach model setup (spatially uniform sediment properties, parameters from published studies) to predictions of coastal erosion in a range of settings, and automate the two-way coupling of a dynamic ground surface in ADCIRC+SWAN. These advancements will continue to improve our understanding of how barrier-island breaching can significantly change the water levels and circulation in lagoonal systems.

Acknowledgements

This project is funded, in part, by the U.S. Coastal Research Program (USCRP) as administered by the U.S. Army Corps of Engineers (USACE), Department of Defense. The content of the information provided in this publication does not necessarily reflect the position or the policy of the government, and no official endorsement should be inferred. The authors acknowledge the USACE and USCRP's support of their effort to strengthen coastal academic programs and address coastal community needs in the United States.

Appendix

ADCIRC has a (relatively undocumented) module for time-varying bathymetry, which allows for changes to the ground surface during the simulation, thus representing the morphodynamics or any variation in ground surface elevation. These changes are implemented by altering the ground surface elevation at specified mesh vertices and over specified durations. Then an offset equal to the ground surface change ($\partial h/\partial t$) is added to the water level change ($\partial \eta/\partial t$), to maintain the total water depth at that location. For example, if the ground surface is lowered by 1 cm at a vertex, then the water surface is also lowered by 1 cm. Then the mass and momentum conservation equations are solved for the new water surface elevations and velocities, respectively, and the wet/dry interface is re-evaluated. This process is repeated at every time step.

Time-varying bathymetry in ADCIRC can be enabled via changes in its existing model control parameter file and a new input file. In the model control parameter file (known as `fort.15`), a new parameter can be added to request updates to the bathymetric elevations in the entire mesh (`NDDT=1`) or only the portion where changes occur (`NDDT=2`). The parameter `BTIMINC` specifies the time intervals at which the surface is updated, and the parameter `BCHGTIMINC` is the duration over which the linear bathymetric changes are implemented. Time-varying data must be provided in a new input file (`fort.141`) with vertex numbers and their new bathymetric elevations. For each time interval, ADCIRC reads and updates linearly the bathymetric elevation of each vertex over the time specified by `BCHGTIMINC`. The `BCHGTIMINC` is used to control how quickly the changes to the ground elevations are implemented and can aid in model stability by "easing in" the changes rather than sudden jumps in values. Furthermore, if `BTIMINC` is a long time period, `BCHGTIMINC` can be used to more quickly implement the changes in the ground elevation during the simulation.

To demonstrate this module, a simple model of a beach with a uniform alongshore bathymetry was created. This configuration is used to resemble the breaching of a barrier island. The domain covers 2 km × 2 km of the beach, and the minimum and maximum mesh resolution are 5 m and 30 m, respectively. The bed level changes take place on a 200 m section alongshore in the middle of the domain. Over a 24-hr period, the water levels on the ocean/south boundary are increased to a maximum of 1.5 m, while the water levels in the lagoon/north are increased to a maximum of 0.5 m. The parameters are set to update the bathymetry on a one-hour (`BTIMINC=3600`) cycle, with the changes to the ground elevations occurring only during the first half hour (`BCHGTIMINC=1800`) of each cycle.

Figure 3.9 (left column) shows the ground surface and water levels over time and location of breaching. The model is stable and can represent the erosion of the beach by lowering the ground surface at the mesh vertices. Figure 3.9 (right column) shows the middle cross-section and the evolution of the breach. The ground surface is lowered slowly. When the water level on the ocean exceeds the dune crest elevation, then the water flows over the dune into the back-barrier region. The wetting/drying algorithm works properly and does not introduce any instabilities to the model. We ran a set of tests to explore the sensitivity of the parameters (with `BTIMINC=3600` and `BCHGTIMINC=900, 1800, 3600`), however, the results did not show significant differences in the water levels or flow through the island, and no instabilities or mass imbalances were added in any cases.

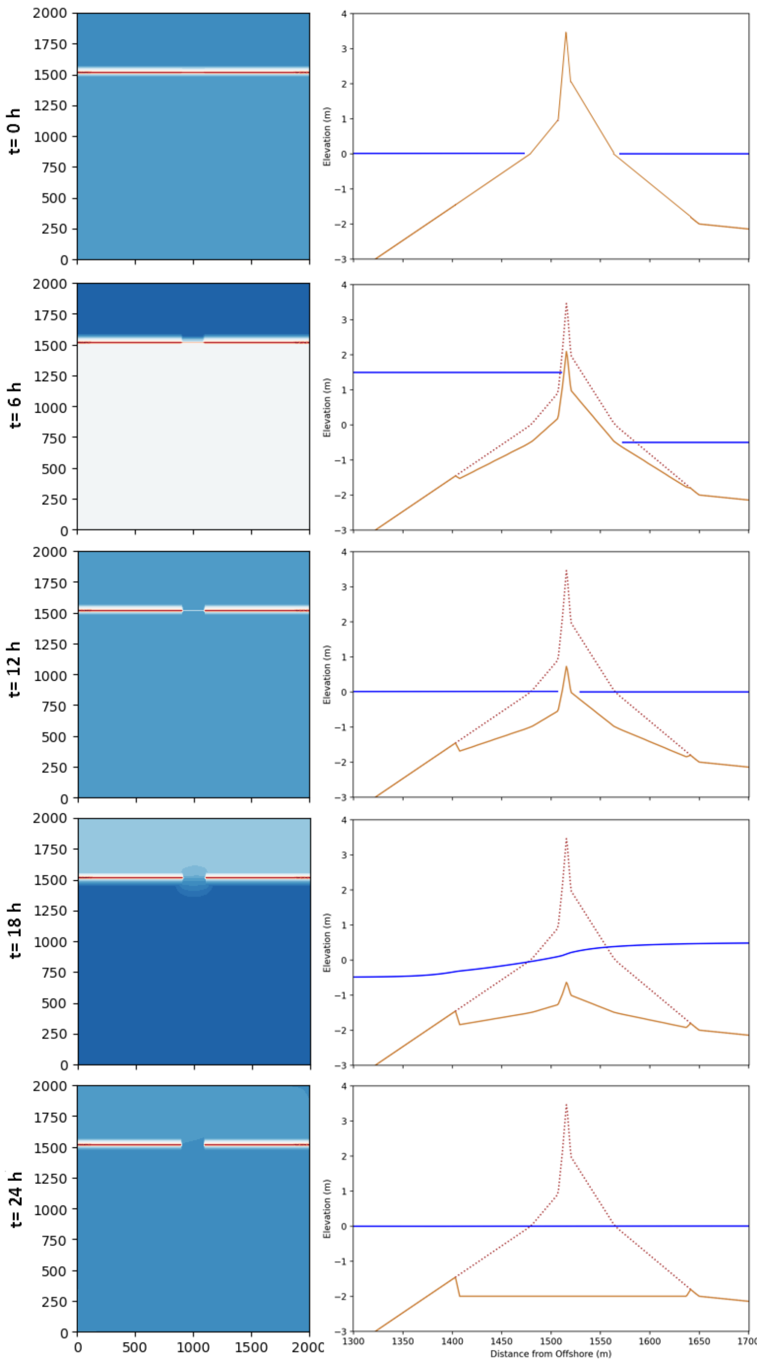

Figure 3.9 Demonstration of time-varying bathymetry in ADCIRC. A breach is opened in an idealized barrier island, as shown in (left) spatial (x, y) plots and (right) cross-section (x, z) profiles. The water levels are increased at the ocean/south boundary to a maximum of of 1.5 m, while the water levels in the lagoon/north are increased to a maximum of 0.5 m. At $t = 15$ hr, the ground surface is lowered enough to allow flow through the breach.

CHAPTER

4

SURROGATE MODEL FOR BEACH NOURISHMENT RESPONSE TO STORMS

4.1 Overview

Coastal areas are prone to severe erosion and subsequent flooding during storms. Among the common ‘soft’ and ‘hard’ mitigation plans, beach nourishment is conducted frequently on U.S. beaches, including in North Carolina. Nourished beaches should withstand extreme conditions during storms, each of which may have a short duration, but which can be repeated over several years. Therefore, to design and plan the nourishment volume and sustaining lifespan, and thus the renourishment frequency, there is a need to consider the morphology changes not from a single design storm but from multiple possible storms in potential future scenarios. As demonstrated in previous chapters of this dissertation, numerical models are great tools for deterministic predictions of how beaches can respond to storm forcing. However, they are expensive, both in computational resources and wall-clock time, which limits their use in forecasting of possible storms. Additionally, the intrinsic uncertainties in the potential future scenarios require a statistical analysis of the information and a probabilistic approach to predict the beach response. Thus, in this chapter, we develop a surrogate model for the prediction of beach nourishment response.

This research is a bit different from the single-storm studies in the preceding chapters, and it is part of a larger study to examine the sustainability of nourishment projects under changing climates. In this chapter, a surrogate model is developed via coupling of deterministic and probabilistic models. The deterministic model is XBeach, which is used to simulate the nourished beach response to 1,250 scenarios of future storms and beach profiles for Nags Head, NC. This library of deterministic predictions is then used to train a probabilistic model, which can then be used as a surrogate for predictions of nourished beach response in related scenarios. This chapter is in preparation to be submitted as a research article to the *Journal of Geophysical Research: Earth Surface*.

4.2 Abstract

Dunes and beaches in coastal areas are vulnerable to erosion and flooding during extreme events. Beaches can be nourished to provide a buffer during such extreme events in the short-term, but this nourishment has a finite lifespan as it erodes due to subsequent storms. Numerical models can predict the morphodynamic response of the beach to extreme events; however, these models are computationally expensive, which hinders their applicability for forecasting of uncertain conditions. In this chapter, we develop a surrogate model by combining deterministic and probabilistic models to predict the nourished beach response to synthetic storms. This surrogate model is focused on Nags Head, NC, which nourishes its beaches frequently to mitigate hazards of storm waves, flooding, and erosion. A high-fidelity, process-based morphodynamic model is used to predict erosion for 1,250 scenarios of future storms and beach profiles in this region. Then this library is used to train a surrogate model to enable predictions of nourished beach response in possible future storm sequences. Therefore, a novel contribution of this research is that the surrogate model is trained not only with the storm parameters, but also with the initial beach profile. It is shown that the surrogate model is capable of predicting the beach response to synthetic storms with high accuracy. When the model is tested for real storms from 2019, the eroded beach profiles were predicted with an excellent Skill Score of 0.66. The cumulative root-mean-square error for the erosion volume predicted by the surrogate was 19.51 m^3/m, while the numerical model errors had the largest contribution to the total error with a root-mean-square error of 18.69 m^3/m.

4.3 Introduction

Beaches and dunes are natural defenses for coastal communities on sandy coasts. Their resilience is affected by extreme storms, changes in sand supply, sea level rise, wave climate variability, and anthropogenic management. They are highly dynamic due to tides, currents, winds, and wave action. Extreme storm events can change the morphology of beaches on timescales of several hours to days, typically removing considerable volumes of sand from the sub-aerial beach to deeper portions of the offshore profile [Gallagher et al., 1998]. Subsequent calm periods can return this sediment on timescales of weeks to months. Over several years to decades, beaches evolve toward equilibrium in response to changes in sea level and sand supply [van Maanen et al., 2008]. Mitigation of both short-term, storm-induced change and long-term, climate-induced change is necessary along developed shorelines where the beaches provide protection from both erosion and flooding.

Mitigation strategies include both ‘hard’ and ‘soft’ engineering, but beach nourishment has been adopted by many coastal municipalities as the preferred form of coastal protection in the

U.S. [Armstrong et al., 2016]. Beach nourishment is the artificial deposition of sand on the shore to replace the eroded sand and maintain the beach width. The practice is widely recognized as an effective shoreline stabilization strategy [Luettich et al., 2014], both as a buffer between infrastructure and storm wave attack and as a source of sand that encourages natural dune building processes [Kaczkowski et al., 2018]. It is difficult to quantify the relative effects of wider beaches compared to larger dunes following beach nourishment, but the combined effect has repeatedly demonstrated the ability to mitigate energetic storm and hurricane risks. Dennis and Floyd (1999) both had impacts on the North Carolina coast, but caused no damages to buildings protected by three U.S. Army Corps of Engineers (USACE) projects while damaging or destroying more than 900 buildings along adjacent unnourished shorelines [Rogers, 2007]. Surveys following Sandy (2012) similarly revealed that nourished beaches prevented overwash and breaching, while unnourished beaches were more likely to have flooded homes behind them [Barone et al., 2014].

The success of these nourishment projects has contributed to an exponential growth of sand volumes placed on U.S. beaches [Elko et al., 2021]. This is due to more towns adopting beach nourishment, and existing projects requiring regular maintenance to combat losses from background erosion and episodic events [Landry, 2011]. North Carolina has spent more than $465 million on about 38 million cubic meters of sand for shore protection and emergency nourishments since 2010, not including nourishments resulting from navigation-related dredging [APTIM, 2021]. Typical nourishment frequencies in the U.S. are every 10 years, with variability dependent on the local background erosion rate [Cuttler et al., 2019]. However, years with the greatest volumes of sand placed have historically followed years with greater hurricane activity in the Atlantic Ocean [Elko et al., 2021].

The specific storm scenarios that a nourishment may experience in its lifetime are unknown, both in number of storms as well as timing and intensity. State-of-the-art frameworks predicting nourishment life-cycles have developed event-based scenarios that randomize the future occurrence of historical storms [Gravens et al., 2007]. For example, Beach-*fx* is a Monte Carlo simulation model developed by the USACE that uses a database of morphological responses estimated by S-Beach [Males et al., 2007].

Predictions of beach nourishment performance are also challenging due to the costs of process-based, deterministic models. The eXtreme Beach (XBeach) model [Roelvink et al., 2009] can simulate nearshore hydro- and morphodynamics during extreme storm events with high accuracy, as shown in several studies. Gharagozlou et al. [2020] modeled the erosion, overwash and inundation on North Carolina barrier island due to Isabel (2003) with high Skill Score. McCall et al. [2010] used XBeach to study the erosion and dune removal of Santa Rosa barrier island during Ivan (2004). While these studies considered a single storm, others have used XBeach to simulate the beach response for a small number of storm scenarios [Mickey et al., 2018; Passeri et al., 2018]. However, XBeach is computationally expensive, often requiring hours for a single simulation on a parallel computer [Nederhoff, 2014; McCall, 2008], and thus most XBeach studies are focused on a single or small number of simulations [Harter & Figlus, 2017; Gharagozlou et al., 2020].

Therefore, recent studies have leveraged probabilistic techniques to improve computational time while preserving the accuracy of deterministic models, thus allowing for a larger number of scenarios to be considered. These probabilistic models define a relationship between the input and output parameters, thus removing the need for time-consuming numerical models. For storm surge predictions, Jia et al. [2016a] used a probabilistic model by approximating the relationship between input and outputs of a computationally expensive numerical model. The model was trained with more than 400 storms for the Gulf of Mexico and could predict the time series of surge for 30 locations with high accuracy. Probabilistic analysis and hydrodynamic modeling have been used to estimate the flood hazard in tidal channels and estuaries [Moftakhari et al., 2019]. Other probabilistic approaches have been used to predict barrier island morphodynamics [Plant & Stockdon, 2012] and to enhance shoreline-change predictions by including dune height, sea level rise, tides and wave height as variables in the model [Plant et al., 2014a]. A combination of detailed probabilistic modeling of offshore storm climate with a process-based morphodynamic model was used to assess and quantify morphodynamic variability of cross-shore beach profiles [Pender & Karunarathna, 2013]. The uncertainty of beach profile response to varying antecedent topographies was investigated by combining the erosion model predictions and statistic functions [Mickey et al., 2020]. In a study on Dauphin Island, 100 synthetic sea storms were generated using a probabilistic model to preserve the full range of possible oceanographic conditions [Wahl et al., 2016], then a surrogate model was developed to predict the geometric parameters of barrier island erosion due to the synthetic storms [Santos et al., 2019].

The combination of probabilistic and deterministic approaches allows for an efficient and accurate modeling of nourished beach erosion due to unknown future scenarios. Previous studies have proved the robustness of statistical-process based models for predicting the beach response to sequence of storms, but the initial state of the beach and its variation over time were not considered in any of these studies. Instead, the sea-storms and resulting morphodynamics were simulated with a reference initial beach profile. Those surrogate models are thus limited in how they handle the evolution of the nourished beach.

In this chapter, we develop a surrogate model that can interpret synthetic, unsimulated conditions and predict the accurate response of the beach to possible storm scenarios. Our goal is to build a surrogate model not only based on the sea-storm parameters but also the initial dune and beach profiles. This model is part of an effort to create a coastal restoration emulator, which will analyse the climate data pattern, generate synthetic storms, predict beach erosion, and ultimately provide information about the sustainability of the beaches and nourishment requirements.

We hypothesize that: (a) simplifying the storms and profiles have minimal effects on the errors, and (b) the developed surrogate model is a reliable and efficient tool that can predict complicated beach morphodynamics accurately in a short amount of time. To test these hypotheses, a procedure to develop a surrogate model based on a combination of probabilistic and numerical models is presented. The surveys of beach profiles and observations of storms are simplified and parameterized into a multivariate space. A large set of hypothetical scenarios are created to explore the beach response to storms, and then a subset of most dissimilar design points (storms and profiles) are selected in a way that they are representative of the large set. These scenarios are simulated with a deterministic morphodynamic model, and the results are used to train the surrogate model. The model is tested for predictions of a nourished beach response to a succession of real storms in 2019. Last, the errors associated with numerical model, parameterization, and surrogate model are quantified by comparing the results to observation and purely numerical model results.

4.4 Background

4.4.1 Nags Head, NC

The town of Nags Head, NC, is an ideal study area, because its beach and dune system are active due to frequent and significant storm events and nourishment activities. The town is located in the Outer Banks and extends from a southern border about 8 km north of Oregon Inlet to a northern border at the town of Kill Devil Hills. Its 18-km ocean shoreline is exposed to both extratropical storms (nor'easters) and tropical cyclones (from the south-southeast). Nags Head experiences semidiurnal tides with a mean range of 0.97 m and a spring tidal range of 1.3 m on the ocean side. The predominant wave direction is from the northeast, exposing Nags Head to some of the highest wave energy along the U.S. Atlantic coast, with mean significant wave heights exceeding 1.3 m at 17 m depth (1985–2015, Field Research Facility (FRF) pier) [Karanci et al., 2018]. The mean significant wave heights from September to April typically range between 1.03 m and 1.19 m. Significant wave heights are usually smaller (0.6 m to 0.92 m) from May to August when dominant southwesterly winds are directed offshore [Coastal Science and Engineering, 2012]. The area is subjected to frequent hurricanes and nor'easter storms and is affected by coastal erosion and sea level rise. For examples, Matthew (2016) generated waves as high as 5 m and storm surge of 1 m, and winter storm Riley (2018) affected the region with wave heights of 4.7 m and storm surge of 0.8 m.

Consequently, erosion has gradually consumed the shoreline of Nags Head. Net shoreline change in the area ranges between 0.23 m/yr (accretion) at the northern end to 2.18 m/yr (erosion) at the southern end of the town [Kana & Kaczkowski, 2012; N.C. Department of Environment and Natural Resources (NCDENR), 2012]. The town is characterized by low-lying areas with elevations lower than 3 m (NAVD88), excluding the dunes. The region had discontinuous dune lines with dune crest heights ranging from 4 to 8 m (NAVD88) before an extensive nourishment in 2011 [Karanci et al., 2018].

4.4.2 Nourishment Projects

Beach nourishment is the preferred mitigation strategy in NC, and Nags Head conducted two nourishment projects in the last 10 years. The first nourishment project was done between May 24 and October 27, 2011, with about 3.5 million m^3 of sand placed along a 16 km stretch of beach. During its lifespan, the nourished beach experienced three major hurricanes (Irene in August 2011,

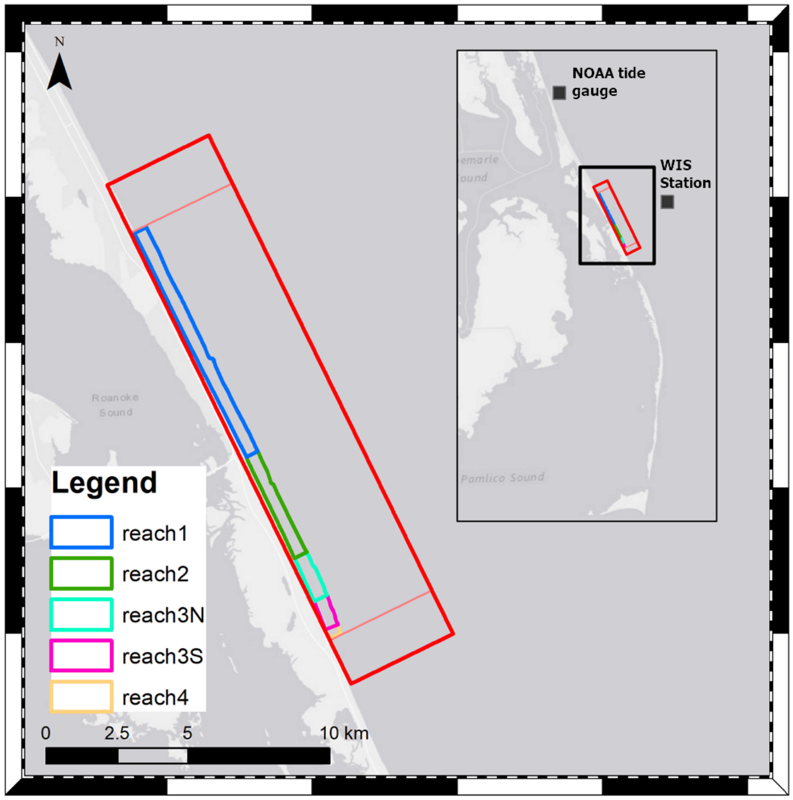

Figure 4.1 Location of Nags Head, NC, in the Outer Banks. The town-surveyed beach reaches are labeled, and the red box shows the extents of the 20-km XBeach computational grid including the buffers on both side. In the inset figure, locations are also shown for the NOAA tide gauge at the USACE Field Research Facility and a synthetic wave buoy in the Wave Information Study.

Sandy in October 2012, and Matthew in October 2016). There was minor damage to oceanfront properties and town infrastructure during these storms. After Matthew, a comprehensive beach condition survey showed that the project area lost 1 million m^3 of sand, which was equivalent to about 30 percent of the nourishment volume placed during the 2011 project [Town of Nags Head, 2017]. Beach width continued to decline in the years following Matthew, necessitating a second nourishment project between May 1 and August 18, 2019. About 3 million m^3 of sand was placed along the same 16 km stretch of beach. Dorian was the first major hurricane of the 2019 Atlantic hurricane season and affected the Outer Banks on 6 September 2019 with waves as high as 5 m and maximum surge level between 1.1 to 1.2 m [Coastal Science and Engineering, 2019]. Pre- and post-Dorian surveys show the region gained sand in the dune and on the back beach due to the wind-generated dune growth after renourishment. However, the net loss of sand caused by Dorian along the 16 km of the beach measured from the foredune to −5.8 m NAVD88 was about 388,000 m^3 [Coastal Science and Engineering, 2019].

For these and earlier nourishments, Nags Head monitored their performance with regular surveys of the bathymetry and topography along the beach and dune system. These surveys have been collected at least once annually, with additional surveys as necessary after nourishments and storm events. For the topographic data, Trimble R-8 GNSS receivers on 2-m rods with Trimble TSC2 Data Collectors running Trimble Survey Pro were used. For the bathymetric data, the RV Southern Echo outfitted with Trimble R-8 (positioning and heave), Odom Echotrac CV100 sounder with a SMSW200-4a transducer (200kHz, 4 degree beam width), and a YSI 6600 for speed of sound calibration were used. The surveys were collected along consistent transects with an average of 150-m spacing, thus providing critical observations of the morphology over the entire beach.

For this study, we consider 10 years of surveys from 2009 to 2019. During this timespan, there were a total of 18 surveys, and for most years, there were surveys both before (in mid-summer) and after (in late fall) the hurricane season. The surveys start from the dune crest and extend to depths between 8 to 12 m below sea level. For this study, each survey was interpolated onto a digital elevation model (DEM) by using the regularized spline tension method. Between the survey profiles, the ground surface was interpolated linearly in each DEM. The root-mean-square errors along the profiles for each interpolated DEM are less than 10 cm. The DEMs cover about 20 km of the beach (about 16 km of which is the focus of our study). For our later analyses, a total of about 25,000 beach profiles were extracted from the 15 DEMs generated from surveys between 2010 to 2019. The profiles were spaced every 10 m along the beach.

These DEMs show how the dune and beach system was changed during and between the nourishments of 2011 and 2019 (Figure 4.2). In the nourishments, sand was placed on the beach, and thus the dune crest elevation was not changed. However, the beach width was extended significantly after each nourishment. The average beach widths in November 2010 and April 2019 (prior to the nourishment projects) were about 50 m and 55 m, respectively. After the 2011 nourishment, the shoreline was extended further toward the ocean and resulted in a wider beach. The average beach width in the northern section after nourishment was about 50 m and in the southern section is about 100 m. Similarly, after the 2019 nourishment, the beach width was about 100 m along most of Nags Head and slightly wider along the southern section.

4.4.3 Wave Climate and Water Levels

Wave data were obtained from the Wave Information Studies (WIS) project [Bryant et al., 2016], which produces a high-quality online database of hindcast, nearshore wave conditions covering U.S. coasts since 1976. These wave estimates are provided using climatology data and third-generation wave models (i.e. WAM and WAVEWATCH III). The results of wave height, period, direction and directional spectral estimates are provided for a set of pre-selected, virtual gauge locations along the coast. For this study, we used the data from a virtual station (ST63222) located 14 km off the Nags Heads head beach at 35.92° N and 75.42° W. The water depth at the station is about 19 m. The wave data cover more than 40 years of hindcast.

Water level data were obtained from the NOAA tide gauge at the USACE Field Research Facility (FRF) in Duck, NC. The water level station (8651370) is located on the FRF pier at 36.17° N and 75.75° W. The study area (Nags Head) is located about 33 km south of this station. The data provide 40

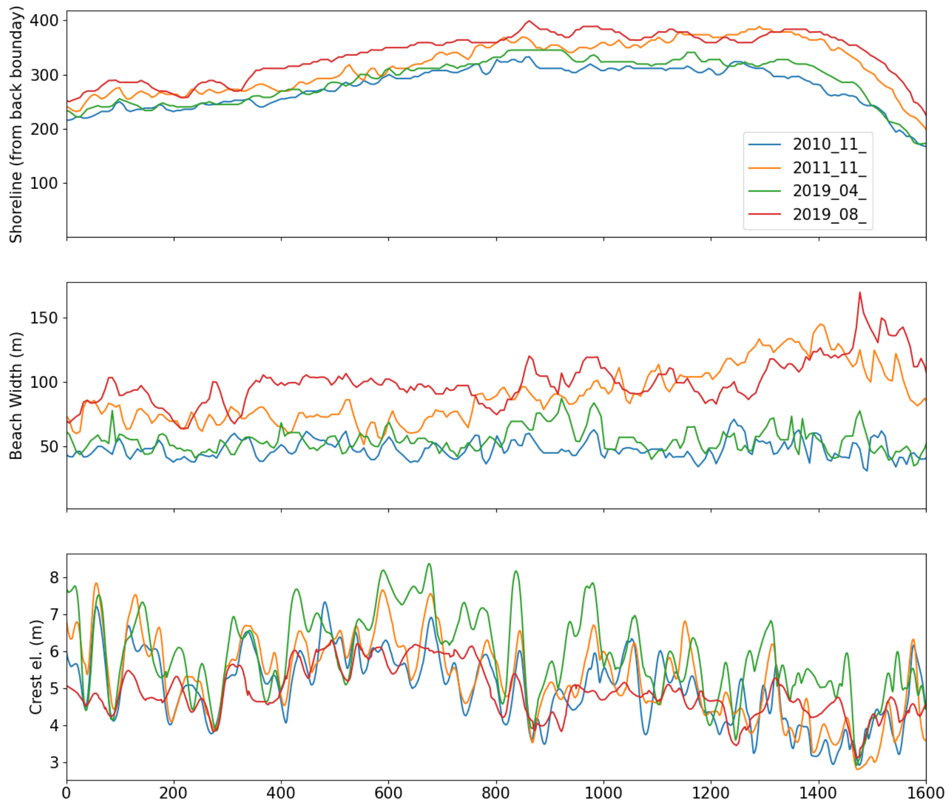

Figure 4.2 Changes in shoreline location (m from back boundary of surveys), beach width (m), and dune crest elevation (m relative to NAVD88) for pre- and post-nourishment in 2011 and 2019. The horizontal axis is the profile number along the shore in Nags Head, NC, with the origin at its north end.

years of predictions and observations of water level and surge. The station has a good coverage of measured data even during major storm events.

We analyzed time series of wave heights and water levels to identify storm events. In the study area, an average of 20 storms occur annually, and thus a nourished beach must withstand several storms per year. The maximum significant wave height experienced during the full time series was about 7.89 m, which occurred in 17 September 2003 during Isabel. The maximum surge level was about 1.43 m, which occurred at the same time during Isabel. We describe below how the storms were selected and compiled into synthetic storm scenarios.

4.5 Methods

In this chapter, the key contribution is a methodology to develop a surrogate model for beach response to hydrodynamic forcings, specifically the scarping of nourished beaches during storms. The surrogate model maps the full dimensionality of the simulator's inputs, or *predictors*, to the simulator's outputs, or *predictands*. In our surrogate model, the predictors will include storm wave and water level conditions that are consistent with the observed and modeled conditions for the

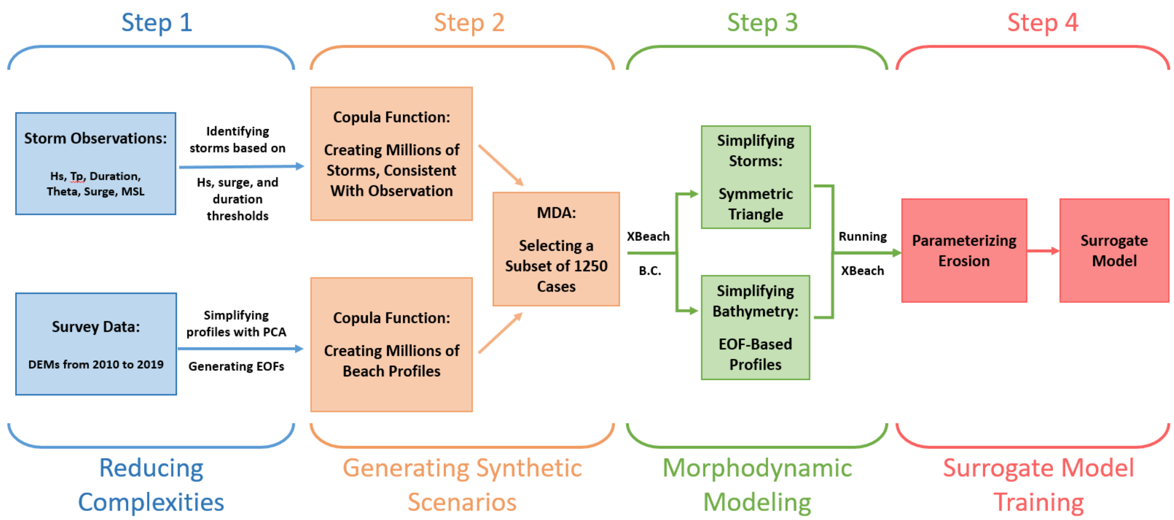

Figure 4.3 Schematic workflow of surrogate model development. First, the observed data are analysed and then parameterized to reduce complexities. Next, a subset of dissimilar scenarios are selected from a library of millions of synthetic cases. Then, the synthetic beach profiles and sea-storm events are used to create boundary conditions and bathymetry for a suite of model simulations. Last, the model predictions are parameterized and used to train the surrogate model.

northeast NC coast, as well as initial beach profiles that are consistent with the surveyed ground surfaces for the beaches in Nags Head. The predictands will include the shape of the scarped beach and thus the volume of sand eroded from the sub-aerial beach. Some of these predictors and predictands are unique components of a surrogate model like ours, i.e. previous studies have included neither beach profiles as inputs nor scarp geometries as outputs. These additional components will increase the complexity of our surrogate model.

If the simulator design is complex, then more predictors are necessary in the surrogate model. This increasing complexity necessitates larger training libraries to capture variability across more dimensions, and thus our library of morphodynamic model simulations will be larger than in previous studies. However, this increasing complexity can also introduce noise if the predictors are not relevant to the variance in the final predictand, and thus we will simplify by describing both predictors and predictands with smaller numbers of parameters.

Our surrogate model development (Figure 4.3) can be described in four major steps: (1) reducing the complexities of the sea-storms and beach profiles, (2) developing scenarios of plausible future conditions, (3) using a process-based morphodynamic model to develop a library of beach responses, and (4) training a surrogate model for predictions of beach scarps and eroded sand volumes. First, the historical sea-storms and surveyed beach profiles are described with a smaller number of parameters, such as the peak significant wave height during a storm or the typical shape of a nourished beach. Next, these parameters are used to create millions of possible future scenarios, which are then sampled to identify a subset of scenarios that are most dissimilar, such as the largest waves or the widest beaches. Then, those scenarios are used as forcing to hundreds of simulations with a full-physics, deterministic model, which will predict the sub-aerial beach erosion. Last, the eroded beaches from the deterministic model simulations are simplified and used as training for a surrogate model. These steps are described in the following subsections.

4.5.1 Step 1: Reducing Complexities of Storms and Beach Profiles

To reduce the complexity of the predictors, the wave, water level, and beach survey data were processed to identify a smaller number of parameters to describe their key attributes. For the wave and water level data, this processing led to the identification of sea-storms that can be described with parameters of duration, wave angle, wave height, wave period, and storm surge. For the beach profiles, this processing led to the identification of principal components (like the shape of the nourished beach) that can be described with simple functions.

4.5.1.1 Parameterizing Sea-Storms

Describing storm events with a set of parameters (wave properties, surge level, etc.) is a straightforward approach and has been used in several recent studies [Wahl et al., 2016; Duo et al., 2020]. For this study, sea-storm events were identified from the historical time series of waves and water levels by using the following procedure. Individual sea-storm events were defined as having the largest 10 percent of significant wave heights in the record, i.e. above a threshold of $H_s = 1.8$ m, and as having a continuous duration greater than 12 hr [Birkemeier et al., 1999; Duo et al., 2020]. The storm duration was defined as the time period that H_s remained above the threshold, plus a 24 hr buffer before and after that time period. If H_s dropped below the threshold and stayed there for more than 24 hr before rising again, then we assumed a new event occurred; otherwise, we assumed that the threshold exceedance was still associated with the same storm incident [Wahl et al., 2016]. This logic assures that events are approximately independent for the subsequent statistical analysis. For each storm event, the maximum significant wave height H_s and the associated wave period T_p and wave direction θ were identified. For the water levels, both the astronomic tides and a linear sea level rise trend were removed from the tide gauge record to obtain non-tidal residuals η driven by storm activity, and the maximum η was identified during each storm event.

Applying this procedure to 40 years of hydrodynamic data, we identified more than 800 independent storm events and extracted their parameters (η, MSL, duration, H_s, T_p, θ). These identified storm events (Figure 4.4) include several major tropical cyclones from the past 20 years: Isabel (2003) had wave heights of 7.89 m and storm surge of 1.43 m, Irene (2011) had wave heights of 6.6 m, Sandy (2012) had wave heights of 5.25 m and storm surge of 1.27 m, and Dorian (2019) had wave heights of 6.3 m and storm surge of 1.1 m. Although the record includes these large storms, it also includes a large number of unnamed storms that affected the nourished beach in Nags Head.

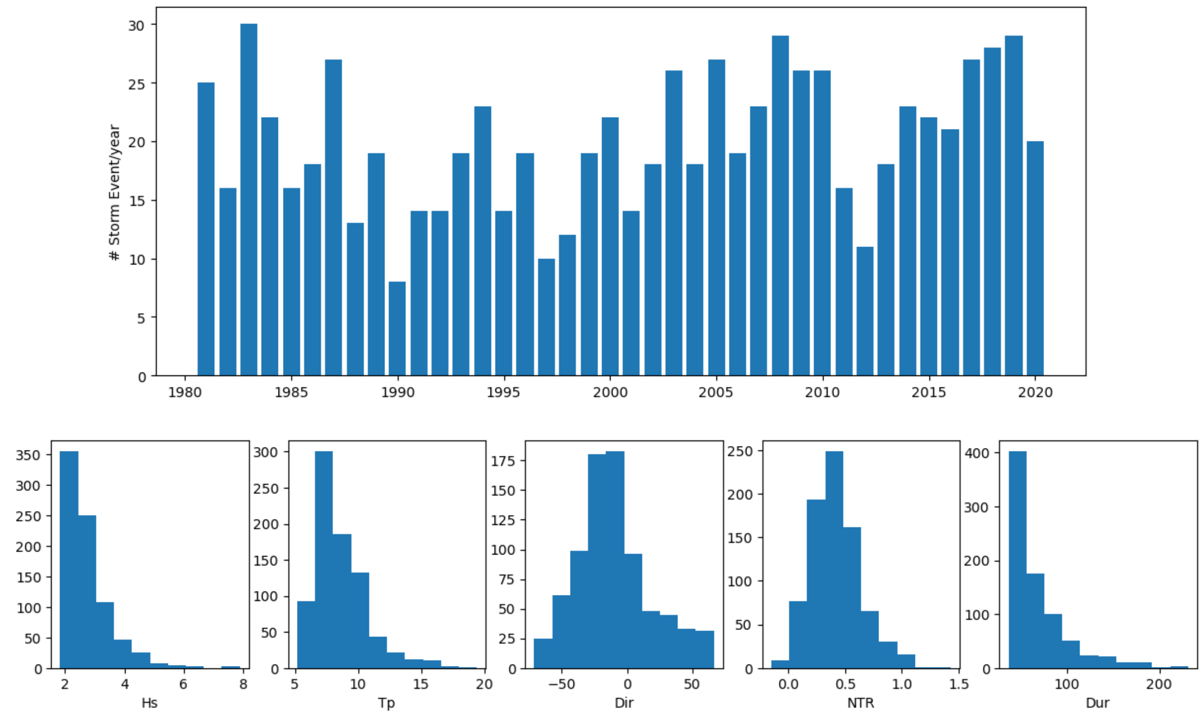

Figure 4.4 For the historical wave and water-level data, (top) the number of individual storm events identified per year, and (bottom) the distributions of storm parameters for significant wave height H_s, wave period T_p, wave direction, θ, non-tidal residual η, and storm duration.

4.5.1.2 Parameterizing Beach Profiles

The surveyed beach profiles were also simplified to describe their key attributes. One method is to parameterize the key characteristics of the profiles, e.g. Santos et al. [2019] defined a set of parameters (beach width, dune height, location of dune toe, etc.) to describe the beach erosion in Dauphin Island, Alabama. However, this method requires additional logic to reconstruct profiles from the parameters. Similarly Karanci et al. [2018] used parameters to represent topographic features in coastal NC. Another method is to represent the beach profile with a simple, smooth function, e.g. Mickey et al. [2020] used a Gaussian fit to island profiles. However, the smoothed profiles may not properly identify key features like the dune.

In this study, we use Principal Component Analysis (PCA) to simplify the beach profiles. PCA finds new variables that are linear functions of those in the original dataset, that successively maximize variance, and that are uncorrelated with each other [Jolliffe & Cadima, 2016]. PCA produces a set of structures called Empirical Orthogonal Functions (EOFs). The shape of each EOF describes an important pattern in the original dataset (such as a nourished beach width). The EOFs can be added together in a linear superposition to recreate members of the original dataset (such as a beach profile), albeit with reduced complexity.

For beach profiles, the dimensionality can be associated with changes in geomorphic features from one profile to another, but it also can be related to the interdependability of multiple features in a single profile, e.g. how the beach width variations correlate to dune height. For example, for our study, a key parameter is the beach width, which has a lot of variability across profiles, both in different years and different parts of Nags Head. If the beach width is the most important parameter to describe the profiles, then its average or representative shape will be described by the first EOF. (The second EOF may describe the average shape of the dune, etc.) By adding together the EOFs, and by varying their weights in the addition, we can create simplified versions of the beach profiles from the survey data (or new beach profiles for future scenarios).

We parameterized the beach profiles with 9 EOFs, which account for more than 97 percent of the total variance (Figure 4.5). As expected, EOF #1 mostly describes the overall shape of the profile with the focus on variability in the dune height and beach width. EOF #2 further modulates the variation in dune and beach geometry, as well as the surf zone portion of the profile, and EOF #3 describes the offshore bar (Figure 4.5). The relative importance of the EOFs changes over time and is sensitive to the temporal variability in beach profiles. For example, EOF #1 shows an increase in 2011, when the nourishment occurred, followed by consistent decrease in subsequent years until 2019, when another beach nourishment took place (Figure 4.5, bottom). These EOFs are then used to generate synthetic profiles.

4.5.2 Step 2: Developing Scenarios of Plausible Future Conditions

The next step is to develop scenarios of plausible future sea-storms and beach profiles. These scenarios will be informed by the 800 parameterized sea-storms and 9 EOFs of beach profile components, but they will not be exact reproductions of them. The EOFs and PCs derived from profiles, along with the sea-storm parameters, are then used to generate synthetic scenarios, while considering the interdependency and correlations between the variables. A copula-based approach is used to generate millions of possible scenarios in which sea-storms and beach profiles will be linked. Then a maximum-dissimilarity algorithm is used to select a subset of possible scenarios that will be most effective in training the surrogate model.

4.5.2.1 Using Copulas to Create Millions of Possible Scenarios

To consider the full range of possible future sea-storms at Nags Head, NC, we should include more than the 800 sea-storms observed in the historical record. Instead, we use the observed sea-storm parameters to develop millions of hypothetical sea-storms.

One possible method is to select randomly from the parameterized sea-storm data. However, this method does not guarantee a correlation between the selected values, and thus the hypothetical storm may not be physically realistic. For example, although it is possible for storms to separately generate waves with a very small height or a very long wave period, it is not realistic that a single storm would have both. A random sampling may not give a realistic representation of the sea-storm.

Instead, we use copula functions to describe the dependence between random variables. Copulas identify correlations by transforming the independent distribution of each variable to a conditional

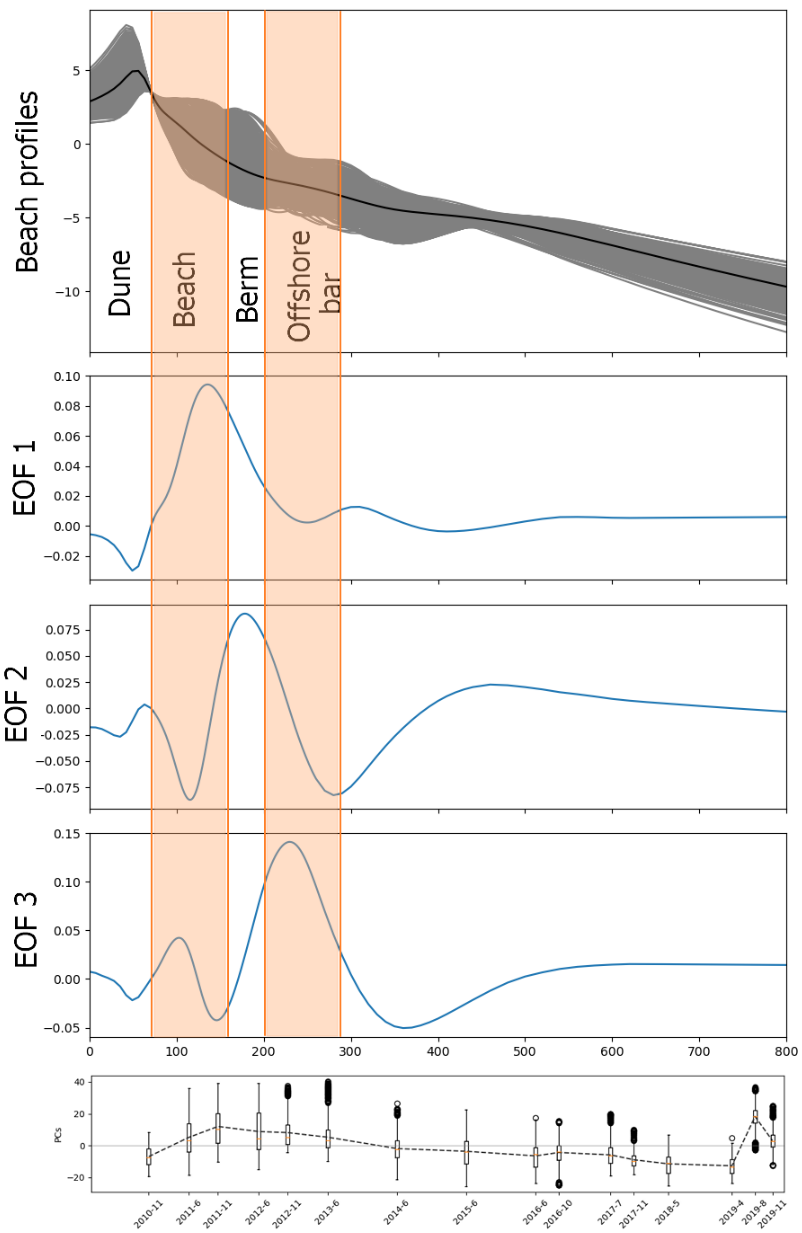

Figure 4.5 Simplifying profiles with EOFs. In the top panel, the mean profile (black line) and the envelope of all profiles (grey) are shown in top panel. The EOFs are used to simplify the profiles. Each EOF modulates part of the profile. In the middle panels, EOFs #1, #2, and #3 are shown. The shaded areas show the portion of the profile that is described by each EOF. In the bottom panel, the temporal variation for EOF #1 is shown. Because EOF #1 is mainly related to beach width, its contribution was sensitive to beach nourishments in 2011 and 2019.

distribution (dependency between variables) and therefore are used to represent relationships between variables. Copulas allow us to consider joint probabilities, so the physical interdependency of variables is maintained. Gaussian copulas are ideal for high-dimensional problems and were shown to ensure realistic co-occurrence for wave and surge conditions in San Diego [Anderson et al., 2019]. In this study, we use copulas to define correlations across dimensions. This means that we differentiate between large and small storms that have specific characteristics; for example, the sea-storms with large waves and shorter duration approach from the south, and sea-storms with lower peak waves and longer duration approach from the north. A copula is an ideal tool to account for these correlations and to create synthetic storms that match the realistic storm behavior.

Wave and water level data are used to determine relationships between hydrodynamic parameters that influence total water level and subsequent erosion and flooding. For the sea-storm data, wave height, period, direction, surge, MSL, and the duration of the storm are correlated, and we used a copula-based approach [Wahl et al., 2016] to create synthetic sea-storms. For the beach profiles, the principal components are correlated, and a separate copula was used to determine the parameters' variability for each transect. We used separate copulas because there is not enough information to correlate the beach profile parameters directly to the sea-storm parameters.

Using these copulas, we generated two sets of synthetic scenarios (one for sea-storm parameters, and one for beach components), each with a million members, by randomly sampling from the multivariate distribution of storm parameters. We considered the joint probability between variables; therefore, these parameters are representative of the realistic observations. Then the two sets of synthetic scenarios were combined, by linking randomly each sea-storm condition to a beach profile. Thus, each of the million realizations has one sea-storm and one profile.

4.5.2.2 Using MDA to Narrow to 1,250 Dissimilar Cases

The generated synthetic scenarios provide the full variability of sea-storm conditions and beach profiles. Although all of the million possible synthetic scenarios could be used in the training of the surrogate model, this would require a million simulations with the morphodynamic model, which would be computationally prohibitive. Therefore, a smaller subset of these scenarios must be selected in a way that still captures the correlations between sea-storm attributes and profiles, while also representing each selected case as a unique, distinct scenario.

A Maximum Dissimilarity Algorithm (MDA) was used to select a subset of the most diverse and dissimilar scenarios. The MDA include extreme events or outliers, as it captures the outer limits of the input boundary space of variables. Using an iterative approach, the MDA selects design points that are most dissimilar. This is achieved by calculating Euclidean distances in multi-dimensional space from the already selected points [Camus et al., 2011] and specifying the dissimilarity of sets as a function of the distances in the dataset. The MDA initially selects the outliers and progressively adds design points located within the center of the multi-dimensional space. This approach assures that the selected scenarios cover a large range of each variables and are representative of all the unique and distinct possible cases.

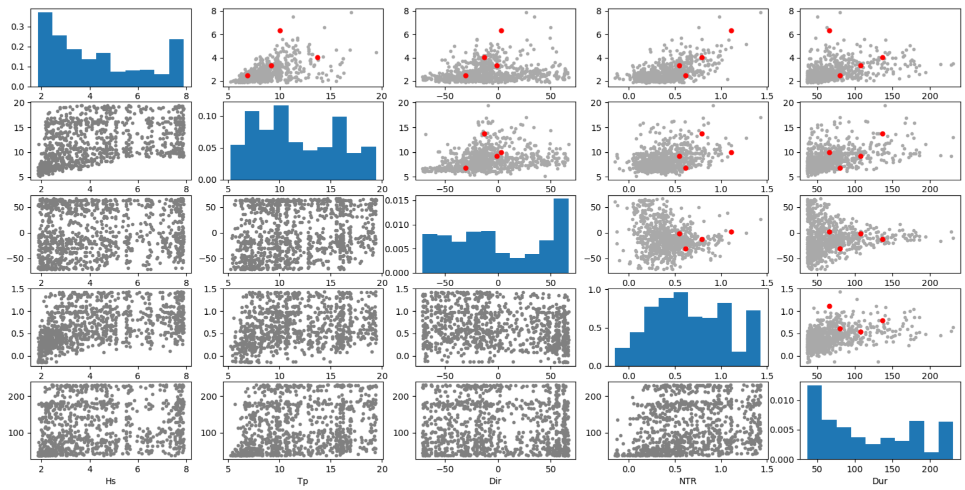

Figure 4.6 Generating millions of synthetic scenarios for storm parameters. Multivariate distributions are shown for (top right) historical storm parameters and (bottom left) selected most-dissimilar storms. The red dots show the parameters for the four major storms between August and November 2019.

In this study, we used MDA to select a subset of 1,250 scenarios of sea-storm events and beach profiles for the XBeach simulations. Figure 4.6 shows the multivariate distributions for the historical storm parameters, as well as for the same parameters for the 1250 selected scenarios. These are the most dissimilar scenarios. Comparing these histograms to the observation data (Figure 4.4) shows that MDA has selected the most dissimilar features (outliers) from the million synthetic scenarios.

The required number of scenarios depends on how the surrogate model errors converge and become stable. Because both the storm and profile parameters are used in the model development (with a total of 16 variables), we need to increase the number of simulations to minimize the errors in training the surrogate model. We tested this with K-fold cross validation (described in Section 4.5.4). The subset of 1,250 synthetic scenarios is much larger than the cases tested in previous studies; e.g. Santos et al. [2019] used only 100 synthetic storms to train their model.

4.5.3 Step 3: Morphodynamic Modeling

The next step is to use these synthetic storm scenarios as forcing to process-based, morphodynamic model simulations of the beach response. The eXtreme Beach (XBeach) model is selected due to its documented skill in predictions of beach and dune erosion during storms [Roelvink et al., 2009; McCall et al., 2010; Nederhoff, 2014]. Model grids are constructed by mapping beach profiles from the library onto synthetic domains, and model hydrodynamic forcings are constructed by using the storm parameters from the library to create 'triangular storms.' Then XBeach simulations are completed for the 1,250 storm/profile scenarios to predict the full physics of the beach response.

Table 4.1 Settings for XBeach input parameters in this study.

Parameter	Description	Value(s)
`morfac`	Morphological acceleration factor	10
`break`	Breaker formulation	`roelvink1`
`gamma`	Breaker parameter	0.42
`alpha`	Wave dissipation coefficient	2.0
`eps`	Threshold water depth for wet cells	0.01
`bdslpeffmag`	Sediment transport based on the bed slope	`roelvink_bed`

4.5.3.1 Numerical Model

XBeach (rev. 5559) is used to predict the beach response to the storm scenarios in Nags Head, NC. The model solves the time-varying, short-wave, action balance equation on wave-group scale to generate the radiation stresses. Then depth-averaged nonlinear shallow water equations are solved to compute the mean flow. The model includes dissipation [Roelvink, 1993], roller models [Svendsen, 1984], and infragravity waves by resolving the short wave variation and the long waves associated with them. Sediment transport is modeled with a depth-averaged advection-diffusion equation, and bed elevations are updated according to the Exner equation. The model is capable of simulating the morphodynamic behavior of coastal regions under different storm impact regimes with excellent Skill Score, as shown in other studies [Gharagozlou et al., 2020; Passeri et al., 2018].

The model is calibrated using several parameters for sediment transport, wave asymmetry and skewness, wave breaking, wetting/drying and avalanching processes (Table 4.1). These parameters differ from the default XBeach settings, but the selected values are consistent with recent studies [Gharagozlou et al., 2020; Kalligeris et al., 2020]. A morphological factor $f_{\text{mor}} = 10$ [McCall et al., 2010] was used to speed up the morphological evolution relative to the hydrodynamic time scale.

4.5.3.2 Representing Synthetic Beach Profiles on XBeach Grids

XBeach represents the nearshore geometry with a structured grid, on which the governing equations are solved at the grid nodes to predict hydro- and morphodynamics. For this study, two model grids were created: a full-domain grid for error evaluation and studies of 2019 nourishment performance, and a smaller-domain grid for batch runs to create a training library for the surrogate model (Figure 4.1). The full-domain grid extends 20 km alongshore (effectively covers 16 km of the nourished beach, with buffers at both ends) and about 4 km offshore on the ocean-side. It has 2000 cells in alongshore with spacing of 10 m and 306 cells in cross-shore with spacing varying from 2 m near the shore to 30 m at the offshore boundary. The bathymetry was interpolated from the August 2019 DEM.

For each batch simulation, a smaller-domain grid was created to represent a synthetic beach profile. These grids extend only 5 km alongshore and 4 km cross-shore, with similar cell spacings to the full-domain grid. These smaller grids enable faster simulations, which was critical for completing hundreds of simulations with a reasonable computational time. For each simulation, a beach profile was constructed from the PCs and corresponding EOFs, and then the beach profile was applied as a uniform alongshore bathymetry on the 2D grid. The 2D model better represents the alongshore currents and wave distributions along the offshore boundary. The beach profiles extend to about 1200 to 1500 m from the back-shore and depths of 8 to 12 m. We extrapolated the bathymetry using a power function to reach the depth of 22 m at the offshore boundary of XBeach. This assumption is reasonable and does not impact the erosion pattern nearshore and on the dunes.

4.5.3.3 Representing Synthetic Storms as XBeach Boundary Conditions

XBeach can receive hydrodynamic forcings at its offshore boundary in the form of time-varying waves and water levels. However, the synthetic sea-storms consist of single (peak) parameters for the hydrodynamic variables, and thus it is necessary to generate time series from the synthetic peak sea-storm parameters to apply as boundary conditions.

Simple approaches have been proposed to adapt a synthetic sea-storm shape to represent real sea-storms. The triangular shape [Corbella & Stretch, 2012; Laface et al., 2016] is the most frequent method applied due to its simplicity, where the storm parameters (i.e. significant wave height, wave period, and storm surge), are increased linearly from a base value to the maximum, and then decreased linearly back to the base value. For a triangular shape, the maximum coincides with the peak of the storm, which may or may not occur halfway through the storm duration. Previous studies have used triangular shape methods to generate the time series. Santos et al. [2019] tested the triangular shape method and showed that it leads to overestimation of the intensity for the most extreme sea-storm events. Therefore, they used standardized representative curves that are derived as the average of the 10 largest events on record. Duo et al. [2020] used symmetric triangular shape, in which the storm peak is assumed to occur halfway through the storm duration. Duo et al. [2020] showed that the energy of the storms, profile characteristics, and water levels did not consistently influence the differences between the synthetic and realistic outputs.

To introduce the time evolution, we used a simple symmetric triangular approach for surge η_{NTR}, wave heights H_s, and wave period T_p. These parameters start at a base value and then increase linearly to a peak (provided by copula and MDA) in the middle of the sea-storm duration, and then decrease linearly to the base value at the end of the event (Figure 4.7). The wave direction was assumed to be constant throughout each simulation. We performed a sensitivity analysis on different methods (realistic time series, asymmetric triangular, and symmetric triangular). In general, the realistic evolution of wave height is centered around the sea-storm peak, therefore, assuming a triangular form for a sea-storm can systematically increase its intensity. However, a sensitivity study showed that the extra erosion due to the symmetric triangular method is negligible. Additionally, this approach simplifies the process of generating time series for boundary conditions, and therefore it is a viable option.

Time series of water levels consist of three components: the surge with a symmetric triangular shape over sea-storm duration; mean sea level due to SLR, which is generated from MDA for each scenario and is added as a constant value to the water level for each storm; and the tides. The SLR

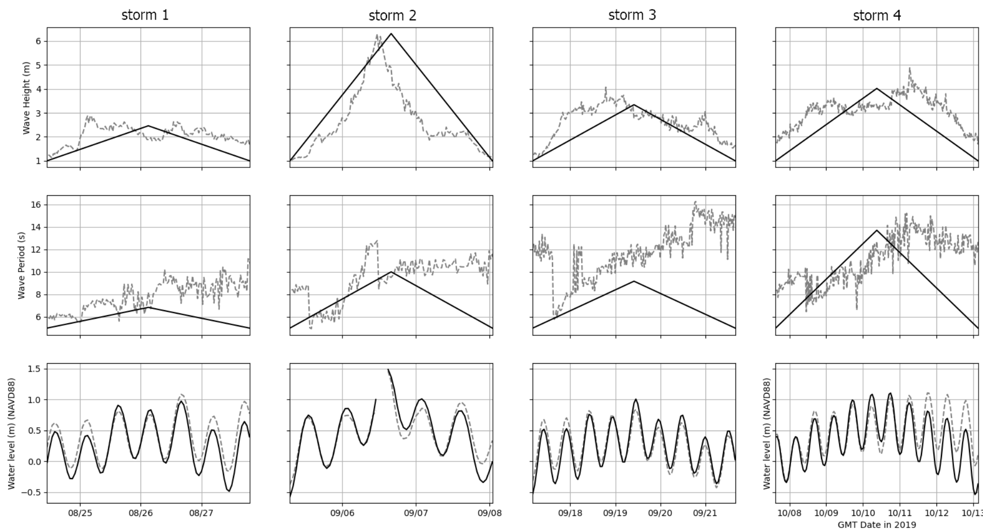

Figure 4.7 Symmetric triangle storm shape for (top) wave heights H_s, (middle) wave periods T_p, and (bottom) surge η_{NTR}. The wave direction (not shown) is assumed to be constant. The total water level includes the tides and MSL correction due to SLR. These four columns correspond to the four storms in Section 4.6.2.

Table 4.2 Tidal constituents and their corresponding amplitude and speed.

Constituent	Amplitude (A)	Speed (σ)
M_2	0.490	28.98
N_2	0.114	28.44
K_1	0.087	15.04
S_2	0.088	30.00

scenario is modeled using the Sea-Level Change Curve Calculator. The sea-level calculator provides a way to visualize the USACE and other authoritative sea level rise scenarios for any tide gauge that is part of the NOAA National Water Level Observation Network (NWLON) [USACE, 2021]. To generate the tides, the four tidal constituents with the largest amplitudes (M_2,N_2,K_1,S_2, Table 4.2) were combined as:

$$\eta = \sum_{i=1}^{N} A_i(\sigma_i . t + \phi_i) \tag{4.1}$$

The phase of the tidal components is generated randomly between 0 and 2π. We assume that the tide level with this phase occurs at the middle of storm duration, and thus the tidal time series are built out from the middle of the storm to the start and end.

4.5.3.4 Running XBeach Simulations

Then these boundary forcings were used to simulate the 1,250 synthetic scenarios of sea-storms and beach profiles. This process was automated to allow for efficient computations in a high-performance computing cluster.

A Python script was used to construct automatically the files for the model parameters, bathymetry and topography, and wave and water level boundary conditions for each XBeach simulation. The script reads a matrix of size 16×1250, which has 16 parameters (6 sea-storm parameters, 1 tidal phase, 9 EOFs) for each simulation. First, the symmetric triangular shapes for wave height, period, and storm surge over each sea-storm duration are generated. Then the tide is created by adding the four constituents. The total water level is generated by adding the tides, MSL, and triangular storm surge. These time series are then saved in a specific format to be used by XBeach.

The beach profiles are recreated from the EOFs and corresponding PCs. Then for each simulation, the script interpolates the profile on the grid to be constant in the alongshore. The bathymetry file is created and saved in a appropriate format for XBeach. Then the script modifies the model control file (`params.txt`) for each simulation based on the newly generated boundary condition and bathymetry file names, and adjusts the wave solver parameters based on wave angle.

The input files for each simulation include the water level and wave boundary condition files, the bathymetry file, model control, the mesh file, and job submission script to run the model on the NCSU high-performance computing cluster. These files are created in a separate folder for each simulation. Then all folders are copied to the HPC cluster and, using a shell script, the jobs are submitted to the computational cores. Each XBeach simulation requires 30 cores to compute the hydro- and morphodynamics and one core to read and write the inputs and outputs.

4.5.4 Step 4: Training the Surrogate Model

The XBeach simulations give process-based predictions of the beach and dune response to the sea-storm forcing, with each simulation representing a single combination of synthetic sea-storm and beach profile. These process-based predictions are complex, and thus they should be simplified before being used as training for the surrogate model. We represent the location and shape of the beach scarp in each XBeach simulation by using a simple function with only three parameters. These parameters are then used as training for the surrogate model.

4.5.4.1 Parameterizing Scarps

Before the XBeach simulation results can be used as training for the surrogate model, their complexity must be simplified. This parameterization could be done similarly to previous studies, e.g. with geometric features [Santos et al., 2019], a Gaussian function [Mickey et al., 2020], or the PCA described above for the input beach profiles. However, the XBeach-simulated shape of the scarped beach is very complex, and thus a large number of EOFs would be required to represent its variability. We want to maintain a small number of variables and a simpler parameterization. Therefore, we

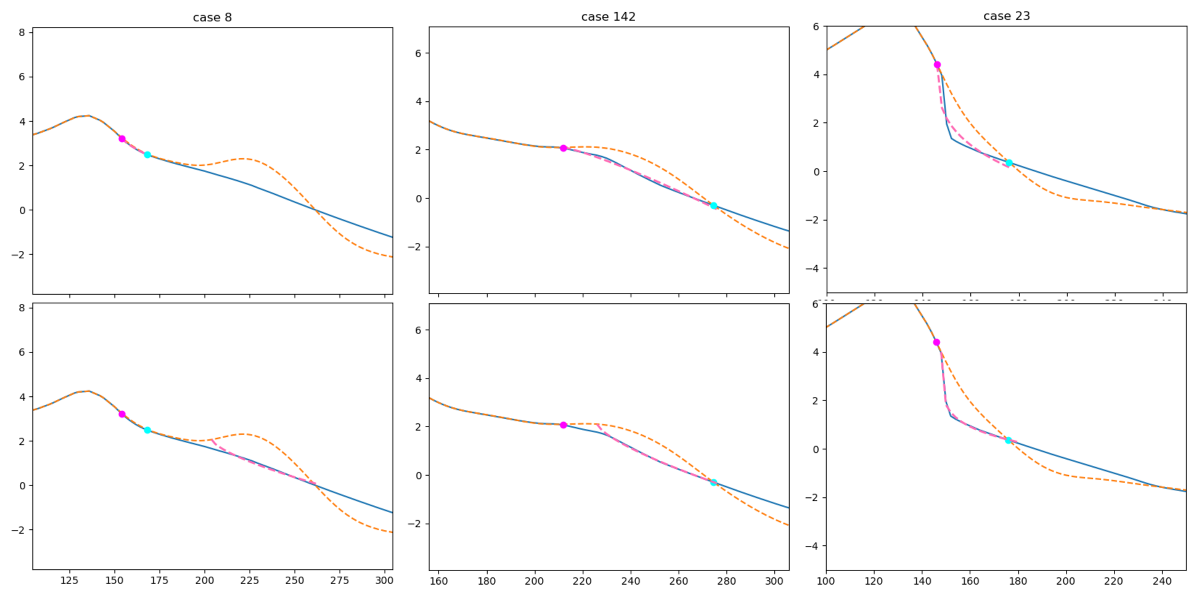

Figure 4.8 Fitting a power function to the scarp and using the parameters (A, B, and D_S) to train the model. The fitted line is shown in dashed magenta color. Top row shows scenarios for which the automated script failed to represent correctly the scarp. Bottom row shows the same scenarios with a manually fixed scarp.)

parameterize the main sub-aerial erosion with a simple power function.

First, for each simulation, we performed a quality check to ensure that the results were acceptable (and instability did not occur during the simulation), and then we extracted the beach profile in the middle of the domain for analyzing the storm-driven erosion. Then, the eroded section (scarp) of the beach was fitted with a power function:

$$z = A \cdot x^B \tag{4.2}$$

in which x is the alongshore distance, z is the ground surface elevation, and A and B are constants. We described the location and shape of each scarp with three parameters. The first two parameters (A and B) are the power function coefficient and exponent, which control the magnitude and curvature of the scarp, and the third parameter (D_s) is the distance of the starting point of the scarp from the shoreline (i.e. zero water level). These three parameters (A, B, and D_s) will be used to train the surrogate model, which will then be able to predict these three parameters (and thus the shape of the scarped beach) for any possible future scenarios.

A script was written to automate the process of finding scarp parameters. This automated approach can find the starting point of the scarp and fit a power function to the eroded profile (with examples in Figure 4.8). However, for some simulations, the script failed to parameterize accurately the scarp. The results were checked manually to be accurate for all profiles. In Figure 4.8a, the initial guess for the scarp was not correct and the code selected a portion with minor erosion on the beach. This was fixed by editing the distance (D_s). Another complex case that needed modification is shown in Figure 4.8b, where the power coefficient of the fitted line is greater than unity, which creates a concave fit. Although this guess is mathematically correct, for the consistency in the parameters we assumed that the fitted lines must be convex ($A < 0$). Therefore, the fitted line was corrected manually by slightly moving the starting point. This process was done for the scarped profiles from all 1,250 simulations, and the erosion data in the form of parameterized scarp shape were used to train the surrogate model. About 20 percent of the profiles had to be adjusted manually, but most adjustments required only a small revision.

4.5.4.2 Surrogate Model

Previous coastal applications have used a number of different statistical methods as the underlying function relating dynamical model inputs and outputs. Nearshore wave and surge predictions have been made using linear interpolation schemes [Allan et al., 2015], radial basis functions [Gouldby et al., 2014], Gaussian process regressions [Jia et al., 2016b; Pullen et al., 2018; Parker et al., 2019], artificial neural networks [James et al., 2018; Kim et al., 2015] and random forests [Tadesse et al., 2020]. We used Gaussian process regression (GPR), also known as kriging, as a machine learning tool to train the surrogate model and emulate the beach response to synthetic sea-storm scenarios. GPRs are commonly referred to as a distribution over functions because each predictand is described by a mean and a covariance function [Rasmussen & Williams, 2006]. GPRs are a supervised machine learning approach, necessitating that the user define the mean and covariance function structure, but automated optimizations subsequently tune free parameters to fit the training data. Their popularity in surrogate modeling is in part because they are highly generalizable, and surrogate models such as neural networks and radial basis funcations collapse to a GPR formulation under certain circumstances [Anjyo & Lewis, 2011].

Common mean functions include constant, linear, and quadratic functions. Covariance functions include exponential, squared exponential, higher order polynomials, and Matern functions that are a product of exponentials and polynomials [Rasmussen & Williams, 2006]. We chose linear functions to describe the mean and a Matern $5/2$ kernel formulation for the covariance. These decisions were made after an iterative tuning process to get the highest correlation between scarp fits and GPR predictions. Validations were performed with K-folding, where the model is trained K number of times and each time removes a portion of the library equal to $1/K$ for validation while using the remaining library for training. Each case in the library is only removed once, such that the model has made an untrained prediction of every case by the end of the validation. We chose K to be 5, and thus calibrated by removing 20 percent of the simulations in each fold.

4.6 Results

In this section, first the surrogate model is developed, by training with and then quantifying its performance against the library of synthetic scenarios. Then the surrogate model is applied, by exploring and quantifying errors in predictions of beach morphodynamics during four storms between August and November 2019.

4.6.1 Surrogate Model Development

We describe how the numerical model was used to simulate the beach erosion for each synthetic scenario. This is a crucial step for training the surrogate model, because: the model will be as accurate as the input data, and any errors in the numerical model prediction can transfer into surrogate model performance. We explore and discuss the variability of the XBeach erosion predictions and the scarp parameterization. Then, we validate the trained surrogate model for the testing set, and we compare the results to numerical model predictions.

4.6.1.1 Generating a Library of Erosion Prediction

The first step was to use XBeach for 1,250 simulations of the synthetic beach profile response to synthetic sea-storm scenarios. As noted previously, this library was larger than in previous studies, and it required automation to generate the XBeach input files and to submit and monitor the XBeach simulations. On the NCSU HPC cluster, each simulation was submitted to 31 cores so that multiple simulations could be executed simultaneously. The cluster hardware is heterogeneous, so the simulation run-times can vary significantly. However, on average, each day of XBeach simulation required about 2 hr of wall-clock time. The library had storms with a cumulative duration of 147,306 hr ($\sim$ 6,138 days), and it required a total wall-clock time of about 12,300 hr. The XBeach simulations were completed over a period of 25 days. The overall process required more than four weeks, including the file preparation, transferring data to and from the cluster, job monitoring, and quality checks.

A small number of simulations failed due to instabilities, especially for simulations with large waves coming from the south and with long durations. For the simulations in which the model crashed due to instability in the boundaries, we analyzed the results and debugged the issues. One issue with XBeach was in the lateral boundary at the northern section of the domain. This boundary was sensitive to waves coming from the south and at a very steep angle (close to shore parallel). For the simulations that crashed due to this issue, we flipped the wave orientation, so the waves approached from the north. This solution does not affect the physics of the simulation, because the bathymetry is uniform and the water level is also uniform along the offshore boundary. These few simulations were re-run to obtain the erosion predictions at their center profiles.

The majority of center profiles in the XBeach simulations experienced considerable erosion. In some simulations, the beach center profile was eroded significantly (Figure 4.9a). Depending on the intensity of the storm and shape of the profile, the erosion could extend to the dune (Figure 4.9b) or even remove the dune face and slightly affect the dune crest (Figure 4.9c). However, this extensive erosion did not occur frequently. The dune crest elevation was changed in only 9 simulations (out of 1250). There were many simulations with moderate to mild erosion, in which the beach was slightly lowered or small scarping occurred on the beach berm (Figure 4.9d). Based on these simulation results, we computed the sub-aerial erosion for the center profiles of the 1250 simulations

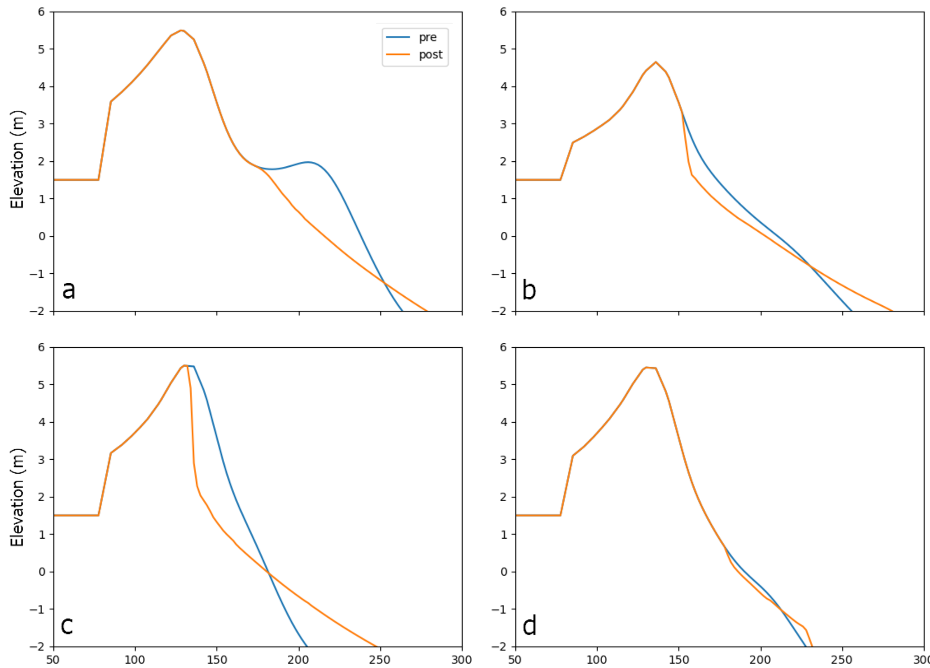

Figure 4.9 Examples of beach response to synthetic storms: (a) significant erosion on the beach and berm, (b) erosion on the beach and dune face, (c) dune erosion, and (d) minor erosion on the beach.

(Figure 4.10-i). The average volume of erosion was about 23.5 m^3/m, and the maximum erosion was 95.4 m^3/m. More than 53 percent of the profiles experienced erosion of more than 20 m^3/m. These data and the distribution of the erosion volumes show that a wide range of potential scenarios were simulated and considered for training the surrogate model. While this information gives details of erosion on the beach, we need to compile it into a format that can be used in surrogate model; therefore, we parameterize the scarps.

Figure 4.10 shows the distribution of the scarp parameters for 1250 scenarios. To keep the analysis consistent, we intentionally parameterized the scarps to be convex. Therefore, the B exponent must be between 0 and 1, and the A coefficient must be less than zero. The shoreline distance D_s had an average of about 31 m with maximum of 90 m. This information, along with the sea-storm and profile parameters, were used to train the surrogate model. Additionally, the validation process was conducted after removing 9 extreme storm scenarios that lowered or removed the dune so completely that the post-storm morphology did not adhere to the exponential fit found in all other simulations. These extreme cases are outliers and including them in the training process could increase the errors in surrogate model.

4.6.1.2 Surrogate Model Training

As described previously, the surrogate model was trained and validated with K-folding. The surrogate model was trained with subsets of 1000 design scenarios, and then its performance was evaluated

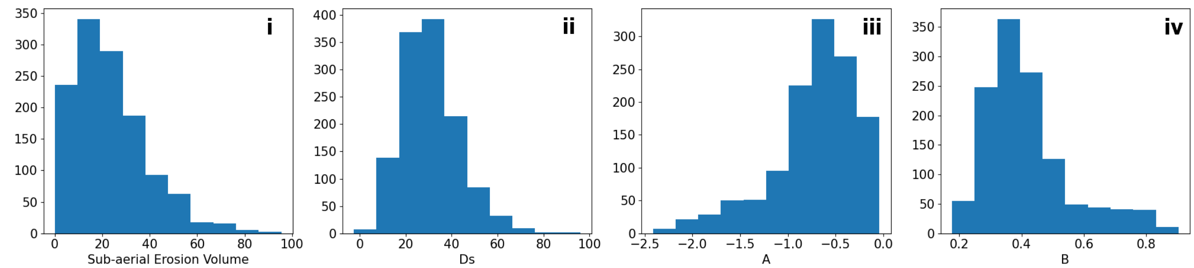

Figure 4.10 Distribution of A, B, and D_s for parameterized scarps and the sub-aerial erosion volume for 1250 modeled results.

against the remaining 241 testing scenarios. For each fold, these remaining scenarios were new to the surrogate model (i.e. the model had not seen or been trained with them).

In comparisons of the scarp predictions between the surrogate model and XBeach, there is a good qualitative match for a majority of scenarios (Figure 4.11). Scenarios (i) to (vi) are representative of the surrogate model's ability to predict the erosion of the profiles. Scenario (i) shows the erosion of a nourished profile. The location where the scarp starts (described with distance D_s from the pre-storm shoreline) is predicted well and the fitted curve (described with parameters A and B) has captured the shape of the scarp. In scenario (ii), a large portion of the beach and the berm were eroded. The prediction matches well with the XBeach results and accurately captures D_s as well as the scarped curve. In scenario (iii), the erosion is extended to the dune face. The surrogate model predicted the starting point accurately and fitted a curve that is very close to the XBeach prediction. Scenarios (iv) and (v) show that the surrogate model produced very reliable results for different beach and erosion conditions. In scenario (vi), the beach is slightly lowered due to erosion and there isn't any significant steep scarp in the profile. Surrogate model replicated the erosion very well. In these representative scenarios, the good match to the scarp will translate into good predictions of the eroded volume.

While these results are great and promising, there are some inaccuracies in the surrogate model predictions (Figure 4.11). For scenario (vii), there is an error in the horizontal start place of the scarp, which is too far landward by about 10 m, therefore, the erosion is over estimated. The predicted curve in this case, however, tries to capture the shape of the eroded scarp. Scenario (viii) shows a considerable error as the beach profile has been predicted to be not steep enough. The errors in D_s and the scarped curve resulted in under-prediction in erosion. Although the starting location of the scarp is predicted accurately in scenario (ix), the fitted curve has overestimated the erosion. These are some of the scenarios that surrogate model could not predict well, however, the number of poorly predicted profiles is much smaller than the accurate predictions. Additionally, our focus is on the sub-aerial erosion of beach profiles. Therefore, any errors in the shape of the scarp in the sub-aqueous will not carry forward to the eroded volumes.

We evaluated the accuracy and errors of the surrogate model predictions for the 1,241 remaining scenarios in each of the K-folds. For each scarp parameter (A, B, D_s), we compare the surrogate

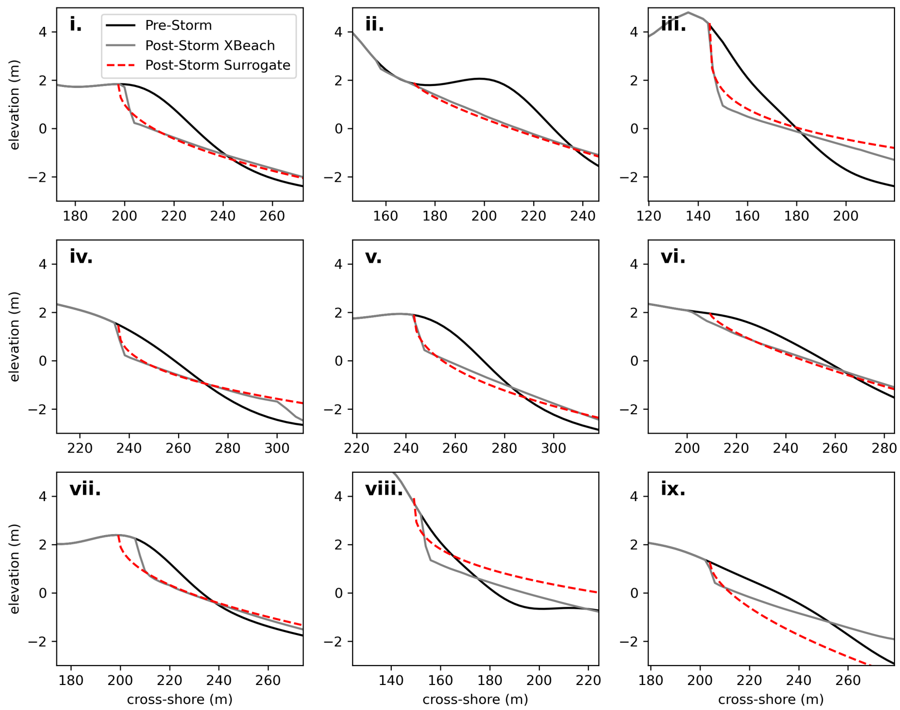

Figure 4.11 Surrogate model prediction of the scarp (red line) compared to XBeach predicted profile (grey): 6 good results on the top rows and 3 bad results along the bottom row.

model predictions with scarps fitted to the XBeach predictions, by using metrics of the correlation coefficient R^2:

$$R^2 = 1 - \frac{\sum_{i=1}^{N}(x_i - f_i)^2}{\sum_{i=1}^{N}(x_i - \bar{x}_i)^2} \tag{4.3}$$

and the root-mean-square error E_{RMS}:

$$E_{RMS} = \sqrt{\frac{\sum_{i=1}^{N}(x_i - \hat{x}_i)^2}{N}} \tag{4.4}$$

in which x is a surrogate model prediction, $\bar{x}$ is the average surrogate model prediction, $\hat{x}$ is the XBeach prediction and f is the linear regression between XBeach and surrogate predictions for N data points. The 5-fold validation of the D_s resulted in an $R^2 = 0.97$, with an $E_{\text{RMS}} = 2.98$ m. The distribution of predicted D_s by XBeach (Figure 4.10) shows that the distance of scarp from the shoreline can be as large as 100 m. The small E_{RMS} proves the accuracy of the surrogate model for this parameter. The A parameter returned an $R^2 = 0.96$ with an average $E_{\text{RMS}} = 0.11$. The B parameter had the lowest $R^2 = 0.91$ and an average $E_{\text{RMS}} = 0.06$. The R^2 values for predicted A,

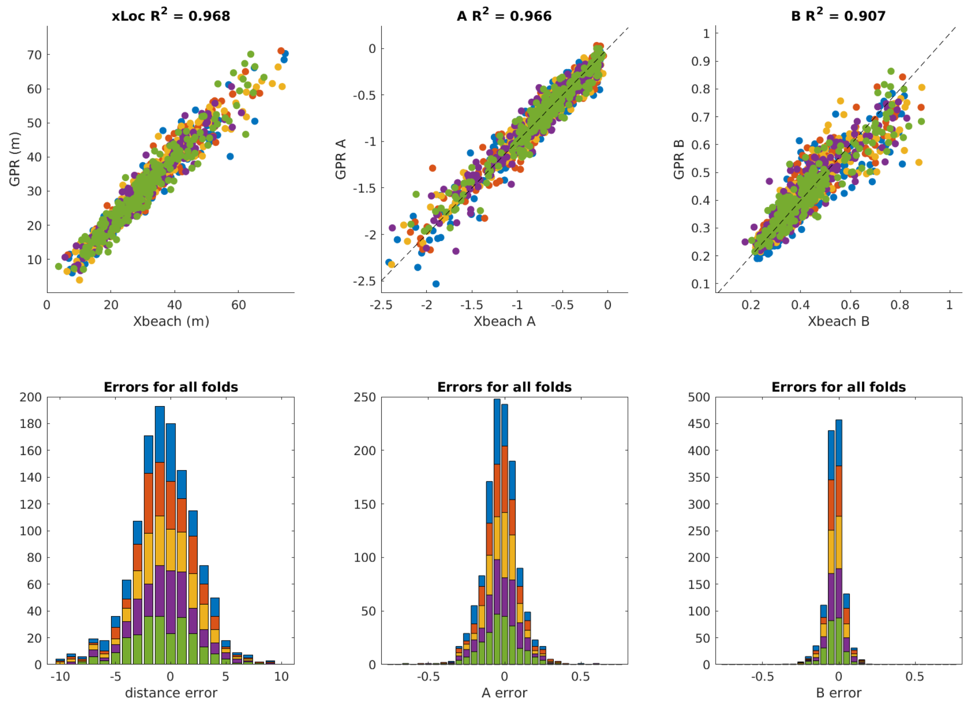

Figure 4.12 K-folding errors for the testing set for each of the scarp parameters A, B, and D_s: (top) scatter plot predictions for surrogate model vs XBeach, and (bottom) distribution of errors (surrogate minus XBeach). Colors show predictions from each of the 5 training tests in the K-fold validation.

B and D_s are very close to unity, and thus the surrogate model performed well in predicting the location of the scarp and the magnitude and curvature of the scarps.

Figure 4.12 shows the distribution of errors for each of the parameters and for each fold. The scatter plots for all folds are very close to the 1:1 line and the R^2 value is close to 1. The distribution of the errors for each fold is similar to a Gaussian distribution, which validates the use of GPR for training the model. Note that in these plots, the distributions of errors for all folds are very similar, and therefore we do not observe any bias for a specific portion of the data set. Additionally, the predicted volumes of erosion for these cases were compared to the XBeach prediction (Figure 4.13). The surrogate model predictions have a close correlation to XBeach, with a median absolute error of 2.53 m^3/m, which is about 11% of the average eroded volume.

These results prove that this approach to develop and train a surrogate model was successful. The trained surrogate model can predict the shape of the eroded beach for many new scenarios (different beach profile and storm condition) within seconds (compared to a traditional numerical model that can take hours). Even though there is a slight overestimation for erosion, given the performance gain, accuracy, and the decrease in computational time, the results are promising. Additionally, the surrogate model will eventually be used for prediction and design of nourished beach erosion. A slight overprediction is a conservative assumption in the design and thus acceptable.

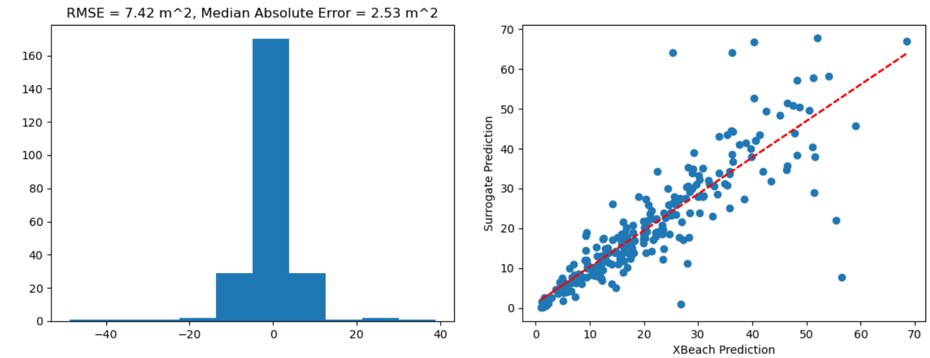

Figure 4.13 Error distribution of erosion volume predicted by surrogate model compared to XBeach predictions for the subset of 241 testing cases.

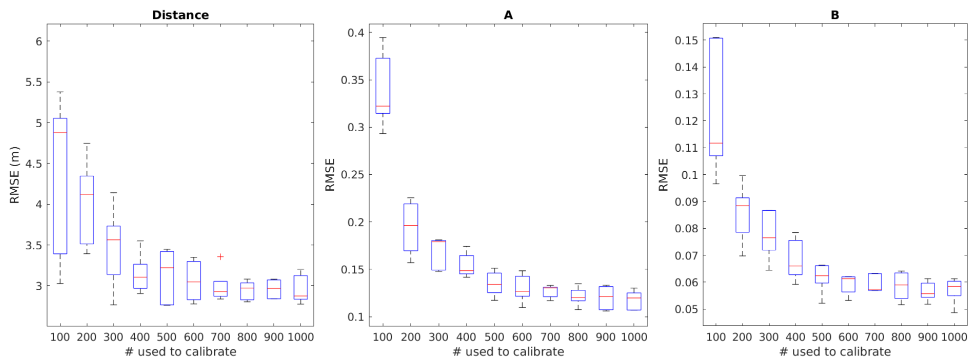

Figure 4.14 The root-mean-squared error for each scarp parameters for different library sizes. The horizontal axis shows the number of scenarios used in 5-folding validation of the model. Errors decrease with larger library sizes. As shown here, the errors reach an asymptote for library size of greater than 600. These box plots show the minimum, the maximum, the median, and the first and third quartiles of the data.

Figure 4.14 shows the decrease in the RMS error for each of the predicted variables (D_s, A, and B) as the number of testing cases is increased. The errors reach an asymptote, which shows that the number of training scenarios is sufficient to minimize the errors. With 1000 training cases, the E_{RMS} for D_s distance is 3 m, and the errors for eroded profile coefficient A and exponent B are 0.11 and 0.06, respectively.

4.6.2 Application to 2019 Nags Head Nourishment and Storm Season

With confidence that the surrogate model is working as designed, its performance is now evaluated for predictions of the response of a real beach nourishment to real storms. Nags Head is an ideal setting for this evaluation, as its most-recent nourishment is described by surveys before and after a busy 2019 storm season. In this section, the surrogate model is applied to predictions of cumulative sub-aerial beach erosion and sand volume losses due to four storms. Then the model performance is deconstructed to quantify errors due to our simplification of real conditions for nearshore processes, waves and water levels, and beach geometries.

4.6.2.1 Storms and Beach Profiles

We applied the surrogate model to predict the beach response in Nags Head, NC. Its nourished beach is surveyed frequently, including multiple surveys per year. During 2019, the beach was surveyed after a nourishment project in August, and it was surveyed again at the end of hurricane season in November. Between these two surveys, the beach was affected by four major storms, which resulted in notable erosion.

The observed waves and water levels for these storm events and the simplified symmetric triangular form of their parameters are shown in Figure 4.7. The first storm started on 11:00 UTC 24 August and had a maximum significant wave height of 2.9 m. A week later on 7:00 UTC 5 September, the second storm (tropical cyclone Dorian) affected Nags Head beach. Dorian had significant wave heights as large as 6.3 m, wave periods of 12 s, and storm surge of 1.1 m. Dorian affected the study area for about 66 hr. The third storm event occurred between 4:00 UTC 17 September and 12:00 UTC 21 September. Its maximum significant wave height was 4 m with maximum surge of 0.5 m. The fourth storm started at 15:00 UTC 7 October and continued for 132 hr with maximum significant wave heights of 4.1 m and surge level of 0.8 m.

The pre-storm bathymetry of the region was extracted from the August 2019 survey and interpolated onto a regular grid. The grid consists of 2000 cross-shore profiles with 10-m spacing alongshore. To maintain stability in the XBeach simulations, there are 400 profiles as buffers at the lateral boundaries of the domain. Therefore, for both XBeach and surrogate model, the storm-driven erosion was predicted on 1600 realistic profiles in the middle of the grid. These profiles were extracted and converted to EOFs and then used in the surrogate model as profile inputs. Additionally, the parameters for the four major storm events were used as the storm inputs (red dots in Figure 4.6).

4.6.2.2 Applying the Surrogate Model to Sequential Storms

The surrogate model was used to predict the beach response to the sequence of storms in a chronological order. These sequential storms require additional processing between predictions, because the output of scarp parameters from one storm must be translated into inputs of EOFs for the next storm. The surrogate model only takes the parameters (i.e. sea-storm parameters, EOFs of beach profile) as inputs, therefore, the initial profile is parameterized in the EOF space. Then it runs for the first storm parameters and predicts the erosion of the beach profile in the form of three scarp parameters (A, B, and D_s). These parameters are then used to reconstruct the full beach profile (from the back-dune to offshore) with the scarp on the beach. Before running the next storm, the scarped profile is converted to EOFs again. Then, the surrogate uses the second storm parameters and the latest EOFs to predict the scarp parameters due to the second storm. This process repeats for all profiles and until all storms are modeled.

Figure 4.15 shows the evolution of one of the profiles as an example. The scarp for the subaerial portion is predicted by the surrogate model, and a straight line is used to connect the zero

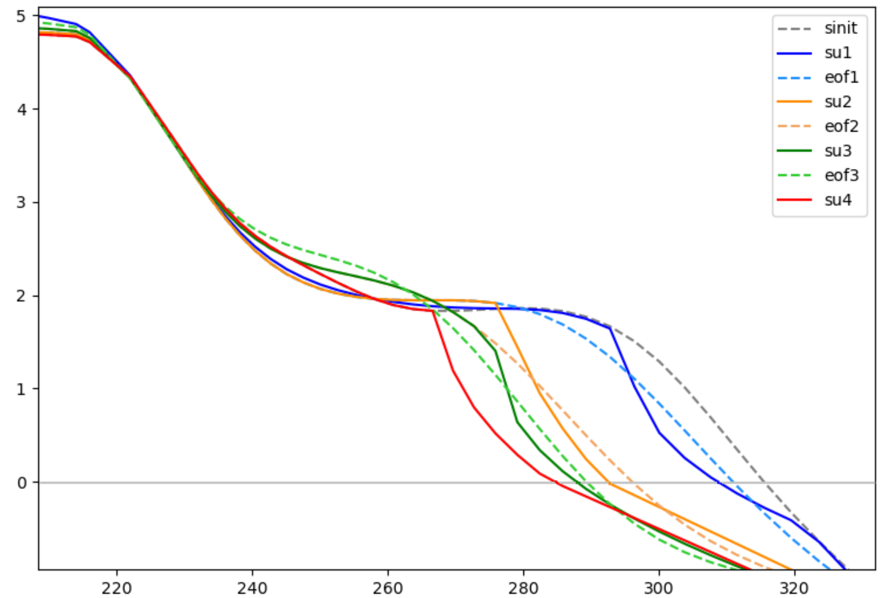

Figure 4.15 Surrogate model prediction after each storm (solid lines) and the re-parameterized profiles with the EOFs (dashed lines) as the initial condition for the next storm. The initial pre-storm profile shown with the dashed grey line. The surrogate model predicted the scarped profile due to first storm (solid blue line). Then this profile is parameterized in EOF space to create the initial profile (dashed blue) for the next storm. This process repeats for second, third and forth storms (orange, green, and red).

contour of the prediction to the −3-m contour of the pre-storm profile. The colored lines show the surrogate model prediction for each storm and the dashed lines show the conversion of each surrogate prediction to EOF form. The model is initiated with the EOF-based DEM (black solid line). Based on this initial profile and first storm parameters, the surrogate model predicts the scarping of the first storm (in the form of A, B, and Ds). The new profile is reconstructed using these parameters (blue line). To run the model for the next storm, the blue line must be parameterized in EOF space (dashed blue line). Then, with this parameterized profile and second storm parameters, the surrogate model predicts the scarp due to the second storm. This process repeats for all four storms. The final predicted profile (red line) affected by all four storms is remarkably close to the post-storm observation of the beach in November 2019. It is noted that we are neglecting the recovery that can occur after storms, which can lead to overprediction of the erosion.

These repetitive steps of parameterizing the scarped profile with EOFs may add errors to the model predictions. As shown for the profiles in Figure 4.15, the dashed lines are shifted seaward at the zero elevation contour due to EOF parameterization. Therefore, for each next storm, the location of scarp D_s may contain this error. To quantify this potential error, we extracted the shoreline (zero elevation) location and the erosion volume for each of these storms and for both the initial surrogate prediction (solid colored lines) and EOF form (dashed grey lines) (Figure 4.15). Figure 4.16 shows

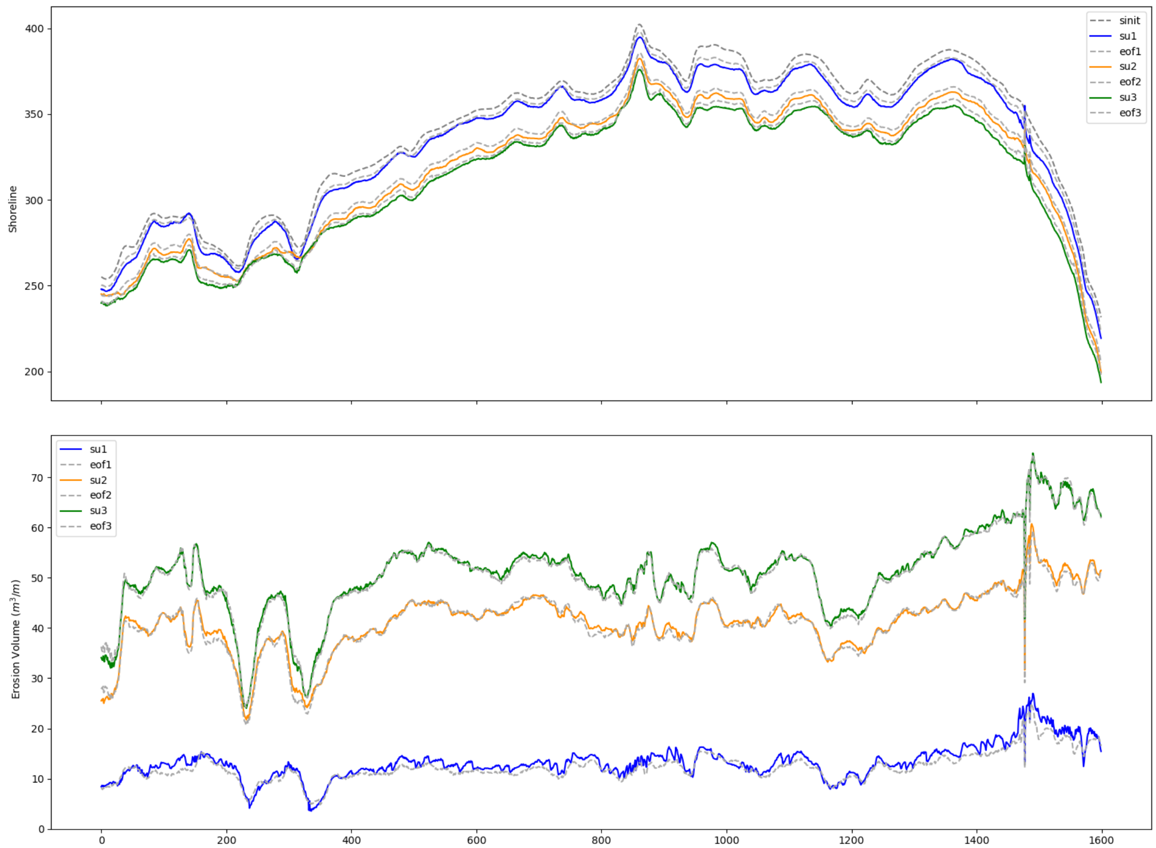

Figure 4.16 Differences due to parameterization of scarped profiles between storms, for (top) shoreline position (m from the back boundary) and the sub-aerial erosion (m^3/m). The horizontal axis shows alongshore profile number from north (left) to south (right).

that the shoreline is shifted toward the ocean when the profiles are recreated with EOFs. This is important because the surrogate model predicts the scarp starting point based on the distance from the shoreline D_s. Therefore, errors in the location of shoreline can ultimately change the stating point of the scarp. Additionally, parameterizing the scarped profile with EOFs will smooth the profile and consequently clip the spike on the berm. This also can add error for prediction of next storm; for example, the dashed orange line smoothed out the berm and has a lower elevation than the solid orange line at that location. Consequently, the predicted scarp for the green line starts at a lower elevation. Although these parameterizations can affect the scarp shape, the predicted total volume of erosion does not change significantly in this process. Figure 4.16 shows the volume of erosion for the surrogate profiles and EOF-based profiles. This analysis shows that the repetitive process of parameterizing the scarped profile with EOFs does not change the volume of erosion. However, the shift in the shoreline and the changes in the shape of the profile can add errors cumulatively to the final predictions.

Figure 4.17 The shoreline location (distance from the back boundary) and the sub-aerial erosion after all storms for each level; realistic forcing and realistic bathymetry (RR), simplified forcing and realistic bathymetry (SR), simplified forcing and bathymetry (SS), and surrogate model predictions.

4.6.2.3 Surrogate Model Predictions of Cumulative Nourishment Response

The final prediction from the surrogate model at the end of four storms was compared to observations and the XBeach predictions. The results for shoreline location show that surrogate predictions are very close to the observations. In Figure 4.17, the surrogate model prediction of the shoreline in the middle and southern part (reaches 2, 3, and 4) is very close to post-storm observed shoreline. In reach 1, there is a significant variation in the location of the observed shoreline between profiles 450 and 700. The surrogate model could not capture all of these small seaward/landward shifts, however the prediction is very close to the overall location of the shoreline. The model predicted an average shoreline shift (compared to pre-storm location) of 23.28 m, which is comparable to observed post-storm shift of 23.40 m. Moreover, the observed sub-aerial erosion volume along the study area shows a huge huge spike in the southern part (reaches 3 and 4) and part of reach 2 (between profile 350 and 650). The surrogate model underpredicted the erosion in these regions; however, for the rest of the domain, the predictions are close to observed erosion. Note that we observe similar patterns of underprediction in the XBeach model results as well. This shows that the inaccuracy in XBeach is the main source of error in surrogate model predictions.

Ultimately, one of the main goals of developing the surrogate model was to reduce the computational time. The surrogate model predicted the erosion of beach profiles due to four storms in a

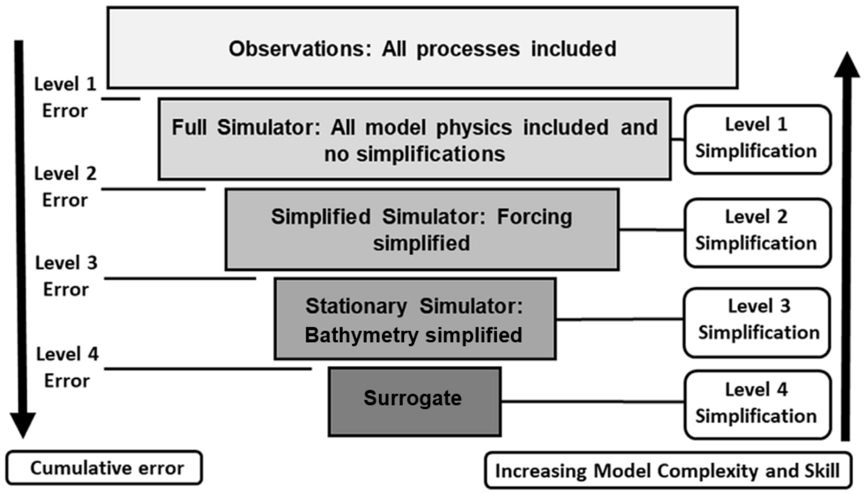

Figure 4.18 Schematic representation of different levels of simplification and associated errors from observation to surrogate model.

very short time of less than 20 s. The computational time required for running all four storms on the larger mesh with XBeach was about 40 hr. This is a significant improvement for the computational time requirement. The other advantage of the surrogate is that it does not require a HPC platform and can run on a laptop/desktop machine. The exact run time for the surrogate model depends on the system's CPU power and available memory, however, it is still thousands times faster than time-consuming numerical models.

4.6.2.4 Quantifying Errors due to Levels of Simplification

Multiple simplifications were used to develop the surrogate model. Storms were parameterized from historical wave and water-level conditions, beach profiles were constructed from principal components of ground surfaces from surveys, and XBeach was used to simulate the storm-driven erosion of the beach and dune system. While these simplifications are necessary to enable the statistical analyses, each simplification has an associated error, and these errors can accumulate in the final predictions (Figure 4.18). In this section, we quantify each error via a systematic analysis of the simplifications in our surrogate model.

Errors can be introduced at each simplification step. First, the real hydro- and morphodynamics were simulated with a process-based, numerical model, which can introduce errors due to its physical parameterizations and numerical discretization. Previous studies have identified that this step can be the largest portion of the cumulative error despite using our best mathematical approximations of the real world [Parker et al., 2019]. The errors from this first step are then compounded by errors in the following steps. Next, the complex time series of waves and water-levels were represented as symmetric, triangular storms. Then, the complex bathymetries and topographies of the Nags Head beach system were represented by profiles reconstructed from EOFs representing

Level	$\overline{E}_{\text{shoreline}}$	$\overline{E}_{\text{volume}}$	$E_{\text{RMS,volume}}$	SS	R^2	Best Fit Slope
1	8.77	12.28	18.69	0.66	0.67	0.48
2	2.21	5.50	7.25	0.93	0.89	0.76
3	0.81	0.79	3.41	0.89	0.92	0.96
4	9.63	10.41	11.58	0.81	0.61	0.90

Table 4.3 These are stepwise metrics - every level compared back to the level immediately above it.

Level	$\overline{E}_{\text{shoreline}}$	$\overline{E}_{\text{volume}}$	$E_{\text{RMS,volume}}$	SS	R^2	Best Fit Slope
1	8.77	12.28	18.69	0.66	0.67	0.48
2	9.56	15.79	23.15	0.63	0.61	0.37
3	9.73	15.87	23.1	0.63	0.64	0.38
4	7.35	11.13	19.51	0.66	0.52	0.40

Table 4.4 These are cumulative metrics - every level compared back to the original surveys.

97 percent of their variance. Last, the process-based numerical model was replaced by a surrogate model, which can introduce errors due to the quality of its training. For all of these levels, the errors can be quantified by comparing both to the previous level (Table 4.3) and to the observed beach nourishment response (Table 4.4). We describe and evaluate each level of error by computing several metrics including Skill Score (defined in an earlier chapter as Equation 2.2), shoreline location, eroded volume, E_{RMS} (Equation 4.4) and R^2 (Equation 4.3).

The first level of error, introduced in the transition from the Nags Head monitoring surveys to a complete XBeach simulation, is expected to be the largest portion of the cumulative error. The embedded error within this step derives from the model inaccuracy to represent complex beach morphodynamics. To evaluate the model accuracy, we calculated the shoreline change, the average volume change above the zero water level, and the Skill Score, and then compared to the expected volume change between the August and November surveys.

The shoreline location and erosion volume for beach profiles along the shore are shown in Figure 4.17. These results show that generally the southern part of the domain is eroded more than the northern part. The average volume of erosion for profiles in reach 3 and 4 is about 110 m^3/m while for reach 1 is about 50 m^3/m. A qualitative comparison of the results show that XBeach underestimated the erosion in a portion of the beach in the middle of the domain (reach 1) and in the southern section (reach 3). The shoreline predicted by XBeach is shifted toward the ocean compared to the final observation (Figure 4.17 top). The average absolute difference between the modeled and observed shoreline is about 8.77 m. Figure 4.19a shows the correlation for the sand volume between the model and the surveyed DEMs for each reach. There is a slight under-prediction of erosion volume by the model that is focused in the southern section of the study area. The regions further north (reach 1 and 2) have a stronger correlation to the observed erosional response. The median absolute difference between the modeled and observed erosion volume is 12.28 m^3/m with

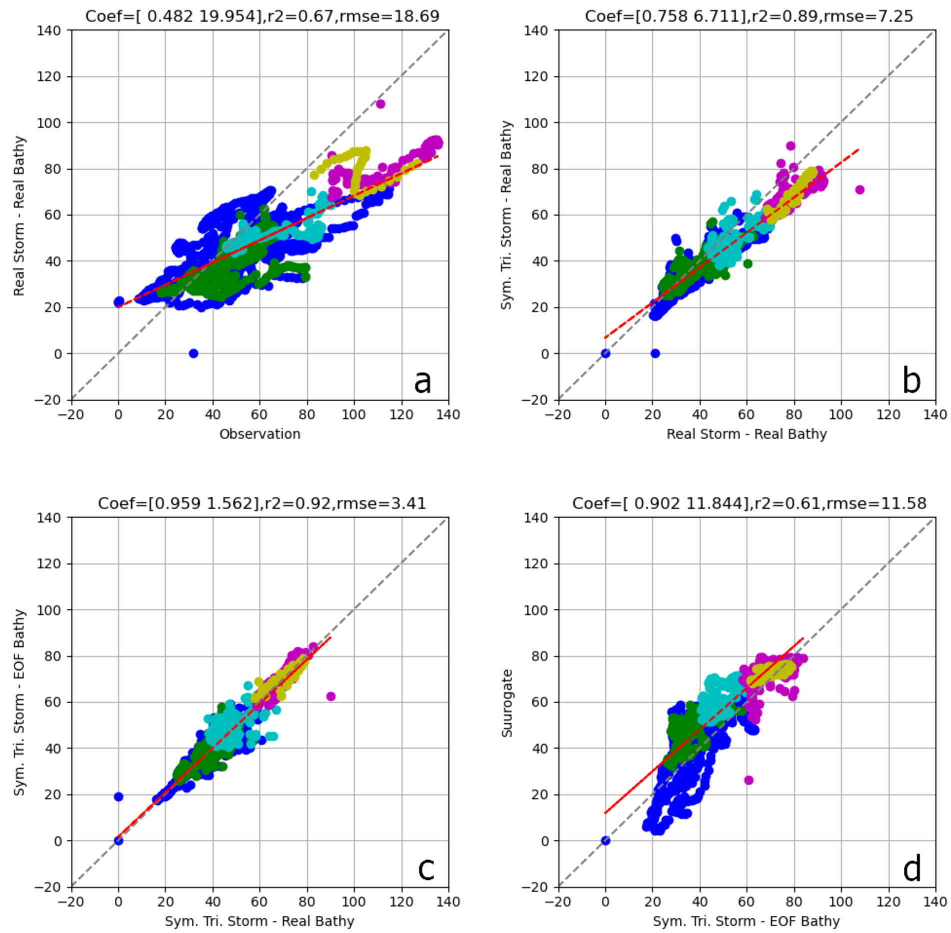

Figure 4.19 Scatter plots of erosion volume comparison for each level of simplification to the previous level (step-wise error).

an $E_{\text{RMS}} = 18.69$ m^3/m and $R^2 = 0.67$. We also computed the Skill Score for the profiles along the shoreline. The average Skill Score is 0.66, which is in the 'excellent' range [Sutherland et al., 2004].

Next, the sea-storm forcings were simplified into symmetrically triangular shapes, in which the peak of the storm hydrodynamics is centered in the middle of the storm duration (Figure 4.7). The shoreline location is very close to previous case with realistic forcings and is eroded less compared to the observed shoreline (Figure 4.17). The average absolute difference between the modeled and observed shoreline is 7.35 m. A comparison between the real and simplified forcing simulations demonstrates the error (Level 2) that is introduced through water forcing simplifications. Simplified forcings resulted in only a slight under-prediction of erosion, mostly in the southern part (reaches 3 and 4) and some locations in the north (reach 1). When compared to the one-to-one line between the real and simplified forcing XBeach simulations, the average volume eroded is correlated very well (Figure 4.19b). The average difference for the erosion volume between these 2 cases is about 5.5 m^3/m. The average Skill Score for for the profiles is 0.63. These results show that Level 2 errors are negligible and simplifying the storms for training the surrogate model is reasonable.

Then, the beach profiles were simplified by using the 9 EOFs for the 2019 DEM. These EOFs were generated from and then used to recreate a simplified form of the bathymetry. It is important to quantify the errors and inaccuracies introduced to the model results by simplifying the bathymetry, because the surrogate model also is trained with parameterized profiles. We simulated the effects of the four simplified storms on the simplified bathymetry. Errors added in this step are computed by comparing the volume of erosion to previous results. Figure 4.19c shows the volume of erosion and deposition compared to previous case. The points are close to one-to-one line and have a strong correlation to the simulation with realistic bathymetry. This also proves that the Level 3 errors are not substantial and are negligible compared to the Level 1 error.

Last, Level 4 includes all previous errors and the uncertainties and inaccuracies in the surrogate model. We tested the model for 2019 major storms. The results for one of the profiles was shown and discussed in section 4.6.2. The Level 4 errors are quantified by calculating the Skill Score and and comparing the erosion volume and E_{RMS} of the surrogate model to observation. The cumulative average absolute errors for the shoreline prediction and the erosion volume are 7.35 m and 11.13 m^3/m, respectively. The E_{RMS} for erosion volume is 19.51 m^3/m. When the surrogate predictions of erosion is compared to Level 3 predictions, it shows an $E_{\text{RMS}} = 11.58$. The scatter plot in Figure 4.19a shows that the Level 1 error comprise the main portion of errors. Figures 4.19b-c show the step-wise Level 2 and Level 3 errors in erosion volume. These scatter plots are very close to the one-to-one line, indicating that parameterizing the sea-storm and beach profiles produced very minor errors ($\bar{E}_{volume} = 5.5$ m^3/m for Level 2 and 0.79 m^3/m for level 3).

Thus, the errors in the surrogate model are mainly due to XBeach errors that transferred into the model during the training steps, and partially due to the process of parameterizing inputs for consecutive storms.

4.7 Discussion

We described a framework to develop a surrogate model by combining deterministic model predictions with a probabilistic-based approach. In this section, we discuss the main findings and the novelty of this study. Our findings have several implications for understanding the performance of the surrogate model and its strengths and weaknesses. Then we provide suggestions for future improvement of the model.

The first novelty of this study is including the initial state of the beach in the training parameters, which enables the surrogate model to account for cumulative erosion due to multiple storms and to be applied to any beach state. Similar studies have not trained for variability in the beach profiles [Santos et al., 2019; Mickey et al., 2020]. We used only 9 EOFs to reduce the dimensionality of the beach profiles, instead of describing the bathymetry variation at every point along the cross-shore profile. The EOF #1 captured variability in the nourished portion of the beach. The model synthesized the a highly variable and dynamic aspect of nourishment profiles into EOFs. As we showed for the beach erosion during the 2019 storm season, the model was able to predict the erosion from a sequence of sea-storms, by carrying forward the beach profiles from sea-storm to sea-storm. This is possible because the surrogate has been trained with a large library of potential beach profile shapes. Therefore, even though the shape of the profile changes after each storm, the resulting profile is (with a high chance) a viable starting point for the next storm and is within the bounds of the training set.

Another novelty was the size of the training library. Previous studies to develop surrogate models have only used sea-storm parameters, and therefore the models were trained with smaller training sets. For example, Santos et al. [2019] trained their model with 100 synthetic storms. We parameterized the beach profile with 9 EOFs in addition to 6 sea-storm parameters. This implementation required an increase in the number of synthetic scenarios for model training to convergence in the surrogate model accuracy (Figure 4.14). Training the model with more scenarios can generally improve the accuracy. The surrogate model was trained by performing 5-folding validation on a library of 1,241 valid scenarios. The E_{RMS} errors for the scarp parameters A and B were 0.11 and 0.06, respectively. Figure 4.14 shows that E_{RMS} for the erosion parameters reach an asymptote for larger library size. Although these results are for synthetic scenarios and only for a single storm, surrogate model could reproduce the XBeach predictions for the testing set with high accuracy.

A third novelty was the parameterizations of the scarps with the power-law function. Previous studies [Santos et al., 2019] have used geomorphic features such as horizontal and vertical changes in dune crest and toe elevations, changes in beach width, etc. While these parameters can be used to estimate the storm impacts, they do not preserve the exact shape of the beach. Using a power function allows us to (a) reduce the number of erosion parameters to three, (b) maintain the volume of erosion and directly calculate the erosion volume, and (c) reconstruct the eroded beach profile shape as the initial condition for the next storm. We used a semi-automated process to identify the scarps in the training set. Although in a few cases the power fit was not able to capture the entire scarp, the surrogate results show a promising performance with $E_{\mathrm{RMSE}} = 7.42\ \mathrm{m}^3/\mathrm{m}$ for the erosion volume of the 241 testing cases.

Another finding was about the contribution of simplification errors to the model. To develop the surrogate model, the parameters were required to be simplified to reduce the dimensions of variability in the inputs. Each of these intended simplifications can introduce different degrees of inaccuracies to the model. We evaluated the errors and uncertainties by testing for a realistic scenario of four storms during 2019. The total error was broken into four levels. The results showed that Level 1 error, which derives from numerical model inaccuracies, has a major contribution to the cumulative error. The errors in volume of erosion for XBeach results compared to observation is $12.28\mathrm{m}^3/\mathrm{m}$ (Table 4.3. It was shown that Level 2 and 3 errors are trivial compared to Level 1 error. When the erosion volume for Level 2 simplification is compared to Level 1, the error is $5.5\mathrm{m}^3/\mathrm{m}$, which shows the added error due to Level 2 simplification is less than half of the Level 1 error. The error due to Level 3 simplification is even smaller ($5.5\mathrm{m}^3/\mathrm{m}$). These results prove that our approach for simplifying the bathymetry and sea-storm parameters is valid and show that these simplifications are reliable and do not introduce errors to the surrogate model.

While these results are very encouraging, there are several components that can be improved and are suggested as future work. Here we discuss these issues and how they can affect the results and contribute to model improvement.

The XBeach calibration can be improved. We initially modeled the synthetic scenarios using XBeach and with a set of parameters that was validated in previous studies for sandy beach response to storms [Kalligeris et al., 2020; Gharagozlou et al., 2020]. We showed that XBeach underpredicted the erosion especially in the southern section of the domain. We suggest that future work consider recalibrating the XBeach model parameters, which will likely improve the accuracy and reduce the Level 1 errors and consequently, will improve the accuracy of surrogate predictions. The calibration may focus on better predicting the sub-aerial erosion and the location of the shoreline, because these parameters are used in identifying the scarps and training the model.

The training library can be smaller. In this study, we set aside 9 extreme scenarios (out of 1,250) because those cases were creating outliers in the training data (i.e. creating unique responses that are not similar to the rest of data set, thus negatively impacting the accuracy). However, the results show that even with a smaller number of training cases (about 600) we could achieve similar accuracy. We increased the library size to 1,250 scenarios to prove that further increasing the size will not improve the errors. Additionally, increasing the library size can be expensive. Training the model requires a full simulation of synthetic scenarios with the numerical model, which can take several weeks. Therefore, there need to be a balance between the required library size and the accuracy.

Some parameters can be neglected. Analysis of the relative importance of each variable in the training of the surrogate model revealed that certain parameters were less useful for predictions. The library size can be reduced if the erosion of the beach is not sensitive such parameters. The relative contribution of each training parameter (on the x axis) for each of the predicting variables (D_s, A, and B) are presented in Figure 4.20. Each training parameter's length scale is indicative of the necessary distance along that axis to become uncorrelated with any other parameter. Length scale is thus inversely related to relevance such that lower values on the scale denote higher importance. EOF #1, which represents the main shape of the sub-aerial portion of the profiles (the nourishment size), is the most-important variable for each scarp parameter. For the library that we tested, the wave direction has a very low impact on variation of the D_s, and the tide parameter also has a very low impact on the results. This seems contrary to the physics of the coastal erosion; however, because the storms have long duration (about 5 days on average), the water level oscillation due to tides may not affect the erosion directly. The future work can investigate whether some of these parameters with low impact can be removed from the set, thus, reducing the minimum required library size.

The surrogate model was used to predict the erosion due to four storms. The model goes through a cycle of parameterizing the profile for the first storm, predicting scarp parameters, recreating the eroded profile and re-parameterizing it for the next storm. The results showed that this process does not add errors to predicted erosion volume, however, it can move the shoreline seaward.

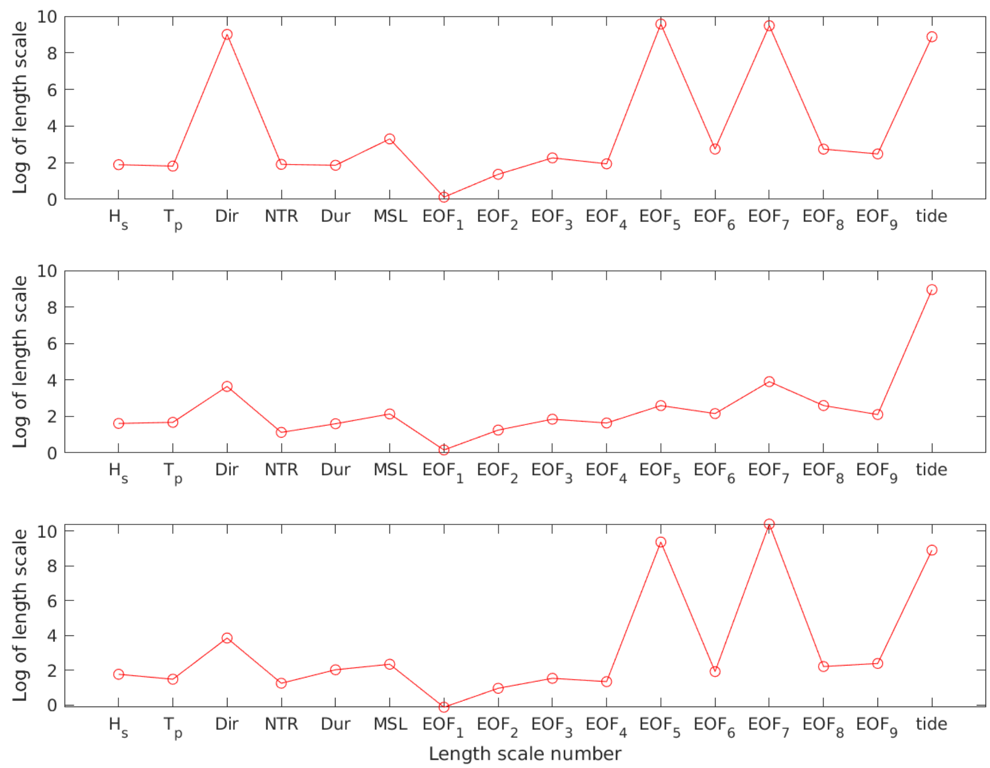

Figure 4.20 Relative importance of input dimensions to scarping parameters (top: D_s, middle: A, and bottom: B). The horizontal axis shows the 6 sea-storm parameters, the 9 EOFs, and the tide parameter. The vertical axis shows the scale of importance for each of these parameters. More-important parameters will have smaller values in this figure.

The cumulative errors in the shoreline location and smoothing the scarped profile can grow to a larger inaccuracy. We suggest that future studies quantify the cumulative errors and either apply corrections to the shoreline location or rework the process of going from scarped profile to new EOF-based profile.

4.8 Conclusion

In this chapter, a framework to develop a surrogate model for storm-driven beach erosion by combining deterministic and probabilistic models was presented. Previous studies have developed surrogate models only based on the sea-storm parameters. The novel contribution of this study is to include both the sea-storm and initial beach profile in the training process. This allows the model to be trained for various beach conditions, and consequently be used for related studies to the impact of possible future sea-storm sequences on the beach morphodynamics.

The surrogate model development required several levels of parameterization of sea-storms and beach profiles, and thus it had several potential sources of error. However, as demonstrated in predictions of observed beach erosion in Nags Head due to four storms in 2019, the surrogate model can predict the nourished beach erosion due to storms considerably well. The major finding of this study are:

1. *Training the surrogate with the parameterized beach profiles enables the prediction of erosion due to multiple storms.* As the main novelty in this study, we trained the model not only with the sea-storm parameters but also with the EOFs of beach profile. Including the variation of beach initial state allows the model to be applicable for storm-sequence studies in which the beach profile changes after each storm. The surrogate model was able to predict the erosion caused by four storms in 2019 by carrying forward the beach profile from one storm to the next.

2. *The surrogate model can be trained with a library of synthetic scenarios and predict the erosion accurately.* The surrogate model was successfully trained with 1,241 synthetic sea-storms, parameterized beach profiles, and XBeach predictions of scarping. The trained model was validated for the testing set and had an acceptable accuracy for predicting the scarp parameters. The RMSE for the scarped parameters reached an asymptote at about 600 testing cases. However, we further increased the number of tests to investigate if it can improve the model accuracy. Qualitative comparison of the predicted profiles for the surrogate and XBeach also shows that for most of the profiles, the surrogate prediction of the scarping is very similar to XBeach. In this study, we focused on the sub-aerial erosion of the beach. The median absolute error of surrogate compared to XBeach predicted erosion was 2.53 m^3/m. This error is less than 11% of the average erosion volume (23.5 m^3/m).

3. *The methodology of identifying the scarps needs further improvement, and the current assumption of power fit limits the predictions for uncommon erosion profiles.* As discussed earlier, the advantage of fitting a power function to scarps is that it reduces the number of parameters and captures the shape of the profile. However, this method can be extended to capture the exact shape of eroded profiles, especially for cases in which the scarped profile could not be approximated with a power function.

4. *The training library was costly to develop, but the trained surrogate model is much faster per prediction than the deterministic model.* While modeling the morphodynamics with XBeach can take several hours, the surrogate can reproduce similar results withing seconds. This incredible advantage of lower computation time, along with the fact that the surrogate can run on cheaper computing systems, makes the model very efficient. Modeling the realistic storms with XBeach took about 40 hours of computational time on 100 cores, whereas the surrogate model predictions were produced in less than 20 seconds. Note that this is the time that surrogate has to run all four storms and go through several loops of re-parameterizing the profiles, and reconstructing the eroded profile. Therefore, running the surrogate for a single storm will be even faster.

5. *The main source of errors in the surrogate model derives from inaccuracies in the numerical model.* Our results show that simplifying the sea-storm with symmetric triangular shape and parameterizing the beach profile with EOFs does not introduce a substantial error to the surrogate. The stepwise scatter plots of erosion (Figure 4.19) show that Level 2 and 3 simplifications have minor contribution to the error, however, Level 1 error is the main source of inaccuracies with $E_{\mathrm{RMS}} = 18.69\mathrm{m}^3/\mathrm{m}$ and $E_{\mathrm{volume}} = 12.28\mathrm{m}^3/\mathrm{m}$, which comes from the numerical model.

The results show that surrogate model is a viable tool for exploring the beach response to futuristic storm scenarios efficiently. While simulating the storms with morphodynamic models can take several hours, the surrogate model can produce similar predictions within seconds. The current developed model can be used to explore the long-term response of similar beaches to Nags Head to futuristic scenarios. Because the model has been trained with the variability of beach profile and with a large number of synthetic scenarios, it is capable of predicting the future storm event and adapt to unforeseen scarped beach profiles in the study area. Therefore, the model can be used to study the sustainability of nourished beaches, and to estimate the frequency of renourishment projects in Nags Head.

These findings are encouraging, however, several components of the model could be revised to improve the model accuracy and its applicability. XBeach could be recalibrated to better capture the sub-aerial erosion and the seaward/landward movement of the shoreline. Then, the parametrization of scarped profiles could be reworked so the eroded profiles for cases with extreme erosion or with shapes that are not similar to power function can be represented by the parameters. Moreover, the parameters that are not affecting the final erosion could be removed to reduce the dimensions in the model and the required library size. Finally, for the prediction of erosion due to storm sequence, the method of re-parameterizing the scarped profile could be revised to reduce the errors due to the seaward shift in the shoreline location.

CHAPTER

5

SUMMARY

Barrier islands are common coastal features and a primary coastal defense. They are vulnerable to storms and can experience erosion, overwash, inundation, and breaching due to large waves and storm surge. Deterministic and probabilistic models have been used to represent the erosion and flooding processes due to a single or a sequence of storms. However, the gaps between these models require further investigation.

In this study, we used a coupled system of numerical, deterministic models to explore the erosion and breaching of a barrier island and its contribution to large-scale hydrodynamic and circulations during a single storm. Then we combined the deterministic and probabilistic models to improve the efficiency and applicability of the models for studying the storm sequence effects on beach erosion. This dissertation contributes to filling the gaps between deterministic and probabilistic models and understanding of beach morphodynamics during storms in the following ways:

1. Application of the morphodynamic model on a large domain and evaluation of its performance and accuracy for prediction of erosion and overwash.

2. Assessment of erosion prediction sensitivity to computational mesh resolution.

3. Modeling the storm-induced breach of a barrier island and its contribution to flooding.

4. Coupling of small- and large-domain deterministic models to explore the interaction of morpho- and hydrodynamics on different scales.

5. Development of a surrogate model by combining probabilistic and deterministic models.

6. Quantification of the surrogate model performance for prediction of nourished beaches response to storm sequence.

Important findings in each of these areas are summarized in the following paragraphs.

Hurricane Isabel was the most powerful storm in 2003 that made landfall in North Carolina Outer Banks. It caused erosion and overwash along the barrier island, and breaching near the town of Hatteras. XBeach was implemented on a very high resolution large domain that covered 30 km of the Outer Banks. The predicted erosion and overwash incidents across the study area match the observations. The Skill Score of the model is 0.59, which is in 'excellent' range. The results show that XBeach successfully predicted the beach and dune erosion, as well as the location of overwash. Additionally, we explored the preliminary steps toward coupling ADCIRC and XBeach. These models run on different scales. To fill the gap between the models, we explored the sensitivity of XBeach results to mesh resolution. A new metric (WOA) was defined to represent the water flow through the barrier island. The mesh spacing in the longshore direction is not affecting the results or the erosion pattern, however, the larger cross-shore spacing significantly reduces the accuracy of the predictions. A spacing of 10 m in cross-shore direction reduces the Skill Score by 50 percent compared to the finer resolution with 3 m spacing.

A loose coupling of ADCIRC and XBeach was implemented in which the ground surface elevation in the ADCIRC mesh was updated with the final ground surface predicted by XBeach. The results show that, even with a fixed bathymetry, the dune erosion can contribute to ADCIRC flooding prediction along the Outer Banks. The predicted extents of inundated regions matched XBeach and post-storm aerial photos. These results were encouraging even with a simple XBeach model setup, and the methodology can be applied in similar studies in other regions. Using a coarser mesh can improve the computational time, however, the prediction of the dune crest and WOA is very sensitive to the cross-shore resolution. Therefore, the optimal resolution depends on the purpose of the modeling and the desired accuracy. The resolution requirements inform the resolution of ADCIRC mesh in the study area to better represent the small-scale changes in the morphodynamics.

Although these results showed the accuracy of XBeach in predicting beach erosion and the improvement in ADCIRC with implementing a fixed bathymetry, there are ways to improve these findings. The dune removal contributed to the flooding, however, breaching though the barrier island and formation of channels has a greater impact on the hydrodynamics in small and large scales. Additionally, the previous methodology with a fixed bathymetry does not account for temporal and spatial evolution of breaching or elevation change on the beach and dunes. Therefore, it is essential to resolve these limitations and to include these impacts for both to consider the more complex morphodynamic of breaching, and to explore the two-way coupled system of ADCIRC and XBeach and account for physical behavior via temporal and spatial evolution.

The breaching of the barrier islands can result in significant changes to the small- and large-scale hydrodynamics and morphodynamics of the region. We explored the breaching and formation of channels on Hatteras Island during Isabel. Then, with a two-way coupled numerical models for coastal erosion and flooding, we explored the effect of the breaching and the subsequent flooding into Pamlico Sound. The breaching effects on the large-scale hydrodynamic are investigated through three scenarios: (a) static mode where the bathymetry is fixed in the coupled models, (b) dynamic mode with DEMs where the bathymetry changes are informed by a linear transition between the pre- and post-storm observed DEMs, and (c) dynamic mode with XBeach where the nodal elevations are updated according to the morphodynamic model predictions.

A time-varying bathymetry module was used to dynamically update the ground surface elevation in ADCIRC+SWAN and represent the evolution of the breach. The results of the dynamic mode were compared to the static mode. The results show that XBeach, with a simple model setup and minimum tuning of the parameters, could predict the initiation and location of the breach. However, the depths and the number of channels were not predicted accurately. The flow from the sound to the ocean has an important role in deepening the channels. Breaching of the barrier island has significant large-scale impacts on the hydrodynamics. The coupled model results show that the water level increased by 1 m near the breach, and the ocean waters extended to 13 km into the sound.

Numerical models are powerful tools for deterministic predictions of beach response to storm forcing. However, they are expensive, both in computational resources and wall-clock time. This will limit their use in forecasting and for scenarios that multiple storms affect the beach. For example, examining the sustainability of nourishment projects under changing climates and designing beach nourishment require considering several futuristic storm scenarios. Using deterministic models for every single scenario is not an efficient solution. Additionally, the intrinsic uncertainties in the potential future scenarios require a statistical analysis of the information and a probabilistic approach to predict the beach response.

We developed a surrogate model by coupling deterministic and probabilistic models to study the nourished beaches response to storms. The study was focused on Nags Head, NC. We compiled more than 40 years of sea-storm data, as well as more than 10 years of surveyed beach profiles to parameterize the data. For the beach profiles, Principal Component Analysis was used to parameterize the profile shape. Statistic functions were applied to generate a large library of synthetic scenarios consisting one million sets of storm and profile parameters. We used copula function to assure that the synthetic storms have preserved the correlation between the parameters and are consistent with the actual observed data. Then a smaller set of 1,250 most dissimilar scenarios were selected and modeled with numerical, deterministic model. The resulting beach erosion was then parameterized in the form of a power function fitted to the scarped profile. Then the surrogate model was trained using the sea-storm parameters, beach profile EOFs, and the scarp parameters and by implementing Gaussian process regression on the data.

The surrogate model was able to predict the erosion of profiles and the results were close to XBeach predictions. We trained the model not only with the sea-storm parameters but also with the EOFs of beach profile. Including the variation of beach initial state allows the model to be applicable for different beach states and for storm-sequence studies where the beach profile changes after each storm. The surrogate model was able to predict the erosion caused by four storms in 2019 by carrying forward the beach profile from one storm to the next. The surrogate model was successfully trained with a library of synthetic sea-storms, parameterized beach profiles, and XBeach predictions of scarping. In this study, we focused on the sub-aerial erosion of the beach. The median absolute error of surrogate compared to XBeach predicted erosion was 2.53 m^3/m. This error is less than 11 percent of the average erosion volume (23.5 m^3/m). Modeling the realistic storms with XBeach took about 40 hours of computational time on 100 cores, whereas it only took less than 20 seconds for surrogate model to produced the results. The main source of errors in the surrogate model derives from inaccuracies in the numerical model.

The findings in this dissertation are very encouraging and have a major contribution to our understanding of (a) multi-scale erosion and breaching and their interaction with hydrodynamics, and (b) surrogate model development and its application for predicting nourished beach response to storm sequences. The methodology described for coupling deterministic models and combining them with probabilistic models can be applied to other regions.

BIBLIOGRAPHY

Allan, J. C. et al. (2015). *Coastal Flood Hazard Study, Tillamook County Oregon*. Tech. rep. Oregon Department of Geology and Mineral Industries, Special Paper 47, 283pp.

Anderson, D et al. (2019). "The time-varying emulator for short- and long-term analysis of coastal flooding". *Journal of Geophysical Research: Oceans*. in review.

Anjyo, K & Lewis, P. L. (2011). "RBF interpolation and Gaussian process regression through an RKHS formuation". *Journal of Math-for-Industry* **3**.6, pp. 63–71.

APTIM (2021). "ASBPA national beach nourishment database". (accessed: 06.13.2021).

Armstrong, S. B. et al. (2016). "Indications of a positive feedback between coastal development and beach nourishment". *Earth's Future* **4**, 626–636.

Avila, L. A. & Cangialosi, J (2013). *Tropical Cyclone Report, Hurricane Irene (AL092011) 21–28 August 2011*. Tech. rep. National Hurricane Center.

Barone, D. A. et al. (2014). "Hurricane sandy: beach-dune performance at New Jersey beach profile network sites". *Shore and Beach* **82** (4), pp. 13–23.

Berg, R (2015). *Tropical Cyclone Report, Hurricane Arthur, 1 - 5 July 2015*. Tech. rep. National Hurricane Center.

Beven, J. L. & Cobb, H (2003). *Tropical Cyclone Report, Hurricane Isabel, 6 - 19 September 2003*. Tech. rep. National Hurricane Center.

Bilskie, M. V. et al. (2016). "Data and numerical analysis of astronomic tides, wind–waves, and hurricane storm surge along the Northern Gulf of Mexico". *Journal of Geophysical Research: Oceans* **121**.5, pp. 3625–3658.

Birchler, J. J. et al. (2019). *Hurricane Matthew: Predictions, observations, and an analysis of coastal change*. Tech. rep. 2019-1095. U.S. Geological Survey, p. 37.

Birkemeier, W. et al. (1999). "Storms, storm groups and nearshore morphologic change". *Proceedings of the Coastal Sediments*, 1109–1122.

Blanton, B. O. & Luettich, R. A. (2008). *North Carolina Coastal Flood Analysis System: Model Grid Generation*. Tech. rep. TR-08-05. Renaissance Computing Institute.

Blanton, B. O. et al. (2008). *Report for State of North Carolina Floodplain Mapping Project Coastal Flood Analysis System*. Tech. rep. TR-08-08. Renaissance Computing Institute.

Blanton, B. O. et al. (2012). "Urgent Computing of Storm Surge for North Carolina's Coast". *Proceedings of the International Conference on Computational Science*. Vol. 9, pp. 1677–1686.

Bonisteel, J. M. et al. (2009). *Experimental Advanced Airborne Research Lidar (EAARL) Data Processing Manual*. Tech. rep. 2009-1078. US Geological Survey, 38p.

Booij, N et al. (1999). “A third-generation wave model for coastal regions, Part I, Model description and validation”. *Journal of Geophysical Research* **104**, pp. 7649–7666.

Bosboom, J et al. (2014). “On the perception of morphodynamic model skill”. *Coastal Engineering* **94**, pp. 112–125.

Bryant, M. A. et al. (2016). *Evaluation Statistics Computed for the Wave Information Studies (WIS)*. Tech. rep. ERDC/CHL CHETN-I-91. U.S. Army Corps of Engineers.

Bunya, S et al. (2010). “A High-Resolution Coupled Riverine Flow, Tide, Wind, Wind Wave and Storm Surge Model for Southern Louisiana and Mississippi: Part I – Model Development and Validation”. *Monthly Weather Review* **138** (2), pp. 345–377.

Camus, P et al. (2011). “Analysis of clustering and selection algorithms for the study of multivariate wave climate”. *Coastal Engineering* **58**.6, pp. 453–462.

Canizares, R & Irish, J. L. (2008). “Simulation of storm-induced barrier island morphodynamics and flooding”. *Coastal Engineering* **55**, pp. 1089–1101.

Clinch, A. S. et al. (2012). “Hurricane Irene and the Pea Island Breach: Pre-storm characterization and storm surge estimation using geospatial technologies”. *Shore and Beach* **80**, pp. 1–10.

Coastal Science and Engineering (2012). *Nags Head Post-Project Monitoring [CSE 2387–Year 1] Semi-Annual Beach Condition Survey – June 2012*. `http://nagsheadnc.gov/`. [Retrieved June 2021].

— (2019). *Nags Head Post-Dorian Beach Condition Survey [CSE 2458–Amendment 3]*. `http://nagsheadnc.gov/`. [Retrieved June 2021].

Corbella, S & Stretch, D. D. (2012). “Multivariate return periods of sea storms for coastal erosion risk assessment”. *Nat. Hazards Earth Syst. Sci.* **12**, pp. 2699–2708.

Cox, A. T. et al. (1995). “An interactive objective kinematic analysis system”. *Proceedings of the Fourth International Workshop on Wave Hindcasting and Forecasting*. Ed. by Dawson, C. N. & Gerritsen, M, pp. 109–118.

Cuttler, E. M. et al. (2019). “A Low-Cost Shoreline Dynamic Simulation Model for proposed Beach Nourishment and Dune Construction: Introducing a New Feasibility Analysis Tool”. *Journal of Coastal Research* **35**.4, pp. 907–919.

Cyriac, R et al. (2018). “Variability in Coastal Flooding Predictions due to Forecast Errors during Hurricane Arthur (2014)”. *Coastal Engineering* **137**, pp. 59–78.

de Vet, P (2014). “Modelling sediment transport and morphology during overwash and breaching events”. MA thesis. Delft University of Technology, Delft, ND.

Dietrich, J. C. et al. (2010). “A High-Resolution Coupled Riverine Flow, Tide, Wind, Wind Wave and Storm Surge Model for Southern Louisiana and Mississippi: Part II – Synoptic Description and Analysis of Hurricanes Katrina and Rita”. *Monthly Weather Review* **138** (2), pp. 378–404.

Dietrich, J. C. et al. (2011a). “Hurricane Gustav (2008) Waves and Storm Surge: Hindcast, Validation and Synoptic Analysis in Southern Louisiana”. *Monthly Weather Review* **139** (8), pp. 2488–2522.

Dietrich, J. C. et al. (2011b). “Modeling Hurricane Waves and Storm Surge using Integrally-Coupled, Scalable Computations”. *Coastal Engineering* **58**, pp. 45–65.

Dietrich, J. C. et al. (2012). “Surface Trajectories of Oil Transport along the Northern Coastline of the Gulf of Mexico”. *Continental Shelf Research* **41** (1), pp. 17–47.

Dietrich, J. C. et al. (2013). “Real-time forecasting and visualization of hurricane waves and storm surge using SWAN+ADCIRC and FigureGen”. *Computational Challenges in the Geosciences*. Ed. by Dawson, C. N. & Gerritsen, M, pp. 49–70.

Dietrich, J. C. et al. (2018). “Sensitivity of Storm Surge Predictions to Atmospheric Forcing During Hurricane Isaac”. *Journal of Waterway, Port, Coastal and Ocean Engineering* **144** (1).

Donnelly, C et al. (2006). “State of knowledge on measurement and modeling of coastal overwash”. *Journal of Coastal Research* **22** (4), pp. 965–991.

Doran, K. S. et al. (2013). *National assessment of hurricane-induced coastal erosion hazards: Mid-Atlantic Coast*. Tech. rep. 2013-1131. U.S. Geological Survey, p. 34.

Dresback, K. M. et al. (2013). “Skill assessment of a real-time forecast system utilizing a coupled hydrologic and coastal hydrodynamic model during Hurricane Irene (2011)”. *Continental Shelf Research* **71**, pp. 78–94.

Duo, E et al. (2020). “How good are symmetric triangular synthetic storms to represent real events for coastal hazard modelling”. *Coastal Engineering* **159**, p. 103728.

Elko, N et al. (2021). “A century of US beach nourishment”. *Ocean & Coastal Management* **199**, p. 105406.

Elsayed, S. M. & Oumeraci, H (2016). “Combined Modelling of Coastal Barrier Breaching and Induced Flood Propagation Using XBeach”. *Hydrology* **3**, p. 32.

— (2017). “Effect of beach slope and grain-stabilization on coastal sediment transport: An attempt to overcome the erosion overestimation by XBeach”. *Coastal Engineering* **121**, pp. 179–196.

Elsayed, S. M. et al. (2018). “Erosion and Breaching of Coastal Barriers in a Changing Climate: Associated Processes and Implication for Contamination of Coastal Aquifers”. *Coastal Engineering Proceedings*. Vol. 1, papers.107.

Emanuel, K (2020). “Evidence that hurricanes are getting stronger”. *Proceedings of the National Academy of Sciences of the United States of America* **117** (24), pp. 13194–13195.

Fauver, L. A. (2005). “Toward predicting barrier island vulnerability: Simple models for dune erosion”. MA thesis. University of South Florida.

Fearnley, S. M. et al. (2009). “Hurricane impact and recovery shoreline change analysis of the Chandeleur Islands, Louisiana, USA: 1855 to 2005”. *Geo-Mar Lett* **29**, pp. 455–466.

FEMA (2020). *Hurricane Michael in Florida: Building Performance Observations, Recommendations, and Technical Guidance*. Tech. rep. FEMA P-2077. Federal Emergency Management Agency.

Fernandez-Montblanc, T et al. (2019). "Towards robust pan-European storm surge forecasting". *Ocean Modelling* **133**, pp. 129–144.

Fritz, H. M. et al. (2007). "Hurricane Katrina storm surge distribution and field observations on the Mississippi barrier islands". *Estuarine, Coastal, and Shelf Science* **74**, pp. 12–20.

Gallagher, E. L. et al. (1998). "Observations of sand bar evolution on a natural beach". *Journal of Geophysical Research* **103**, pp. 3203–3215.

Gencarelli, R et al. (2009). "Beach Profile Evolution and Dune Erosion due to the Impact of Hurricane Isabel". *International Conference on Coastal Engineering*, pp. 1697–1709.

Gharagozlou, A et al. (2020). "Storm-Driven Erosion and Inundation of Barrier Islands from Dune- to Region-Scales". *Coastal Engineering* **158**.103674.

Giordano, L et al. (2006). "Beach nourishment design: An integrated approach". *International Offshore and Polar Engineering Conference Proceedings*. Vol. 3, pp. 778–781.

Gouldby, B. et al. (2014). "A methodology for deriving extreme nearshore sea conditions for structural design and flood risk analysis". *Coastal Engineering* **88**, pp. 15–26.

Gracia, V et al. (2013b). "Breaching of a barrier under extreme events. The role of morphodynamic simulations". *Journal of Coastal Research* **65**, pp. 951–956.

Gracia, V et al. (2013a). "Breaching of a barrier under extreme events. The role of morphodynamic simulations". *Journal of Coastal Research* **Special Issue**.65, pp. 951–956.

Gravens, M. B. et al. (2007). "Beach-fx: Monte Carlo life-cycle simulation model for estimating shore protection project evolution and cost benefit analyses". *Shore and Beach* **75**.1, p. 12.

Grzegorzewski, A. S. et al. (2009). "The influence of barrier islands on hurricane-generated storm surge and waves in Louisiana and Mississippi". *Proceedings from the 31st International Conference of Coastal Engineering*. Hamburg, Germany.

Grzegorzewski, A. S. et al. (2011). "Interaction of Barrier Islands and Storms: Implications for Flood Risk Reduction in Louisiana and Mississippi". *Journal of Coastal Research* **59**, pp. 156–164.

Haigh, I. D. et al. (2014). "Estimating present day extreme water level exceedance probabilities around the coastline of Australia: tides, extra-tropical storm surges and mean sea level". *Climate Dynamics* **42** (1–2), pp. 121–138.

Hanson, H et al. (2002). "Beach nourishment projects, practices, and objectives - a European overview". *Coastal Engineering* **47** (2), pp. 81–111.

Hardin, E. J. (2013). "A Transient Landscape: Geospatial Analysis and Numerical Modeling of Coastal Geomorphology in the Outer Banks, North Carolina". PhD thesis. North Carolina State University.

Harter, C & Figlus, J (2017). “Numerical modeling of the morphodynamic response of a low-lying barrier island beach and foredune system inundated during Hurricane Ike using XBeach and CSHORE”. *Coastal Engineering* **120**, pp. 64–74.

Hope, M. E. et al. (2013). “Hindcast and Validation of Hurricane Ike (2008) Waves, Forerunner, and Storm Surge”. *Journal of Geophysical Research: Oceans* **118**, pp. 4424–4460.

Hovis, J et al. (2004). *EFFECTS OF HURRICANE ISABEL ON WATER LEVELS DATA REPORT, April 2004*. Tech. rep. National Oceanic and Atmospheric Administration.

James, S. C. et al. (2018). “A machine learning framework to forecast wave conditions”. *Coastal Engineering* **137**.February, pp. 1–10.

Jia, G. F. et al. (2016a). “Surrogate modeling for peak or time-dependent storm surge prediction over an extended coastal region using an existing database of synthetic storms”. *Natural Hazards* **81** (2), pp. 909–938.

Jia, G. et al. (2016b). “Surrogate modeling for peak or time-dependent storm surge prediction over an extended coastal region using an existing database of synthetic storms”. *Natural Hazards* **81**.2, pp. 909–938.

Jolliffe, I. T. & Cadima, J (2016). “Principal component analysis: a review and recent developments”. *Philosophical Transactions of the Royal Society A: Mathematical, Physical, and Engineering Sciences* **374** (2065), p. 20150202.

Kaczkowski, H. L. et al. (2018). “Beach-fill equilibration and dune growth at two large-scale nourishment sites”. *Ocean Dynamics* **68**, pp. 1191–1206.

Kalligeris, N et al. (2020). “Calibration and assessment of process-based numerical models for beach profile evolution in southern California”. *Coastal Engineering* **158**, p. 103650.

Kana, T. W. & Kaczkowski, H. L. (2012). “PLANNING, PRELIMINARY DESIGN, AND INITIAL PERFORMANCE OF THE NAGS HEAD BEACH NOURISHMENT PROJECT”. *Coastal Engineering proceeding* **1(33)**.sediment.109, p. 12.

Karanci, A et al. (2014). “Land Cover Effect on Dune Erosion and Overwash”. *International Conference on Coastal Engineering*.

Karanci, A et al. (2018). *Beach Management Practices and Occupation Dynamics: An Agent-Based Modeling Study for the Coastal Town of Nags Head, NC, USA*. Springer, pp. 373–395.

Kennedy, A. B. et al. (2011). “Origin of the Hurricane Ike Forerunner Surge”. *Geophysical Research Letters* **38(8)**.

Kim, S.-W. et al. (2015). “A time-dependent surrogate model for storm surge prediction based on an artificial neural network using high-fidelity synthetic hurricane modeling”. *Natural Hazards* **76** (1), pp. 565–585.

Kossin, J. P. et al. (2020). “Global increase in major tropical cyclone exceedance probability over the past four decades”. *Proceedings of the National Academy of Sciences of the United States of America* **117** (22), pp. 11975–11980.

Kraus, N. C. & Wamsley, T. V. (2003). *Coastal barrier breaching, Part 1: Overview of breaching processes*. Tech. rep. US Army Corps of Engineers.

Kraus, N. C. et al. (2002). “Barrier Breaching Processes and Barrier Spit Breach, Stone Lagoon, California”. *Shore and Beach* **70**.4, pp. 21–28.

Kurum, M. O. & Overton, M. F. (2013). “Scenario Testing on the Impact of Topography, Land Cover and Sea-Level Rise on Barrier Island Breaching”. *Proceedings of Coastal Dynamics 2013*, pp. 1025–1036.

Kurum, M. O. et al. (2010). “Effects of Coastal Landform Changes on Storm Surge along the Hatteras Island Breach Area”. *Proceedings of Coastal Engineering 2010*, pp. 1–8.

Laface, V et al. (2016). “Peak over threshold vis-à-vis equivalent triangular storm: return value sensitivity to storm threshold”. *Coastal Engineering* **116**, pp. 220–235.

Landry, C. E. (2011). “Coastal Erosion as a Natural Resource Management Problem: An Economic Perspective”. *Coastal Management* **39**.3, pp. 259–281.

Lindemer, C. A. et al. (2010). “Numerical simulation of a low-lying barrier island’s morphological response to Hurricane Katrina”. *Coastal Engineering* **57**, pp. 995–995.

Luettich, R. A. et al. (1992). *ADCIRC: An Advanced Three-Dimensional circulation model for shelves coasts and estuaries, report 1: Theory and methodology of ADCIRC-2DDI and ADCIRC-3DL*. Tech. rep. United States Army Corps of Engineers.

Luettich, R. A. et al. (2014). *Reducing Coastal Risk on the East and Gulf Coasts*. Washington, DC: The National Academies Press.

Lugt, M. A. van der et al. (2019). “Morphodynamic modeling of the response of two barrier islands to Atlantic hurricane forcing”. *Estuarine, Coastal and Shelf Science* **229**.106404.

Males, R. M. et al. (2007). “Beach-fx: Life-cycle Risk Analysis of Shore Protection Projects”, pp. 4069–4081.

Mallinson, D. J. et al. (2010). “Geological characteristics and spatial distribution of paleo-inlet channels beneath the outer banks barrier islands, North Carolina, USA”. *Estuarine, Coastal and Shelf Science* **88**, pp. 175–189.

Mattocks, C & Forbes, C (2008). “A real-time, event-triggered storm surge forecasting system for the state of North Carolina”. *Ocean Modelling* **25**, pp. 95–119.

McCall, R (2008). “The longshore dimension in dune overwash modelling”. MA thesis. Delft University of Technology, Delft, ND.

McCall, R. T. et al. (2010). “Two-dimensional time dependent hurricane overwash and erosion modeling at Santa Rosa Island”. *Coastal Engineering* **57**, pp. 668–683.

Mickey, R. C. et al. (2018). “A framework for modeling scenario-based barrier island storm impacts”. *Coastal Engineering* **138**, pp. 98–112.

Mickey, R. C. et al. (2020). “Sensitivity of Storm Response to Antecedent Topography in the XBeach Model”. *Journal of Marine Science and Engineering* **8** (10), p. 829.

Miselis, J. L. et al. (2016). “Evolution of Mid-Atlantic Coastal and Back-Barrier Estuary Environments in Response to a Hurricane: Implications for Barrier-Estuary Connectivity”. *Estuaries and Coasts* **39**, pp. 916–934.

Mitasova, H et al. (2005). “Simultaneous spline approximation and topographic analysis for lidar elevation data in open-source GIS”. *IEEE Geoscience and Remote Sensing Letters* **2** (4), pp. 375–379.

Mitasova, H et al. (2009). “Raster-Based Analysis of Coastal Terrain Dynamics from Multitemporal Lidar Data”. *Journal of Coastal Research* **25**.2, 507—514.

Moftakhari, H et al. (2019). “Linking statistical and hydrodynamic modeling for compound flood hazard assessment in tidal channels and estuaries”. *Advances in Water Resources* **128**, 28—38.

Morgan, K. L. M. & Sallenger, A (2009). *Coastal Change during Hurricane Isabel 2003*. Tech. rep. 2009-3025. US Geological Survey.

Morton, R. A. (2002). “Factors controlling storm impacts on coastal barriers and beaches – a preliminary basis for near real-time forecasting”. *Journal of Coastal Research* **18**, pp. 486–501.

Morton, R. A. & Sallenger, A. H. (2003). “Morphological Impacts of Extreme Storms on Sandy Beaches and Barriers”. *Journal of Coastal Research* **19** (3), pp. 560–573.

Muis, S et al. (2016). “A global reanalysis of storm surges and extreme sea levels”. *Nat. Commun.* **7**.11969.

Mulligan, R. P. et al. (2015). “Storm Surge and Surface Waves in a Shallow Lagoonal Estuary during the Crossing of a Hurricane”. *Journal of Waterway, Port, Coastal, and Ocean Engineering* **141** (4).

N.C. Department of Environment and Natural Resources (NCDENR) (2012). *North Carolina 2011 long-term average annual oceanfront erosion rates. Raleigh, NC.* `https://files.nc.gov/ncdeq/`. [Retrieved June 2021].

Nederhoff, C. M. (2014). “Modeling the Effects of Hard Structures on Dune Erosion and Overwash: Hindcasting the Impact of Hurricane Sandy on New Jersey with XBeach.” MA thesis. Delft University of Technology, Delft, ND.

Oertel, G. F. (1985). “The barrier island system”. *Marine Geology* **63** (1-4), pp. 1–18.

Ormondt, M van et al. (2020). “Morphodynamic modelling of the wilderness breach, Fire Island, New York. Part I: Model set-up and validation”. *Coastal Engineering* **157**.103621.

Overton, M. F. & Fisher, J. S. (2004). “Hurricane Isabel and the NC12 Hotspots”. *Shore and Beach* **72** (1), pp. 30–35.

Overton, M. F. & Smyre, E. A. (2013). “Evolution of the Pea Island Breach, Outer Banks, North Carolina”. *Shore and Beach* **81**, pp. 23–27.

Parker, K et al. (2019). “Emulation as an approach for rapid estuarine modeling”. *Coastal Engineering* **150**, pp. 79–93.

Passeri, D. L. et al. (2015). “On the significance of incorporating shoreline changes for evaluating coastal hydrodynamics under sea level rise scenarios”. *Natural Hazards* **75**.2, pp. 1599–1617.

Passeri, D. L. et al. (2018). “The influence of bed friction variability due to land cover on storm-driven barrier island morphodynamics”. *Coastal Engineering* **132**, pp. 82–94.

Pender, D & Karunarathna, H (2013). “A statistical-process based approach for modelling beach profile variability”. *Coastal Engineering* **81**, pp. 19–39.

Peng, M et al. (2004). “A numerical study of storm surge and inundation in the Croatan-Albemarle-Pamlico Estuary System”. *Estuarine, Coastal and Shelf Science* **59**, pp. 121–137.

— (2006). “Tropical cyclone induced asymmetry of sea level surge and fall and its presentation in a storm surge model with parametric wind fields”. *Ocean Modelling* **14**, pp. 81–101.

Pierce, J. W. (1970). “Tidal inlets and washover fans”. *Journal of Geology* **78**, pp. 230–234.

Plant, N. G. & Stockdon, H. F. (2012). “Probabilistic prediction of barrier-island response to hurricanes”. *Journal of Geophysical Research: Earth Surface* **117**, F03015.

Plant, N. G. et al. (2014a). “Coupling centennial-scale shoreline change to sea-level rise and coastal morphology in the Gulf of Mexico using a Bayesian network”. *Earth’s Future* **4** (5), 143–158.

Plant, N. G. et al. (2014b). “Predictions of barrier island berm evolution in a time-varying storm climatology”. *Journal of Geophysical Research: Earth Surface* **119**, pp. 300–316.

Pullen, T et al. (2018). “Bayonet GPE: A generic and practical overtopping model that includes uncertainty”. *Maritime Engineering* **171**.3.

Rasmussen, C. E. & Williams, C. K. (2006). *Gaussian processes for machine learning*. 39. MIT Press.

Rego, J. L. & Li, C (2010). “Storm surge propagation in Galveston Bay during Hurricane Ike”. *Journal of Marine Systems* **82**, pp. 265–279.

Riggs, S. R. et al. (1995). “Influence of inherited geologic framework on barrier shoreface morphology and dynamics”. *Marine Geology* **126**, pp. 213–234.

Roelvink, D et al. (2009). “Modelling storm impacts on beaches, dunes and barrier islands”. *Coastal Engineering* **56**, pp. 1133–1152.

Roelvink, D et al. (2010). *XBeach Model Description and Manual*. Tech. rep. UNESCO-IHE Institute for Water Education, Deltares and Delft University of Technology.

Roelvink, J. A. (1993). “Dissipation in random wave groups incident on a beach”. *Coastal Engineering* **19**, pp. 127–150.

— (2006). “Coastal morphodynamic evolution techniques”. *Coastal Engineering* **53** (2-3), pp. 277–287.

Rogers, S. M. (2007). “Beach Nourishment for Hurricane Protection: North Carolina Project Performance in Hurricanes Dennis and Floyd”. *Shore and Beach* **75** (1), pp. 37–42.

Rogers, S. M. & Tezak, E. S. (2004). “Hurricane Isabel Damage to Coastal North Carolina Buildings”. *Shore and Beach* **72** (2), pp. 38–44.

Ruggiero, P et al. (2001). “Wave runup, extreme water levels and the erosion of properties backing beaches.” *Journal of Coastal Research* **17(2)**, 407—419.

Safak, I et al. (2016). “Barrier island breach evolution: Alongshore transport and bay-ocean pressure gradient interactions”. *Journal of Geophysical Research: Oceans* **121**, pp. 8720–8730.

Sallenger, A. H. (2000). “Storm impact scale for barrier islands”. *Journal of Coastal Research* **16** (3), pp. 890–895.

Sallenger, A. H. et al. (2004). “Assessing Storm-Induced Damage and Dune Erosion using Airborne Lidar: Examples from Hurricane Isabel”. *Shore and Beach* **72** (1), pp. 25–29.

Sallenger, A. H. et al. (2007). *Extreme changes to barrier islands along the central Gulf of Mexico coast during Hurricane Katrina*. Tech. rep. 1306. United States Geological Survey, pp. 113–118.

Santos, V. M. et al. (2019). “Combining numerical and statistical models to predict storm-induced dune erosion”. *Journal of Geophysical Research: Earth Surface* **124**, 1817–1834.

Schambach, L et al. (2018). “Assessing the impact of extreme storms on barrier beaches along the Atlantic coastline: Application to the southern Rhode Island coast”. *Coastal Engineering* **133**, pp. 26–42.

Sciaudone, E. J. et al. (2016). “Spatial and temporal variability in dune field: Pea Island, North Carolina”. *Shore and Beach* **84** (2), pp. 49–58.

Sebastian, A. G. et al. (2014). “Characterizing Hurricane Storm Surge Behavior in Galveston Bay using the SWAN+ADCIRC Model”. *Coastal Engineering* **88**, pp. 171–181.

Sheng, Y. P. et al. (2010). “Simulation of storm surge, wave, currents, and inundation in the Outer Banks and Chesapeake Bay during Hurricane Isabel in 2003: The importance of waves”. *Journal of Geophysical Research* **115**, p. C04008.

Sherwood, C. R. et al. (2014). “Inundation of a barrier island (Chandeleur Islands, Louisiana, USA) during a hurricane: Observed water-level gradients and modeled seaward sand transport”. *J. Geophys. Res. Earth Surf.* **119**, pp. 1498–1515.

Sherwood, C. R. et al. (2020). “Morphologic changes from sound-side inundation of North Core Banks, Cape Lookout National Seashore, North Carolina, USA during Hurricane Dorian”.

Smallegan, S. M. & Irish, J. L. (2018). “Barrier Island Morphological Change by Bay-Side Storm Surge”. *Journal of Waterway, Port, Coastal, and Ocean Engineering* **143** (5), p. 04017025.

Sopkin, K. L. et al. (2014). *Hurricane Sandy: Observations and analysis of coastal change*. Tech. rep. 2014-1088. U.S. Geological Survey, p. 54.

Stewart, S. R. (2017). *Tropical Cyclone Report for Hurricane Matthew, 28 September - 9 October 2016*. Tech. rep. National Hurricane Center.

Stutz, M. L. & Pilkey, O. H. (2011). “Open-Ocean Barrier Islands: Global Influence of Climatic, Oceanographic, and Depositional Settings”. *Journal of Coastal Research* **27** (2), pp. 207–222.

Suh, S. W. et al. (2015). “An efficient early warning system for typhoon storm surge based on time-varying advisories by coupled ADCIRC and SWAN”. *Ocean Dynamics* **65** (5), pp. 617–646.

Sutherland, J et al. (2004). “Evaluating the performance of morphological models”. *Coastal Engineering* **51**, pp. 917–939.

Svendsen, A (1984). “Wave heights and set-up in a surf-zone”. *Coastal Engineering* **8**, pp. 303–329.

Tadesse, M. et al. (2020). “Data-Driven Modeling of Global Storm Surges”. *Frontiers in Marine Science* **7**.

Thomas, A et al. (2019). “Influence of Storm Timing and Forward Speed on Tide-Surge Interactions during Hurricane Matthew”. *Ocean Modelling* **137**, pp. 1–19.

Thornton, E. B. et al. (2007). “Rip currents, mega-cusps, and eroding dunes”. *Marine Geology* **240**, pp. 151–167.

Town of Nags Head (2017). *Town of Nags Head Comprehensive Plan*. `https://www.nagsheadnc.gov/241/2017-Results`. [Retrieved June 2021].

U.S. Geological Survey (2018). `https://coastal.er.usgs.gov/hurricanes/isabel/`. [Retrieved 20 July 2018].

— (2019a). `https://coastal.er.usgs.gov/data-release/doi-F76W9879/`. [Retrieved November 2019].

— (2019b). *USGS Current Water for the Nation*. `https://waterdata.usgs.gov/nwis/rt`. [Retrieved 28 April 2019].

USACE (2021). *Sea-Level Change Curve Calculator (Version 2021.12)*. `https://cwbi-app.sec.usace.army.mil/rccslc/slcc_calc.html`. [Retrieved June 2021].

van Maanen, B et al. (2008). “Onshore sandbar migration at Tairua Beach (New Zealand): Numerical simulation and field measurements”. *Marine Geology* **253** (3-4), pp. 99–106.

Velasquez, L et al. (2015). “Multi-temporal geospatial analysis of the evolution and closing of Pea Island Breach, NC”. *Proceedings of Coastal Sediments 2015*. World Scientific, pp. 1–11.

Velasquez-Montoya, L et al. (2018). “Observation and modeling of the evolution of an ephemeral storm-induced inlet: Pea Island Breach, North Carolina, USA”. *Continental Shelf Research* **156**, pp. 55–69.

Wahl, T et al. (2016). “Probabilistic assessment of erosion and flooding risk in the northern Gulf of Mexico”. *Journal of Geophysical Research: Oceans* **121**, 3029–3043.

Wamsley, T. V. & Hathaway, K. K. (2004). “Monitoring Morphology and Currents at the Hatteras Breach”. *Shore and Beach* **72** (2), pp. 9–14.

Wamsley, T. V. et al. (2009). “Influence of Landscape Restoration and Degradation on Storm Surge and Waves in Southern Louisiana”. *Journal of Natural Hazards* **51** (1), pp. 207–224.

Weaver, R. J. & Luettich, R. A. (2010). “2D vs 3D Storm Surge Sensitivity in ADCIRC: Case Study of Hurricane Isabel”. *Estuarine and Coastal Modeling 2009*, pp. 762–779.

Westerink, J. J. et al. (2008). “A Basin to Channel Scale Unstructured Grid Hurricane Storm Surge Model Applied to Southern Louisiana”. *Monthly Weather Review* **136** (3), pp. 833–864.

Wurtkowski, M (2004). “Hatteras Breach Closure”. *Shore and Beach* **72** (1), pp. 20–24.

Zijlema, M (2010). “Computation of wind-wave spectra in coastal waters with SWAN on unstructured grids”. *Coastal Engineering* **57**, pp. 267–277.

APPENDIX

APPENDIX

A XBEACH PARAMETERS

This is an example of XBeach parameters and output log file. This is a log file for version 5559, however, it still shows an older version in the header, likely due to a minor bug in the source code.

```
 **********************************************************
                    Welcome to XBeach

             version 1.23.5526 XBeachX release
              dateTue Feb  2 21:48:12 EST 2021
    URL:URL: https://svn.oss.deltares.nl/repos/xbeach/trunk
 **********************************************************

 Simulation started: YYYYMMDD    hh:mm:ss     time zone (UTC)
                     20210803  15:22:03     -0400

   running in:/gpfs_common/share01/jcdietri/agharag/new_4storm_2019/

 General Input Module
  MPI version, running on         100processes
 Reading input parameters:
  XBeach reading fromparams.txt
 --------------------------------
 Backward compatibility:
```

```
Warning: Specification of instat using parameter 'wbctype'
                   instat =jons_table
 --------------------------------
 Physical processes:
                wavemodel =surfbeat
                   cyclic =0 (no record found, default value used)
                    swave =1 (no record found, default value used)
               single_dir =0 (no record found, default value used)
                    lwave =1 (no record found, default value used)
                     flow =1 (no record found, default value used)
                 sedtrans =1
               morphology =1
               avalanching =1 (no record found, default value used)
                   gwflow =0 (no record found, default value used)
                    ships =0 (no record found, default value used)
               vegetation =0 (no record found, default value used)
                 setbathy =0 (no record found, default value used)
                viscosity =1 (no record found, default value used)
                advection =1 (no record found, default value used)
                     wind =1 (no record found, default value used)
 --------------------------------
 Grid parameters:
                 gridform =delft3d
                  depfile =Nags_20km_2019_08_ext_fill.dep
                   xyfile =Nags_matt_20km_extended.grd
                     xori =.0000 (no record found, default value used)
                     yori =.0000 (no record found, default value used)
                     alfa =.0000 (no record found, default value used)
                   posdwn =-1.0000
                       nz =1 (no record found, default value used)
                 thetamin =-50.0000
                 thetamax =190.0000
                thetanaut =1
                   dtheta =20.0000
 --------------------------------
 Model time parameters:
                      CFL =.5000
                    dtset =.0000 (no record found, default value used)
                    tstop =288000.0000
```

```
                maxdtfac =50.0000 (no record found, default value used)
--------------------------------
Physical constants:
                     rho =1025.0000 (no record found, default value used)
                       g =9.8100 (no record found, default value used)
              depthscale =1.0000 (no record found, default value used)
--------------------------------
Initial conditions:
              zsinitfile = None specified
--------------------------------
Wave boundary condition parameters:
                 wbctype =jonstable
                  bcfile =2019-08-24_real_wave_revised.txt
                   taper =100.0000 (no record found, default value used)
                    nmax =.8000 (no record found, default value used)
             lateralwave =neumann (no record found, default value used)
--------------------------------
Wave-spectrum boundary condition parameters:
                  random =0
                 fcutoff =.0000 (no record found, default value used)
                 trepfac =.0100 (no record found, default value used)
                 sprdthr =.0800 (no record found, default value used)
              Tm01switch =0 (no record found, default value used)
              wbcversion =3
            nspectrumloc =1 (no record found, default value used)
--------------------------------
Flow boundary condition parameters:
                   front =abs_2d (no record found, default value used)
                    left =neumann
                   right =neumann_v
                    back =abs_2d (no record found, default value used)
                     ARC =1 (no record found, default value used)
                   order =2.0000 (no record found, default value used)
                highcomp =0 (no record found, default value used)
                freewave =0 (no record found, default value used)
                    epsi =-1.0000 (no record found, default value used)
                tidetype =velocity (no record found, default value used)
--------------------------------
Tide boundary conditions:
```

```
                 tideloc =1
                 zs0file =2019-08-24_real_wl_revised.txt
--------------------------------
Discharge boundary conditions:
          disch_loc_file = None specified
   disch_timeseries_file = None specified
              ndischarge =0 (no record found, default value used)
             ntdischarge =0 (no record found, default value used)
                    beta =.1000
--------------------------------
Wave breaking parameters:
                   break =roelvink1
                   gamma =.4200
                  gammax =2.0000 (no record found, default value used)
                   alpha =2.0000
                       n =10.0000 (no record found, default value used)
                   delta =.0000 (no record found, default value used)
                      fw =.0200
                  fwfile = None specified
                fwcutoff =1000.0000 (no record found, default value used)
            breakerdelay =1.0000 (no record found, default value used)
--------------------------------
Roller parameters:
                  roller =1 (no record found, default value used)
                     rfb =0 (no record found, default value used)
--------------------------------
Wave-current interaction parameters:
                     wci =0 (no record found, default value used)
                    hwci =.1000 (no record found, default value used)
                 hwcimax =100.0000 (no record found, default value used)
                    cats =4.0000 (no record found, default value used)
--------------------------------
Flow parameters:
             bedfriction =chezy (no record found, default value used)
             bedfricfile = None specified
             bedfriccoef =55.0000 (no record found, default value used)
                   droot =.5000 (no record found, default value used)
                   dstem =.5000 (no record found, default value used)
                   maxcf =.0400 (no record found, default value used)
```

```
                 nuh =.1000 (no record found, default value used)
              nuhfac =1.0000 (no record found, default value used)
                smag =1 (no record found, default value used)
--------------------------------
Coriolis force parameters:
              wearth =.0417 (no record found, default value used)
                 lat =.0000 (no record found, default value used)
--------------------------------
Wind parameters:
                rhoa =1.2500 (no record found, default value used)
                  Cd =.0020 (no record found, default value used)
            windfile = None specified
               windv =.0000 (no record found, default value used)
              windth =270.0000 (no record found, default value used)
--------------------------------
Sediment transport parameters:
                form =vanthiel_vanrijn (no record found, default
                value used)
            waveform =vanthiel (no record found, default value used)
                 sws =1 (no record found, default value used)
                 lws =0
               BRfac =1.0000 (no record found, default value used)
               facua =.1000 (no record found, default value used)
               facSk =.1000 (no record found, default value used)
               facAs =.1000
               Tbfac =1.0000 (no record found, default value used)
                turb =bore_averaged (no record found, default value
                used)
             turbadv =none (no record found, default value used)
                 sus =1 (no record found, default value used)
                 bed =1 (no record found, default value used)
                bulk =0 (no record found, default value used)
               facsl =.1500 (no record found, default value used)
                  z0 =.0060 (no record found, default value used)
                smax =-1.0000 (no record found, default value used)
         bdslpeffmag =roelvink_bed
         bdslpeffini =none (no record found, default value used)
         bdslpeffdir =none (no record found, default value used)
         reposeangle =30.0000 (no record found, default value used)
```

```
                   tsfac =.1000 (no record found, default value used)
                   Tsmin =.5000 (no record found, default value used)
                   facDc =1.0000 (no record found, default value used)
                     lwt =0 (no record found, default value used)
                   betad =1.0000 (no record found, default value used)
              fallvelred =0 (no record found, default value used)
               dilatancy =0 (no record found, default value used)
--------------------------------
Bed composition parameters:
                     ngd =1
                      nd =3
                     por =.4000 (no record found, default value used)
                     D50 =.0003
                     D90 =.0005
                    rhos =2650.0000 (no record found, default value
                    used)
                     dzg =.1000 (no record found, default value used)
                    dzg1 =.1000 (no record found, default value used)
                    dzg2 =.1000 (no record found, default value used)
                    dzg3 =.1000 (no record found, default value used)
                  sedcal =1.0000
 ucrcal =1.0000 (no record found, default value used)
--------------------------------
Morphology parameters:
                  morfac =10.0000
               morfacopt =1
                morstart =3600.0000
                 morstop =288000.0000 (no record found, default
                 value used)
                  wetslp =.3000
                  dryslp =1.0000 (no record found, default value used)
                 hswitch =.1000 (no record found, default value used)
                   dzmax =.0500 (no record found, default value used)
                  struct =0 (no record found, default value used)
--------------------------------
Output variables:
                 timings =1 (no record found, default value used)
                  tunits = None specified
                  tstart =.0000
```

```
                    tint =1.0000 (no record found, default value used)
                tsglobal = None specified
                   tintg =72000.0000
                tspoints = None specified
                   tintp =1.0000 (no record found, default value used)
                  tsmean = None specified
                   tintm =288000.0000 (no record found, default value
                   used)
              nglobalvar =5
 nglobalvar: Will generate global output for variable:zs
 nglobalvar: Will generate global output for variable:zb
 nglobalvar: Will generate global output for variable:ue
 nglobalvar: Will generate global output for variable:ve
 nglobalvar: Will generate global output for variable:H
                 npoints =0 (no record found, default value used)
                nrugauge =0 (no record found, default value used)
               npointvar =0 (no record found, default value used)
               nrugdepth =1 (no record found, default value used)
 rugdepth =.0000 (no record found, default value used)
                nmeanvar =0 (no record found, default value used)
            outputformat =netcdf
         outputprecision =double (no record found, default value used)
              ncfilename = None specified
netcdf output to:xboutput.nc
            remdryoutput =1 (no record found, default value used)
--------------------------------
Output projection:
              projection = None specified
                  rotate =1 (no record found, default value used)
--------------------------------
Wave numerics parameters:
                  scheme =warmbeam (no record found, default value
                  used)
                  snells =0 (no record found, default value used)
--------------------------------
Flow numerics parameters:
                     eps =.0100
                  eps_sd =.5000 (no record found, default value used)
                    umin =.0000 (no record found, default value used)
```

```
                    hmin =.2000
                secorder =0 (no record found, default value used)
--------------------------------
Sediment transport numerics parameters:
                thetanum =1.0000 (no record found, default value used)
                    cmax =.1000 (no record found, default value used)
--------------------------------
Bed update numerics parameters:
                 frac_dz =.7000 (no record found, default value used)
                  nd_var =2 (no record found, default value used)
                   split =1.0100 (no record found, default value used)
                   merge =.0100 (no record found, default value used)
--------------------------------
MPI parameters:
             mpiboundary =man
                    mmpi =5
                    nmpi =20
--------------------------------
Finished reading input parameters
--------------------------------
------------------------------------
Building Grid and Bathymetry
------------------------------------
 processor grid:           5 X          20
Initializing .....
 readtide: reading tide time series from real_wl_revised.txt ...
--------------------------------
Initializing spectral wave boundary conditions
--------------------------------
--------------------------------
```